Ph.D. DISSERTATION

Integrated Pressure/Temperature Sensor Array Based on Nickel Conductive Composite

니켈 전도성 복합재료 기반의
압력/온도 집적 센서 어레이 구현에 관한 연구

BY

SANGWOO KIM

FEBRAURY 2014

DEPARTMENT OF ELECTRICAL ENGINEERING AND
COMPUTER SCIENCE
COLLEGE OF ENGINEERING
SEOUL NATIONAL UNIVERSITY

Ph.D. DISSERTATION

Integrated Pressure/Temperature Sensor Array Based on Nickel Conductive Composite

니켈 전도성 복합재료 기반의 압력/온도 집적 센서 어레이 구현에 관한 연구

BY

SANGWOO KIM

FEBRAURY 2014

DEPARTMENT OF ELECTRICAL ENGINEERING AND COMPUTER SCIENCE
COLLEGE OF ENGINEERING
SEOUL NATIONAL UNIVERSITY

Integrated Pressure/Temperature Sensor Array Based on Nickel Conductive Composite

니켈 전도성 복합재료 기반의 압력/온도 집적 센서 어레이 구현에 관한 연구

지도교수 홍 용 택

이 논문을 공학박사 학위논문으로 제출함

2014 년 2 월

서울대학교 대학원

전기컴퓨터 공학부

김 상 우

김상우의 공학박사 학위논문을 인준함

2014 년 2 월

위 원 장 : _____ (인)

부위원장 : _____ (인)

위 원 : _____ (인)

위 원 : _____ (인)

위 원 : _____ (인)

Abstract

Integrated Pressure/Temperature Sensor Array Based on Nickel Conductive Composite

SANGWOO KIM

DEPARTMENT OF ELECTRICAL ENGINEERING AND COMPUTERSCIENCE

COLLEGE OF ENGINEERING

SEOUL NATIONAL UNIVERSITY

Implementation of electronic artificial skin has been widely studied, from basic concept to prototypes, for potential applications in robot engineering and prosthetic replacement. Electronic Artificial skin plays a key role of sensing external environment, such as pressure and temperature, and delivering transformed signals either to robot control or human nerve system.

In order to truly mimicking human skin, artificial skin at least needs to

contain both pressure and temperature sensing elements in an array format. In fact, a couple of trials have been attempted to integrate sensing both elements onto single skin. Combination of commercial temperature sensing chips with printed pressure sensitive resistor or assembly of separately fabricated sensor arrays of each type has been demonstrated. These hybrid type integration or assembly approach renders rather complicated processes and thus increases fabrication cost.

For sensing elements, conductive composite materials have been commonly used, whose resistance changes as geometrical dimension changes with applied pressure or temperature. In most cases, the conductive composite materials have been used only for single type of sensing element, either pressure or temperature sensor. It is challenging to differentiate two type of sensing part in one substrate with single conductive composite material and to independently read out each signal. Therefore, there have been no reported researches on using single conducting composite materials to a multi-sensing device.

In addition, the conductive composite materials were typically fabricated

"on" either flexible or stretchable substrate only after readout active-matrix circuitry was fabricated on the substrate. Therefore, there can be limitation in selection of materials and device structure, and process incompatibility that can makes mass manufacturing of the active-matrix sensor arrays difficult. However, when the sensor arrays are separately fabricated by embedding the sensing elements in the substrate, they can be easily incorporated into passive-matrix system or can be simply laminated on the separately fabricated active-matrix circuitry, as in case of the electronic paper front-plane technology.

In this thesis, a simple fabrication method of integrated pressure/temperature sensor arrays by embedding conductive nickel (Ni) particles in poly(dimethyloxane) (PDMS) medium for electronic artificial skin application will be elucidated. The pressure and temperature sensing parts are formed in one pixel but have different heights, which are implemented by introducing a corrugated structure to Ni/PDMS composite with a pre-patterned aluminum mold. Since Ni particles are ferromagnetic materials, Ni/PDMS mixture can be patterned by

exposure to patterned magnetic fields. Magnetic field exposure helps both lateral patterning and vertical particle alignment, which directly improved sensitivity and linearity of the sensor. Independent and stable read-out signals for pressure and temperature sensors are successfully obtained even under repeated measurements. This technology has advantages of simple tuning for sensitivity and operation ranges by changing particle concentration and device physical dimension, easy scaling-up to large area by seamlessly bonding small arrays or using large-area magnetic field modulator, and potential implementation of the sensor frontplane for active-matrix backplane read-out circuitry. Electronic artificial skin passive-matrix system with about 10 ppi resolution with the integrated 16 by 16 pressure and 15 by 15 temperature sensor arrays have been finally demonstrated.

Furthermore, a highly stretchable electrode with demonstration of a resolution sustaining lighting device by fully utilizing the magnetic patterning/aligning method will be also studied. This stretchable electrode based on conductive composite shows unique property that is negative strain-dependency in

electrical resistance. Although cyclic behavior of pure nickel composite needs more improvement, nickel-based composite materials have excellent advantages over other materials in terms of simple patterning and in-situ embedding in the matrix. This novel technology would be one of the key enabling technology in implementing future stretchable electronic display devices.

Kew Words: Electronic Artificial Skin, Conductive Composite Materials, Magnetically Patterning/Aligning, Stretchable Electrodes, Stretchable Electronics

Student Number: 2008-20840

Contents

List of Figures

List of Tables

Chapter 1

Introduction

1.1 Motivation

There are famous saying ‘Imitation is the Mother of Creation’. In fact, this adage is modifying of ‘Failure is the Mother of Success’ by famous inventor Thomas Edison; however, it has very meaningful substance. Typically, the word named ‘Imitation’ implies negative meaning; however, it has been very powerful means in history of human race. One of a common epithet for human beings is ‘Animals which the most well use tools’. Ancestors of the human race made tools and used it using by two free hands which is caused by upright walking. The first tool of human beings may rocks or part of trees that had been easily found around themselves. Why did they use these crude tools? Just guess they have wanted to

imitate strong physical abilities of large carnivorous animals which have been located at the very top of the food chain by using rocks and tree clubs. By doing so, they might be able to buildup weak physical abilities of themselves. The limitation has been started from this purpose, being create greatly marvelous and useful results even at this moment. There is sketch at the famous note from Leonardo da Vinci, who was a representative painter, sculptor, mathematician, engineer and inventor of the Renaissance era, is showed Figure 1.1. It is 'Flying Machine' based on flying mechanisms of various winged animals such as birds, bats and flying insects which are easily observed from nature. Actually, his effort toward the 'Flying Machine' was disastrously failed, however, after 400 years the Wright brothers were invent first controlled and powered airplane. This airplane has been great invention which completely changes notions about time and space.

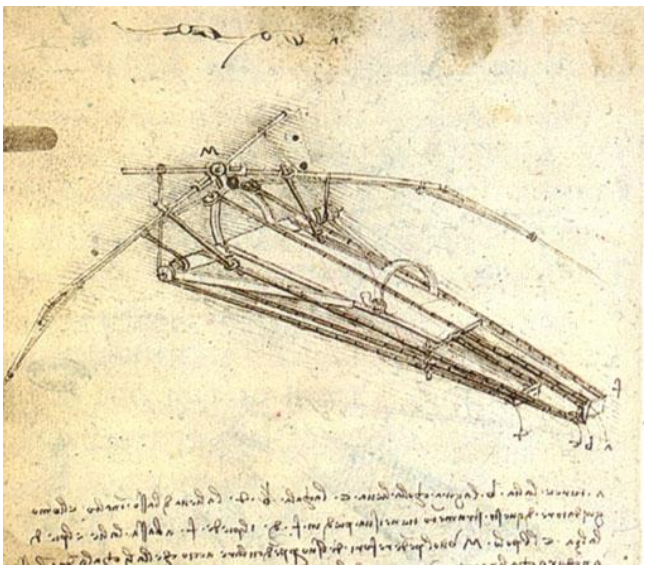

Figure 1.1 A design for the flying machine by Leonardo da Vinci. (Reference [70])

Almost imitations have been based on outer environment what is covering human so far; recently, there are many cases of imitations about human themselves. These are based on bio engineering, mechanical engineering and electrical engineering which being greatly developed. There are some representative cases, artificial organs and a human clone technology which are based on bio engineering, artificial muscles and actuators which are based on mechanical engineering and mimicking various sensory organs and nerve systems which are based on electrical engineering. (Mimicking human abilities or human itself might be caused by curiosity about us; however, there is strong desire to improve our insufficient physical abilities or to make something which resembles ourselves.

It is hard and a meaningless to determine the rank of numerous human physical abilities according to its importance, however, there would be no objection on fact that is the five senses are very important. Human can sense and respond a change of environment around ourselves through the five senses. To date, there have been numerous researches which are related to artificially mimicking the ability of human senses by using several techniques based on electrical, mechanical, chemical and biological methods.

Leaving the researches about a prosthetic eye [1], which is just mimicked appearance of human eye, aside, there have been great progress about artificial visual, such as image sensor technologies including a charge-coupled device (CCD)

and a complementary metal-oxide-semiconductor (CMOS) sensor [2-3], and visual information processing techniques, based on signal process and computer technology, such as object tracking [4-5]. Even in the recent, there have been hemispherical electronic eye systems similar with real structure of the human eye. These systems are made by mimicking structural and functional characteristic of the retina, iris and crystalline lens that could not be realized in the past [6-8].

Of all the human senses mimicking, an artificial auditory is the oldest and the most mature technology. Hearing aids are one of the well-known realizations of the artificial auditory. Historically, the first hearing aids were created in the 17th century. Early hearing aids simply allowed that a user could hear louder using mechanical structure similar with trumpet. By the late 19th, with the telephone technology, electronic hearing aids were developed. Since then, have repeated developments, a digital type hearing aid was developed. In addition to the hearing aid, a voice recognition technology is being intensively researched for a robotic or a handheld device application [9-11].

The sense of olfactory and sense of gustatory have been mimicked with an analogous principle. A view of a distinguishing of a specific chemical molecule, these two senses have same purpose and functionalities. Numerous electrochemical sensors have been developed for artificial olfactory [12-15], and gustatory system [16-18]. Although there are some problems remaining such as multi-sensing

capability and re-use issue, present electrochemical sensors have significantly enhanced sensing capabilities than olfactory and gustatory sense of a human being. These ‘electronic nose’ and ‘electronic tongue’ are used in wide application fields even in illness diagnosis [14].

However, comparing with other senses, there has been only a few achievements regarding realization of the artificial sense of touch. It is come from both morphological and functional characteristics of the human skin which senses the sense of touch. The human skin is largely covered onto whole surface of the human body, and can sense multitudinous touch which includes pressure, temperature, vibration and slip.

Moreover, it can sustain its functionality of the sense of touch when it is compressed or stretched, and even restore its morphology and functionality itself under some extent of destruction. There are already many tactile or pressure sensors, based on micro-electromechanical systems (MEMS) and silicon technology [19-21], which are very superior to the human skin’s tactile receptors. Such a good sensing ability however, nonetheless, there have been many difficulties to make artificial skin due to lack of the foregoing real human skin’s feature such as conformability, stretchability, scalability and multi-functionality.

Over the past decade, however, with rapid developments of the stretchable electronics, several developments have been presented regarding ‘Electronic Skin’

that has both morphological and functional properties which are comparable to the human skin. Stretchable electronics technology aims to flexible and stretchable mechanical characteristics of electrical devices that cannot be accomplished with conventional manner which is mainly based on a silicon fabrication technology [22-24]. For attainment of the stretchability, many alternative ways have been researched including materials and fabrication methods. Various elastomer materials, which have an inherent stretchability, have been used as a substrate instead of rigid silicon or glass [25-26]. And electrodes have been given stretchability by using thin metal films that are designed to various structures [28-30], or new materials such as carbon nanotubes (CNTs) [31], silver (Ag) nanowire [32] and conductive composite materials [33]. Furthermore, organic and nanowire materials which have inherently flexible characteristics have used as semiconductor, and several techniques have been developed to minimize mechanical stress which is applied to electronic devices [34-35]. In addition, various solution and printing techniques, which are appropriate for alternative materials, have been intensively researched. Typically, stretchable devices show relatively deficient performance than conventional silicon based devices. Even though they show inferior performance than existing techniques, stretchable electronic devices can be easily adopted to new application area, which the existing silicon based devices could not be adopted to, owing to the fact that notable mechanical characteristics and scalability.

The Electronic skin is one of the new applications that stretchable electronics can have inaugurated. Techniques of Stretchable electronics have allowed making skin-like electronic device structures which are able to be stretched with scalability. More details will be discussed in following chapter.

1.2 Human Sense of Touch

Where is a baseline to make the electronic skin? It is obvious that the electronic skin must possess at least human skin's capability, in terms of its purpose which is home service robot's sensor system or further alternative medical prosthetic skin application. In this point of view, understanding of the real human skin characteristics and mechanism of the sense of touch is the starting point for the development of the electronic skin.

Physiologically, human have various touch sense capabilities at different sites on the body as shown in Figure 1.2 [36]. Most of all, It is well known that skin on finger tips show the most outstanding performances. For this reason, almost researches that are related to make an electronic skin or a tactile sensor system aim at having human finger tips characteristics. Whatever applications of the electronic skin are, it must be granted human touch sense capability. In fact, this requisite is a starting point where the all researches, that are related on electronic skin. In the following chapter, the human skin and its ability to the sense of touch will be concretely discussed.

The human sense of touch is housed in the largest and heaviest of the sense organs: the skin, which covers an area of 1.8 m^2 and weighs 4 kg in the case of the average adults. The skin is composed of touch receptors, the outer layer, epidermis,

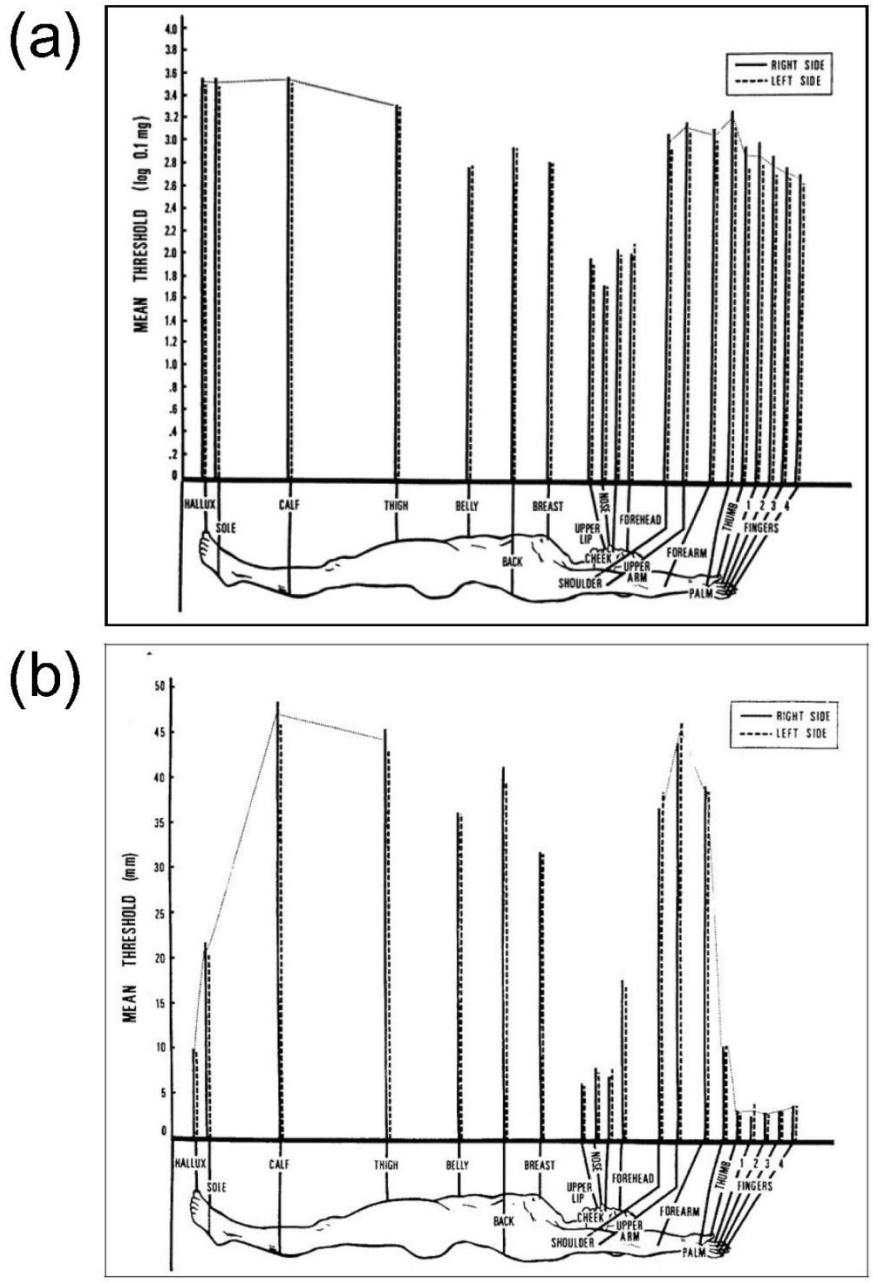

Figure 1.2 (a) Pressure sensitivity threshold and (b) two-point discrimination threshold for males for different areas of the body. (Reference [36])

and the underlying layer, dermis, as shown in Figure 1.3. Various touch receptors are embedded in both the epidermis and the dermis with different densities in sites of the body [69]. Most of all, the skin on the hand (especially, on the finger tip) has the best ability to touch sense.

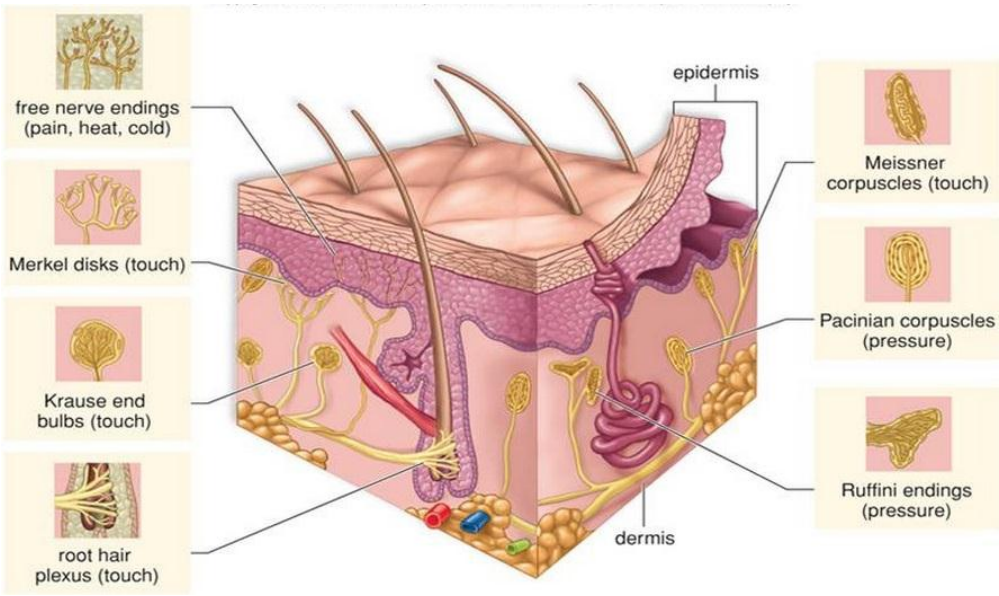

Figure 1.3 Cross section of skin, schematically demonstrating the locations of the mechanoreceptors. (Reference [69])

A concept of the sense of touch includes detecting heat transfer and pain as well as applied pressure to the skin. Human can feel external sensual stimulate by using various receptors which are located in the skin, as well as in mucous membranes, muscles, tendons and joints. Receptors act as a transduction device which can convert physical stimulates such as pressure and temperature into a electrical signal. It has been known, a human being has four types of receptors, tactile receptors, kinesthetic receptors, thermoreceptors, and nociceptors, respectively. Tactile receptors and thermoreceptors are located in the skin. However, kinesthetic receptors lie within muscles, tendons and joints. Nociceptors are found in any area of the body that can sense pain skin, muscle, joints and viscera [38]. Receptors will be discussed with type of stimulation.

1.2.1 Tactile Receptors

Tactile receptors are composed of four receptor types known as Meissner corpuscles, Merkel cell neurite complexes, Pacinian corpuscles, and Ruffini endings. These are also called mechanoreceptors because they accept mechanical stimulations such as pressure and vibration. These four types of tactile receptors have been classified according to size of the receptive field and rate of adaptation. Fast-adapting (FA) receptors respond with occurrence of action potentials when mechanical stimulus is applied and when it is eliminated. There are two types of FA receptors according as size of the receptive field. Meissner corpuscles, named FA I

units, which are characterized by a small receptive field; and Pacinian corpuscles, named FA II units, which are characterized by a large receptive field. Slow-adapting (SA) receptors continuously respond during mechanical stimulation contacts on its receptive field. SA receptors are categorized into two units, Merkel cell neurite complexes which have small receptive filed, also named SA I units, and Ruffini endings which have large receptive field, also named SA II units [39]. Each receptor has a different feature of tactile sensing, shown as below.

1. FA I units (Meissner corpuscles) respond to low-frequency vibrations (3-40 Hz), flutter, slip and motion [37]. They innervate the skin densely (about 140 units/cm^2) [71]. For example, if an object which is held by our hand begins to slip across our fingers, this motion on our skin will cause vibrations, and FA I receptors will react and calibrate our grip before miss the object.

2. FA II units (Pacinian corpuscles) (about 20 units/cm^2) respond to high-frequency vibrations (40-500 Hz) which are generated when an object first make contact onto the skin [37, 71]. FA II receptors assist to determine temporal changes in skin deformation.

3. SA I units (Merkel cell neurite complexes) (about 70 units/cm^2) respond to compressive strain which especially important to recognize fine form and texture [37, 71]. Some activities that are particularly dependent on this receptor include reading Braille and determining the location and orientation of the slot on the head

of screw that can be felt but not be seen.

4. SA II units (Ruffini endings) (about 10 units/cm^2) respond to sustained downward pressure, and particularly to lateral skin stretch when we grasp an object [37, 71]. These receptors participate in finger position, motion detection to perceive a shape of an object. When you rich out for an object, this receptors help determine when our fingers are shaped properly for stable grasping.

1.2.2 Thermoeceptor

Thermo-receptors, which are located in both the epidermal and dermal layers of the skin, inform us about changes in skin temperature. There are two types of thermo-receptors. First, warmth fibers which fire when the temperature of the skin surrounding the fibers increases. Second, cold fibers which fire when the skin temperature decreases [37]. Thermo-receptors start its activity when we touch an object which is warmer or colder than the skin. We can use this thermal conduction information, through contact between the skin and objects, for identification of an object besides using a visual and texture information.

1.2.3 Nociceptors

Nociceptors have responsiveness of pain perception. The pain means noxious stimulation which cause damage or potential damage to the skin. The pain perception is one of the most significant ability, because if we cannot be aware of

the pain signals, which encompass strong or sharp pressure and extreme skin temperatures lower than 15℃ or higher than 45℃, we would be easily deprived of an our part of body, or even an our life. Nociceptors are composed of some fibers [37]. A-delta fibers respond to strong pressure or heat and they are myelinated, which allows them to conduct signals to the brain very rapidly. C fibers are unmyelinated and respond to extreme pressure, heat or cold and even noxious chemicals [37].

1.2.4 Kinesthetic Receptors

In fact, there is one more kind of receptors, known as kinesthetic receptors. These are sort of mechanoreceptors which lie within muscles, tendons, and joints. They play an important role in sense of where our limbs are and what kind of movements we are making. The sense of touch includes a perception by kinesthetic receptors, in terms of the physiology. However, we do not consider this kind of sensation as a purpose for the mimicking of the human skin in this research because it can be artificially made to a form of individual sensor such as strain sensor, not a large area skin-like sensor array.

1.2.5 Tactile Sensitivity and Acuity

It is also important that how sensitive is the human skin to various sensations, as well as how many sensations can it sense. Figure 1.2(a) shows sensitivity to pressure at different sites on the body [36]. In general, there are differences between

each side of the body, and women are more sensitive than men. However, these differences are negligible and there is a common distribution at body sites. Typically, pressure sensitivity of the touch receptors on the face is highest. The torso and upper extremities are followed [37].

In fact, the most significant ability of the human skin, especially on finger tips, is that how finely we can resolve spatial details. This characteristic is known as two point touch threshold. The human hand can make elaborate work with a fine pressure spatial distribution which is gained by the skin on fingers and palm. Figure 1.2(b) shows the minimal separation between two points needed to perceive them as separate, at different sites of the body [36]. Similar with the pressure sensitivity, the extremities show the good results. There is a little difference between each experimental method, however, in general, finger tips can resolve two points pressure which are separated in only about 3 mm.

1.2.6 Stretchability of Human Body

As mentioned at the beginning of this chapter, morphological characteristics are also important at development of the electronic skin. The most important morphological feature of the human skin is the stretchability. There have been many researches about elastic limit of the human skin. There are somewhat deference by experimental methods, age/sex of test subjects and anatomical region. It is known that regular adult shows an elastic limit with an averagely 20-30 % tensile strain [40-

47]. Unfortunately, there has been no searched previous result about functionality limitation of the human skin under stretching condition. However, we can easily extrapolate that the human skin cannot normally operate above elastic limit

1.3 Transduction Principles for Electronic Skin Applications

Many researchers have tried to mimic the human skin in terms of functionalities, such as pressure, temperature, and vibration, and sensitivity. As mentioned before, sensors for the electronic skin can be conformable which including flexibility and stretchability, because the electronic skin can be used at crumple and stretched location similar with the human skin. Elastomer based sensors are apposite to the skin-like structure. In fact, most of the sensors what have been researched for the electronic skin are based on elastomeric materials. Several types of sensing mechanisms for the electronic skin based on piezoresistive, piezoelectric, capacitive and optical devices have been used for sensing elements. Unfortunately, however, most of the research regarding electronic skin application has been focused on pressure or tactile sensing devices. Representative researches of each sensing mechanism are presented, as follow.

1.3.1 Piezoresistive

Piezoresistive type materials have been widely developed and commonly used for tactile sensor applications. It is also well known as conductive composites or conductive elastomers. Transduction principles of these materials are very simple and well revealed by many researchers during nearby 50 years. Typically, piezoresistive type materials are composed of elastomeric insulating matrix and conductive fillers. This type of materials initial bulk resistivity has variability

according to a content ratio of conductive fillers. The conductive composite materials act as an elastomer when conductive filler concentrations are not enough certain level. However, their electrical resistivity is rapidly decreases when conductive filler concentrations are reached above certain level. This certain level is known as the ‘Percolation Threshold’. The percolation threshold is depends on conductive filler properties such as type of filler material, filler size, aspect ratio and degree of dispersion into an elastomer matrix. Electrical characteristics of conductive composite materials due to an interaction between an elastomer matrix and conductive fillers are explained by the percolation theory. The percolation theory will be elaborately discussed in further chapter.

The tactile sensing principles of a piezoresistive type materials are based on the change of electrical resistivity come from a mechanical deformation. Electrical resistivity is either decreased or increased due to electrical conduction paths are either constructed or deconstructed, while it is deforming by applied mechanical stress. Deformations of material affect spacing between adjacent conductive fillers. Generally, electrical resistance component of applied pressure direction is decreased when normal pressure apply onto the surface. The piezoresistive type conductive composite materials have advantage on the mimicking of the human skin; intrinsic properties regarding its conformability originate from elastic matrix as well as low fabrication cost and easy scalability. To date, there have been so many researches

regarding characteristics observation of the conductive composite itself by environmental variables, such as pressure and temperature, and its mechanisms. In contrast, there have been insufficient researches about application of the conductive composite materials. As mentioned before, this lacking in application development derived from immaturity of relation technologies. In the past decade, however, stretchable electronics technology have been rapidly developed, accordingly many applications, especially regarding the electronic skin, have been presented.

Someya et al. developed conductive composite based electronic skin which can detect applied pressure [48]. This electronic skin can express spatial distribution of applied pressure by using OTFT (organic thin film transistor) array on a plastic substrate which is laminated onto conductive composite sheet. However, it can only sense pressure information and has flexibility not stretchability. For solve these limitations, they used net-shaped conductive composite to give stretchability, and added organic diodes as temperature sensors [49]. It has been still remained as an one of few researches which can sense applied pressure and temperature simultaneously and be stretched, although it has problems such as complex fabrication method and performance non-uniformity among sensing cells.

National Taiwan University presented flexible electronic skin which is composed of patterned conductive composite as pressure sensor and commercially available temperature sensor chips [50]. Sensing cell separation methods including

dispensing process for conductive composite patterning is too complex and its output is not efficient to enhance the uniformity. Additionally, rigid bulky IC chips are not adequate in conformal applications. Same research group in National Taiwan University, developed piezoresistive material based temperature sensor array on a flexible polyimide film by using same fabrication method above [51].

Recently, researchers of University of California, Berkeley developed conductive composite and nano-wire active matrix based electronic skin which is capable of pressure sensing [52]. It has 2.5 mm spatial resolution and low operating voltages. They also demonstrated net-shaped type stretchable electronic skin with pressure sensing capability.

The piezoresistive type elastomeric sensor is the simplest way to sense medium range of pressure (10-50 kPa). However, it shows some weaknesses regarding fundamental sensor characteristics such as hysteresis and temporal response. Also, there has been few researches about its application as temperature sensor even it has a temperature sensitivity.

1.3.2 Piezoelectric

Piezoelectric materials generate electric charges when it experience a mechanical stress by virtue of an applied force. This phenomenon is named piezoelectricity.

The piezoelectric effect is a reversible process which can transform either mechanical stress into electrical signal (generation of electrical charge resulting from an applied mechanical stress) or the opposite (generation of a mechanical movement resulting from an applied electric field). Piezoelectric materials have been used to many application fields such as sensors, actuators and even energy devices. Piezoelectric materials show very good sensitivity to applied pressure. And also piezoelectric materials based on polymers are show good conformability.

Polyvinylidene fluoride (PVDF) is the most commonly used in flexible tactile sensor applications due to not only its good as pressure sensor characteristics but also mechanical characteristics such as inherent flexibility, dimensional stability and low weight [53]. There have been many researches about PVDF and its copolymers based tactile sensor systems since Dario et al. [54]

Dahlia et al. presented piezoelectric material (PVDF-TrFE) based skin-like sensor array [55-56]. The sensor array is composed of 32 sensing elements and shows a linear response to applied pressure in the range of 0.02-4 N and a high pressure sensitivity with a 0.2 V/N and 0.4 V/N for 25 μm and 50 μm thickness of films, respectively. In this type of sensor array, however, significant cross-talk

problem is arisen between adjacent sensing elements due to electrically connection of the whole inside PVDF-TrFE film. For reducing cross-talk problem, piezoelectric film is directly spin coated onto FET devices. In this way, each sensor cells shows a linear response in the range of 0.2-5 N and a pressure sensitivity of 0.5 V/N with reducing cross-talk issue.

In spite of superior sensor properties, the piezoelectric materials including PVDF have a major drawback besides highly dependency of temperature which has been well known [57]. It is a transient response to applied mechanical stresses. A pressure sensor which is based on the piezoelectric material response only when a pressure is first applied. This characteristic is very unfit to develop the electronic skin which must distinguish between a static and a transient pressure.

1.3.3 Capacitive

A capacitive type sensor, which has been developed for electronic skin application, is composed of parallel two electrodes and dielectric material which are located between electrodes. Elastomers can be used as dielectric materials or elastic substrates. Capacitance which is build up between two electrodes changes when the elastomer is deformed by applied mechanical stress.

Cotton et al. have demonstrated stretchable multifunctional sensor based on gold thin films embedded in poly (dimethylsiloxane) (PDMS) [68]. This sensor can detect one-dimensional tensile strain as well as applied pressure. However, they

have not yet shown large area implementation with having a spatial resolution.

Recently, a highly sensitive stretchable pressure sensor array has been demonstrated by Mannsfeld et al [59]. They used micro-structured PDMS layer as dielectric layer. The micro-structured capacitive sensor was more sensitive than the unstructured one; even it can sense a fly on the sensor. Moreover, its temporal response was better than the unstructured sensor. The micro-structured capacitive sensor shows 100 ms below temporal response compared to 5 s for the unstructured sensor. These type of sensors attained highest pressure sensitivity among elastomeric based sensors, however, there still have been some problems. Although, signal to noise ratio is significantly increased by fabricating as thin as a few micrometers compared to past elastomeric capacitive sensors, it must be problem when arraying large numbers of sensors because a baseline capacitance is still quite low, about 1 pF. Besides, it has aimed observation of monotonic capacitance variation by only an applied pressure, which is limited narrow range, not other factors such as temperature. Furthermore, it is hard to distinguish between pressure and tensile strain, structurally.

It is known that one of the major challenges with using a capacitive elastomeric sensor system is limitation of spatial resolution, as described by Tee et al [60]. Because absolute scale of output capacitance is proportionally to overlapping area between two electrodes, extremely small output capacitance, which is generated

in high spatial resolution condition, will bring about some major problems. While these small value of output capacitance can be read by a high performance readout circuitry, this approach is not adequate due to some reasons including cost and noise issues in large area application which is prerequisite for developing of the electronic skin.

1.3.4 Optical

The aforementioned transduction principles for electronic skin application have been mainly based either electrical or electrochemical mechanisms. Recently, however, there is interesting new type of elastomeric sensors which use an optical mechanism. Typically, optical sensor systems detect the change in light intensity to detect pressure or strain.

Heo et al. presented 3 x 3 flexible tactile sensor array using fiber Bragg gratings (FBG) [61]. They demonstrated two types of sensor arrays. First one is a large area with low spatial resolution, similar with human body skin. Second one is a small area with high spatial resolution, similar with human finger tips. In the case of a second one, it has pressure resolution as low as 0.001 N with the spatial resolution of 5 mm. And, they also demonstrated a flexible optical sensor using the micro-bending optical fiber (MBOF) [62]. The Light loss is occurred in the optical fiber when the optical fiber was bended. Especially, when the optical fiber's radius of curvature by bending is under millimeter scale (micro-bending), the light loss is

significantly increased that it can be useful for applied contact force sensing. By using this mechanism, they presented 8 x 8 flexible tactile sensor array which is based on MBOF.

There is another optical method which can detect mechanical force by modulate of light direction in waveguide. Ohka et al. developed optical three-axis tactile sensor which is able to acquire normal and shearing force, with the aim of mounting it on a robotic finger [63]. The tactile sensor is based on the principle of an optical waveguide mechanism, which is composed of an acrylic hemispherical dome, a light source, an array of rubber sensing elements, and a CCD camera. It shows high repeatability when 1000 cycles of load-unload experiment, with the respective error of the normal and shearing forces was 2 and 5%. Similar with this mechanism, Koeppe et al. demonstrated waveguide touch pad system, which is composed of PDMS as a waveguide and PEDOT:PSS based large area organic photodiode [64]. This optical sensor is able to detect applied pressure over about 5 N with a sensitivity of 250 nA/N.

Optical sensor has some important advantages, especially in tactile sensor application. It shows high selectivity. That means, optical sensors are less affected by undesired environmental changes such as temperature, electromagnetic and chemical effect, distinct from other type of sensing mechanisms. When it is made to the form of array, there are no cross-talk issues between sensing cells. However,

being highly sensitive to bending deformation, optical fibers are not adequate in case of flexible condition. As mentioned before, characteristic of light loss due to micro-bending can be used for pressure sensing. However, it also shows light loss in macro-bending situation which is caused when optical fiber is bended more than its allowed radius of curvature. Generally, it is well known that the radius of curvature of the single-mode optical fiber must be more than 25 mm [65-67]. When the optical fiber is bended under 25 mm radius of curvature, bending modifies the guiding properties of optical fibers causing light loss increasing, especially toward long wavelengths,. In most cases, the macro-bending in the field of optical elastomeric sensor application is happened under an unexpected deformation such as bending at joint movement location and crushing by external force. These optical signal alterations by the unexpected deformations affect conformability of the electronic skin as unfavorable factors.

1.4 The Goal and Outline of This Thesis

There are many kinds of transduction principles for electronic skin application. Table 1.1 shows transduction principles and some representative researches about electronic skin applications that were mentioned in previous sections. As shown in the table, almost researches have focused only on mimicking the tactile receptors to develop the electronic skin. However, as mentioned at the beginning of this chapter, the electronic skin must possess sensing abilities of the human skin including tactile, temperature and pain perception. Moreover, deformable characteristic is also important. The electronic skin must maintain its functionalities even under stretching condition as well as bending.

According to our preliminary study, conductive composite materials based on the piezoresistive principle have the most required conditions for mimicking the human skin including multi sensing capability, spatial resolving property under 5 mm, and mechanically stretchable characteristics. In this point of view, the piezoresistive type conductive composite materials are most suitable candidate for the electronic skin application. However, there are some disadvantages comparing with other transduction mechanisms such as low sensitivity or cross-talk issues. These weaknesses have to be considered in detail and improved.

Table 1.1 Comparison of transduction principles and applications for electronic skin

Transduction Principle	Advantages	Disadvantages	Ref.	Mechanical Characteristics		Sensor Characteristics			Array	
				Deformability	Implementation Method	Sensing Capability	Sensitivity	Dynamic Range	No. of Sensors	Spatial Resolution
Piezoresistive (Conductive Composite Material)	-Mechanically flexible or stretchable -Large-area and simple fabrication techniques possible -Various sensing capable	-Low sensitivity -Hysteresis -Cross-talk	48	Flexible	Sheet of pressure sensitive composite	Pressure	N/A	10-30 kPa	256 (16x16)	2.54 mm
			49	Stretchable	Net-shaped structure	Pressure and Temperature	N/A	<30 kPa	144 (12x12)	4 mm
			50	Flexible	Polyimide as substrate	Pressure	N/A	N/A	64 (8x8)	5 mm
			51	Flexible	Polyimide as substrate	Temperature	N/A	20-110 ℃	64 (8x8)	N/A
			52	Stretchable	Net-shaped structure	Pressure	~30 $\mu S \cdot kPa^{-1}$	<6 kPa	96 (12x8)	~5 mm
Piezoelectric	-High sensitivity -Mechanically flexible -Low weights and thin structure possible	-Not stretchable -High temperature dependency -Transient response	55	Rigid	Implemented on silicon wafer	Pressure	0.4 $V \cdot N^{-1}$	0.01-10 N	32	1 mm
			56	Rigid	Implemented on silicon wafer	Pressure	0.5 $V \cdot N^{-1}$	0.2-5 N	N/A	N/A
Capacitive	-High sensitivity -Mechanically flexible or stretchable -Simple fabrication techniques possible	-Low spatial resolution -Cross-talk -Highly sensitive to electromagnetic interference	68	Stretchable	Gold thin film embedded in PDMS	Pressure and Strain	0.014~0.016 $fF \cdot kPa^{-1}$ (pressure) ~3 fF·% (strain)	<160kPa (pressure) <20% (strain)	1	N/A
			59	Flexible	Micro-structured PDMS film	Pressure	0.55 kPa^{-1} (<2 kPa) 0.15 kPa^{-1} (>2 kPa)	0.003-40 kPa	64 (8x8)	2 mm
Optical	-No cross-talk -Protected from electromagnetic interference	-Optical signal alteration by bending	61	Flexible	Flexible optical fiber sensor	Pressure	1 mN (sensing resolution)	<5 N	9 (3x3)	25 mm
			62	Flexible	Flexible optical fiber sensor	Pressure	0.05 N (sensing resolution)	<15 N	64 (8x8)	N/A
			63	Rigid	Optical fiber embedded in acrylic dome	Pressure	N/A	<2 N	40	N/A
			64	Flexible	Organic photodiodes on PET	Pressure	250 $nA \cdot N^{-1}$	5-20 N	25 (5x5)	15 mm

This thesis studies characteristics improvement method for conductive composite material and fabrication technique of a pressure/temperature integrated stretchable sensor array based on conductive composite material for electronic skin application. Chapter 2 will elucidate electrical characteristics improvement for the conductive composite material by using a magnetically conductive aligning method. Chapter 3 will present fabrication of the pressure/temperature integrated stretchable sensor array based on conductive composite material based on a modified magnetically aligning and patterning method. Furthermore, Chapter 4 will elaborate magnetically aligned conductive composite for stretchable electrode application. Conclusions will be given in Chapter 5.

Reference

[1] P. Benson, “The fitting and fabrication of a custom resin artificial eye,” Journal of prosthetic dentistry, vol. 38, no. 5, pp. 532–538, 1977.

[2] W. S. Boyle and G. E. Smith, “Charge-coupled devices-a new approach to MIS device structures,” IEEE Spectrum, vol. 8, no. 7, pp. 18–27, 1971.

[3] M. Bigas, E. Cabruja, J. Forest and J. Salvi, “Review of CMOS image sensors,” Microelectronics Journal, vol. 37, no. 5, pp. 433–451, 2006.

[4] D. Koller, K. Daniilidis and H.-H. Nagel, H.-H, “Model-based object tracking in monocular image sequences of road traffic scenes,” International Journal of Computer Vision, vol. 10, no. 3, pp. 257–281, 1993.

[5] D. Comaniciu, V. Ramesh and P. Meer, “Kernel-based object tracking,” IEEE Transactions on Pattern Analysis and Machine Intelligence, vol. 25, no. 5, pp. 564–577, 2003.

[6] H. C. Ko, M. P. Stoykovich, J. Song, V. Malyarchuk, W. M. Choi, C.-J. Yu, J. B. Geddes III, J. Xiao, S. Wang, Y. Huang and J. A. Rogers, “A hemispherical electronic eye camera based on compressible silicon optoelectronics,” Nature, vol.454, no. 7205, pp.748–753, 2008.

[7] G. Shin, I. Jung, V. Malyarchuk, J. Song, S. Wang, H. C. Ko, Y. Huang, J. S. Ha

and J. A. Rogers, “Micromechanics and Advanced Designs for Curved Photodetector Arrays in Hemispherical Electronic-Eye Cameras,” Small, vol. 6, no. 7, pp. 851–856, 2010.

[8] I. Jung, J. Xiao, V. Malyarchuk, C. Lu, M. Li, Z. Liu, J. Yoon, Y. Huang and J. A. Rogers, “Dynamically tunable hemispherical electronic eye camera system with adjustable zoom capability,” Proceedings of the National Academy of Sciences of the United States of America, vol. 108, no. 5, pp. 1788–1793, 2011.

[9] Y. Sakagami, R. Watanabe, C. Aoyama, S. Matsunaga, N. Higaki and K. Fujimura, “The intelligent ASIMO: System overview and integration,” in Proc. of 2002 IEEE/RSJ International Conference on Intelligent Robots and Systems (IROS 2002), Lausanne Switzerland, September 30-October 4, 2002, pp. 2478-2483.

[10] C. Breazeal and L. Aryananda, “Recognition of affective communicative intent in robot-directed speech,” Autonomous robots, vol. 12, no. 1, pp. 83–104, 2002.

[11] R. Stiefelhagen, C. Fugen, R. Gieselmann, H. Holzapfel, K. Nickel and A. Waybill, “Natural human-robot interaction using speech, head pose and gestures,” in Proc. of 2004 IEEE/RSJ International Conference on Intelligent Robots and Systems (IROS 2004), Sendai, Japan, September 28-October 2,

2004, pp. 2422-2427.

[12] M. S. Freund and N. S. Lewis, “A chemically diverse conducting polymer-based" electronic nose",”. Proceedings of the National Academy of Sciences of the United States of America, vol.92, no. 7, pp. 2652–2656, 1995.

[13] S. Ampere and J. O. Bosset, “The electronic nose applied to dairy products: a review,” Sensors and Actuators B: Chemical, vol. 94, no. 1, pp. 1–12. 2003.

[14] J. W. Gardner, H. W. Shin and E. L. Hines, “An electronic nose system to diagnose illness,” Sensors and Actuators B: Chemical, vol. 70, no. 1, pp. 19–24 2000.

[15] D. James, S. M. Scott, Z. Ali and W. T. O’Hare, “Chemical Sensors for Electronic Nose Systems,” Microchimica Acta, vol. 149, no. 1-2, pp. 1–17. 2004.

[16] J. J. Lavigne, S. Savoy, M. B. Clevenger, J. E. Ritchie, B. McDoniel, S.-J. Yoo, E. V Anslyn, J. T. McDevitt, J. B. Shear and D. Neikirk, “Solution-based analysis of multiple analytes by a sensor array: toward the development of an “electronic tongue”,” Journal of the American Chemical Society, vol. 120, no. 25, pp. 6429–6430, 1998.

[17] A. Legin, A. Rudnitskaya, Y. Vlasov, C. D. Natale, E. Mizzen and A. D'Amico, A, “Application of electronic tongue for quantitative analysis of mineral water

and wine," Electroanalysis, vol. 11, no. 10-11, pp. 814–820, 1999.

[18] P. Ivarsson, S. Holmin, N.-E. Höjer, C. Krantz-Rülcker and F. Winquist, "Discrimination of tea by means of a voltammetric electronic tongue and different applied waveforms," Sensors and Actuators B: Chemical, vol. 76, no. 1, pp. 449–454, 2001.

[19] Z. Chu, P. M. Sarro and S. Middelhoek, "Silicon three-axial tactile sensor," Sensors and Actuators A: Physical, vol. 54, no. 1, pp. 505–510, 1996.

[20] D. J. Beebe, D. D. Denton, R. G. Radwin and J. G. Webster, "A silicon-based tactile sensor for finger-mounted applications," IEEE Transactions on Biomedical Engineering, vol. 45, no. 2, pp. 151–159, 1998.

[21] L. Wang and D. J. Beebe, "A silicon-based shear force sensor: development and characterization," Sensors and Actuators A: Physical, vol. 84, no. 1, pp. 33–44. 2000.

[22] D.-H. Kim and J. A. Rogers, "Stretchable Electronics: Materials Strategies and Devices," Advanced Materials, vol. 20, no. 24, pp. 4887–4892, 2008.

[23] D.-H. Kim, J. Xiao, J. Song, Y. Huang and J. A. Rogers, "Stretchable, Curvilinear Electronics Based on Inorganic Materials," Advanced Materials, vol. 22, no. 19, pp. 2108–2124, 2010.

[24] D. J. Lipomi and Z. Bao, “Stretchable, elastic materials and devices for solar energy conversion,” Energy & Environmental Science, vol. 4, no. 9, pp. 3314-3328, 2011.

[25] S. P. Lacour, J. Jones, Z. Suo and S. Wagner, “Design and Performance of Thin Metal Film Interconnects for Skin-Like Electronic Circuits,” IEEE Electron Device Letters, vol. 25, no. 4, pp. 179–181, 2004.

[26] P. Lee, J. Lee, H. Lee, J. Yeo, S. Hong, K. H. Nam, D. Lee, S. S. Lee and S. H. Ko, “Highly Stretchable and Highly Conductive Metal Electrode by Very Long Metal Nanowire Percolation Network,” Advanced Materials, vol. 24, no. 25, pp. 3326–3332, 2012.

[27] G. D. Moon, G.-H. Lim, J. H. Song, M. Shin, T. Yu, B. Lim and U. Jeong, “Highly Stretchable Patterned Gold Electrodes Made of Au Nanosheets,” Advanced Materials, vol. 25, no. 19, pp. 2707–2712, 2013.

[28] D. Brosteaux, F. Axisa, M. Gonzalez and J. Vanfleteren, “Design and fabrication of elastic interconnections for stretchable electronic circuits,” IEEE Electron Device Letters, vol. 28, no. 7, pp. 552–554. 2007.

[29] J. Xiao, A. Carlson, Z. J. Liu, Y. Huang, H. Jiang and J. A. Rogers, “Stretchable and compressible thin films of stiff materials on compliant wavy substrates,” Applied physics letters, vol. 93, no. 1, pp. 013109-013109-3, 2008.

[30] D.-H. Kim, J. Song, W. M. Choi, H.-S. Kim, R.-H. Kim, Z. Liu, Y. Y.Huang, K.-C. Hwang, Y.-W. Zhang and J. A. Rogers, “Materials and noncoplanar mesh designs for integrated circuits with linear elastic responses to extreme mechanical deformations,” Proceedings of the National Academy of Sciences, vol.105, no. 48, pp. 18675–18680. 2008.

[31] L. Cai, J. Li, P. Luan, H. Dong, D. Zhao, Q. Zhang, X. Zhang, M. Tu, Q. Zeng, W. Zhou and S. Xie, “Highly Transparent and Conductive Stretchable Conductors Based on Hierarchical Reticulate Single-Walled Carbon Nanotube Architecture,” Advanced Functional Materials, vol. 22, no. 24, pp. 5238–5244. 2012.

[32] F. Xu and Y. Zhu, “Highly Conductive and Stretchable Silver Nanowire Conductors,” Advanced Materials, vol. 24, no. 37, pp. 5117–5122. 2012.

[33] T. Sekitani, Y. Noguchi, K. Hata, T. Fukushima, T. Aida and T. Someya, “A Rubberlike Stretchable Active Matrix Using Elastic Conductors,” Science, vol. 321, no. 5895, pp. 1468–1472, 2008.

[34] I. M. Graz, D. P. J. Cotton, A. Robinson and S. P. Lacour, “Silicone substrate with in situ strain relief for stretchable thin-film transistors,” Applied physics letters, vol. 98, no. 12, pp. 124101-123101-3, 2011.

[35] R. M. Erb, K. H. Cherenack, R. E. Stahel, R. Libanori, T. Kinkeldei, N.

Münzenrieder, G. Tröster and A. R. Studart, “Locally Reinforced Polymer-Based Composites for Elastic Electronics. ACS Applied Materials & Interfaces, vol. 4, no. 6, pp. 2860–2864. 2012.

[36] S. Weinstein, “Intensive and Extensive Aspects of Tactile Sensitivity as a Function of Body Part, Sex, and Laterality,” in The Skin Senses (Ed. by D.R. Kenshalo) Springfield, Thomas, Springfield, IL, pp.195-222, 1968.

[37] J. M. Wolfe, K. R. Kluender, D. M. Levi, L. M. Bartoshuk, R. S. Herz, R. L. Klatzhy and S. J. Lederman, “Ch. 12 Touch,” in Sensation & Perception, Sinauer Associates, Sunderland, MA, pp. 286-313, 2006.

[38] M. S. Gold and G. F. Gebhart, “Nociceptor sensitization in pain pathogenesis,” Nature Medicine, vol. 16, no. 11, pp. 1248–1257, 2010.

[39] A. B. Vallbo and R. S. Johansson, “Properties of cutaneous mechanoreceptors in the human hand related to touch sensation,” Human Neurobiol, vol. 3, no. 1, pp. 3–14, 1984.

[40] D. A. Danielson, “Human skin as an elastic membrane,” Journal of Biomechanics, vol. 6, no. 5, pp. 539–546, 1973.

[41] H. L. Stark. “Directional variations in the extensibility of human skin,”. British Journal of Plastic Surgery, vol. 30, no. 2, pp. 105–114, 1977.

[42] J. L. Leveque, J. De Rigal, P. G. Agache and C. Monneur, “Influence of ageing on the in vivo extensibility of human skin at a low stress” Archives of Dermatological Research, vol. 269, no. 2, pp. 127–135, 1980.

[43] P. G. Agache, C. Monneur, J. L. Leveque and J. De Rigal, “Mechanical properties and Young's modulus of human skin in vivo,” Archives of Dermatological Research, vol. 269, no. 3, pp. 221–232, 1980.

[44] C. Escoffier, J. de Rigal, A. Rochefort, R. Vasselet, J.-L. Lévêque and P. G. Agache, P. G, “Age-related mechanical properties of human skin: an in vivo study,” Journal of Investigative Dermatology, vol. 93, no. 3, pp. 353–357, 1989.

[45] A. B. Cua, K.-P. Wilhelm and H. I. Maibach, “Elastic properties of human skin: relation to age, sex, and anatomical region,” Archives of Dermatological Research, vol. 282, no. 5, pp. 283–288, 1990.

[46] S. Diridollou, V. Vabre, M. Berson, L. Vaillant, D. Black, and J. M. Lagarde, “Skin ageing: changes of physical properties of human skin in vivo,” International Journal of Cosmetic Science, vol. 23, no. 6, pp. 353–362, 2001.

[47] C. Pailler-Mattei, S. Bec and H. Zahouani, “In vivo measurements of the elastic mechanical properties of human skin by indentation tests,” Medical Engineering & Physics, vol. 30, no. 5, pp. 599–606, 2008.

[48] T. Someya, T. Sekitani, S. Iba, Y. Kato, H. Kawaguchi and T. Sakurai, “A

large-area, flexible pressure sensor matrix with organic field-effect transistors for artificial skin applications," Proceedings of the National Academy of Sciences of the United States of America, vol. 101, no. 27, pp. 9966-9970, 2004.

[49] T. Someya, Y. Kato, T. Sekitani, S. Iba, Y. Noguchi, Y. Murase, H. Kawaguchi and Takayasu Sakurai, "Conformable, flexible, large-area networks of pressure and thermal sensors with organic transistor active matrixes," Proceedings of the National Academy of Sciences of the United States of America, vol. 102, no. 35, pp. 12321-12325, 2005.

[50] M.-Y. Cheng, W.-Y. Chang, L.-C. Tsao, S.-A. Yang, Y.-J. Yang, W.-P. Shih, F.-Y. Chang, S.-H. Chang and K.-C. Fan, "Design and fabrication of an artificial skin using PI-copper films," in Proc. of 2007 IEEE 20th International Conference on Micro Electro Mechanical Systems (MEMS 2007), Hyogo, Japan, January 21-25, 2007, pp. 389-392.

[51] L.-C. Tsao, M. Y. Cheng, I.-L. Chen, W.-P. Shih, Y. J. Yang, F. Y. Chang, K. C. Fan and S.-H. Chang, "Flexible Temperature Sensor Array using Electro-Resistive Polymer For humanoid Artificial Skin," in Proc. of 2007 Solid-State Sensors, Actuators and Microsystems Conference (TRANSDUCERS 2007), Lyon, France, June 10-14, 2007, pp. 2287-2290.

[52] T. Takahashi, K. Takei, A. G. Gillies, R. S. Fearing and A. Javey, "Carbon

Nanotube Active-Matrix Backplanes for Conformal Electronics and Sensors," Nano Letters, vol. 11, no. 12, pp. 5408–5413, 2011.

[53] J. R. Flanagan and A. M. Wing, "Modulation of grip force with load force during point-to-point arm movements," Experimental Brain Research, vol. 95, no.1, pp. 131–143, 1993.

[54] P. Dario and D. de Rossi, "Tactile sensors and gripping challenge: Increasing the performance of sensors over a wide range of force is a first step toward robotry that can hold and manipulate objects as humans do," IEEE Spectrum, vol. 22, no. 8, pp. 46–53, 1985.

[55] R. S. Dahiya, M. Valle, G. Metta, L. Lorenzelli, C. Collini, "Tactile sensing arrays for humanoid robots," in Proc. of 2007 Research in Microelectronics and Electronics Conference (PRIME 2007. Ph.D.), Bordeaux, France, 2-5, 2007, pp. 201–204.

[56] R. S. Dahiya, M. Valle, G. Metta, L. Lorenzelli, "Bio-inspired tactile sensing arrays", in Proc. of SPIE 7365, Bioengineered and Bioinspired Systems IV, Dresden, Germany, May 20, 2009, 73650D-9.

[57] R. S. Dahiya, G. Metta, M. Valle and G. Sandini, "Tactile sensing—from humans to humanoids," IEEE Transactions on Robotics, vol. 26, no. 1, pp. 1-20, 2010.

[58] R. K. Kramer, C. Majidi and R. J. Wood, “Wearable tactile keypad with stretchable artificial skin,” in Proc. of 2011 IEEE International Conference on Robotics and Automation (ICRA 2011), Shanghai, China, May 9-13, 2011, pp. 1103-1107.

[59] S. C. B. Mannsfeld, B. C.-K. Tee, R. M. Stoltenberg, C. V. H.-H. Chen, S. Barman, B. V. O. Muir, A. N. Sokolov, C. Reese and Z. Bao, “Highly sensitive flexible pressure sensors with microstructured rubber dielectric layers,” Nature Materials, vol. 9, no. 9, pp. 1-6, 2010.

[60] B. C. K. Tee, S .C .B. Mannsfeld and Z. Bao, “Elastomer-Based Pressure and Strain Sensors” in Stretchable Electronics (ed. by T. Someya), Wiley-VCH, Weinheim, Germany, pp. 325-353, 2013.

[61] J.-S. Heo, J.-H. Chung and J.-J. Lee, “Tactile sensor arrays using fiber bragg grating,” Sensors and Actuators A: Physical, vol. 126, no. 2, pp. 312–327, 2006.

[62] J.-S. Heo, J.-Y. Kim and J.-J. Lee, “Tactile sensors using the distributed optical fiber sensors,” in Proc. of 3rd International Conference on Sensing Technology (ICST 2008), Tainan, Taiwan, November 30-December 3, 2008, pp. 486–490.

[63] M. Ohka, H. Kobayashi, J. Takata and Y. Mitsuya, “Sensing precision of an optical three-axis tactile sensor for a robotic finger,” in Proc. of 15th IEEE

International Symposium on Robot and Human Interactive Communication (RO-MAN 2006), Hatfield, United Kingdom, September 6-8, 2006, pp. 214–219.

[64] R. Koeppe, P. Bartu, S. Bauer and N. S. Sariciftci, “Light- and Touch-Point Localization using Flexible Large Area Organic Photodiodes and Elastomer Waveguides,” *Advanced Materials*, vol. 21, no. 34, pp. 3510-3514, July 2009.

[65] E. A. J. Marcatili, “Bends in optical dielectric guides,” *The Bell System Technical Journal*, vol. 48, no. 7, pp. 2103–2132. 1969.

[66] L. Faustini and G. Martini, “Bend loss in single-mode fibers,” *Journal of Lightwave Technology*, vol. 15, no. 4, pp. 671-679, 1997.

[67] T. Sorensen, J. Broeng, A. Bjarklev, E. Knudsen and S. B. Libori, “Macro-bending loss properties of photonic crystal fibre,” *Electronics letters*, vol. 37, no. 5, pp. 287–289, 2001.

[68] D. P. J. Cotton, I. M. Graz, and S. P. Lacour, “A Multifunctional Capacitive Sensor for Stretchable Elctronic Skin,” *IEEE Sensors Journal*, vol. 9, no. 12, pp. 2008–2009, 2009.

[69] S. S. Mader, “Ch. 14 Senses,” in Human Biology, Mcgraw Hill, New York, NY, 2008.

[70] “Leonardo_da_Vinci.” *Wikipedia: The Free Encyclopedia.* Wikimedia Foundation, Inc., date last updated (16 January 2014). Web. Date accessed (25 January 2014). < http://en.wikipedia.org/wiki/Leonardo_da_Vinci>

[71] C. Lucarotti, C. M. Oddo, N. Vitiello, and M. C. Carrozza, “Synthetic and Bio-Artificial Tactile Sensing: A Review,” *Sensors*, vol. 13, pp. 1435–1466, 2013.

Chapter 2

Nickel Conductive Composite Material : Characteristics Enhancement by Magnetic Aligning Method

2.1 Introduction

As briefly introduced at Chapter 1, the conductive composite materials are well known as one of the piezoresistive type materials. Generally, the conductive composite materials are composed of electrically insulating matrix and conductive filler. The conductive fillers that can be added into the insulating matrix include various carbonaceous particles (carbon black (CB) [1-2], carbon fibers (CFs) [3-4], carbon nano-fibers (CNFs) [5], carbon nanotubes (CNTs) [6-7], graphite [8-9],

graphite nano-sheets [10], and graphene [11-12]) and most metals (aluminum [13], cobalt [14], copper [15-16], gold [17-18], iron [13] and its oxidized substances [20-22], nickel [23-25], silver [26-27], and zinc [28-29]), and metal based nano-fibers [30] and nanowires [31-32]. By compounding of these conductive fillers into the insulating matrixes, the insulating matrix is given electrical conductivity.

Elastomer materials, such as poly (dimethylsiloxane) (PDMS) and polyurethane (PU) which can be elastically deformable, have been generally used as an insulating matrix in the field of sensor application. Elastic deformation of the elastomer materials can be occurred due to various environmental factors such as applied force, temperature variation and infiltration of specific chemical molecules. According to directions of deformation, such as compression or expansion, electrical characteristics are varied with construction or destruction of conductive paths. This has led to the development of the conductive composite materials for applications as pressure sensors [33], temperature sensors [34-35], and chemical sensors [36]. For sensor applications, the conductive composite materials are prepared with conductive filler volume with certain level. In this condition, conductive composite materials have sensitive characteristics by various environmental factors with the electrical conductivity [37].

The electrical characteristics of the conductive composite materials can be explained with a conductive path formation in the conductive composite materials.

Most simple explanation for the conductive path formation in the conductive composite materials is related with a volume fraction of the conductive fillers. It can be easily inferred that more conductive paths are formed with more conductive fillers. The electrical conductivity of the conductive composite material will be more increased, if more conductive paths are formed. However, the electrical conductivity variation with the volume fraction of the conductive fillers does not show directly proportion characteristic. When the volume fraction of the conductive fillers is not reached at a specific level, the conductive composite materials show fully insulating properties.

The electrical conductivity of the conductive composite materials is given as a power-law relationship, follows in Equation (2.1) [38]:

$$\sigma = \sigma_0 (V_f - V_c)^s \tag{2.1}$$

where σ is the electrical conductivity of the conductive composite materials, σ_0 is the electrical conductivity of the conductive filler, V_f is the volume fraction of the conductive filler, V_c is the percolation threshold, and s is a conductivity exponent. However, there are more factors that can affect the electrical conductivity of the conductive composite materials such as geometrical shape of the filler particle, particle orientation in the insulating matrix, polymer-particle interaction, and a degree of dispersion. For this reason, the value of the conductivity exponent s is not

a constant, varies with each different type of conductive composite system [39].

As mentioned before, a behavior of the electrical conductivity variation with the conductive filler volume fraction is divided in three ranges, as shown in below Figure 2.1 [40].

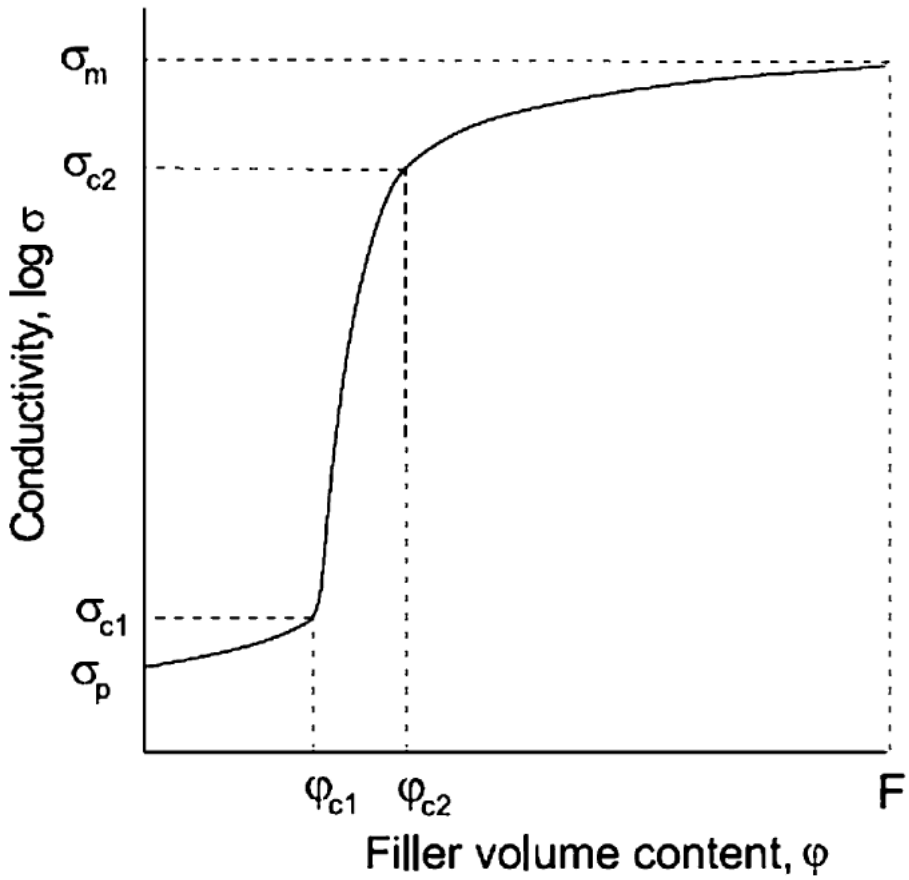

Figure 2.1 Typical dependences of electrical conductivity on conductive filler volume content. (Reference [40])

The conductive composite materials show electrically insulating property when the conductive filler volume fraction is below the percolation threshold (V_c or φ_{c1}). When the conductive filler volume fraction is above the percolation threshold, conductive paths are formed in the conductive composite materials and it becomes electrically conductive. And the electric conductivity is rapidly increased until the conductive filler volume fraction is reached at certain level that is above the percolation threshold. This sharply increasing range ($\varphi_{c1}<\varphi<\varphi_{c2}$) is called the smearing region [41]. The maximum conductivity is attained at the certain level of the filler volume fraction that is above the percolation threshold [42].

In spite of simple transduction mechanism and fabrication method, there are some critical problems of the conductive composite materials for high performance sensor applications, such as a low electrical conductivity and a location of a dynamic range. In cases of pressure or tactile sensors based on the conductive composite materials, these sensors cannot well detect a low to medium pressure range (0-100 kPa), which is an important for mimicking the human skin, because dynamic ranges are generally located at a high pressure region (~MPa). This is due to the low electrical conductivity and a narrow range of the smearing region. Another problem is that the conductive composite materials show severe hysteresis characteristic under a repeat operation due to a viscoelastic property of the elastomer matrix [50].

There have been numerous researches to modify well known drawbacks of the

conductive composite materials [43-49]. According to the previous researches, conductive filler size, shapes, its distribution in the elastomeric matrixes and so on are most important factors that affect to aforementioned problems. Furthermore, an interface interaction between the elastomer and conductive filler is also important. Most extensive research trend to solve the problems is that using new type of conductive fillers such as CNTs, nanowires, or its compounds. Recently, some remarkable results have been reported that show the high electrical conductivity by using specially treated materials such as silver nano-particle attached CNTs [51-54]. In view of practical use, however, they require a complex fabrication process and a high cost to attain a high initial electrical conductivity. Large-area fabrication is an essential factor for making an electronic skin. In this point of view, more practical approach is needed for realization of the electronic skin.

In this work, spherical-shape nickel micro particle and PDMS, which are easily approachable materials, were used as the conductive filler and the elastomeric matrix, respectively. Furthermore, magnetic field exposure method was used for shape modification and aligning of the nickel conductive filler. In the following sections, magnetic field exposure effect will be analyzed by the effective medium theory and shown by experimental results. Further, electrical characteristics improved nickel conductive composite materials were used as pressure and temperature sensor applications.

2.2 Theoretical Analysis with the Maxwell Theory and the Effective Medium Theory

Under the external magnetic field, nickel particles are aggregated along the magnetic field direction. Through this process, randomly distributed nickel conductive fillers become a highly ordered structure which has high axial ratio. According to the previous researches, a structure of the conductive filler is one of important factors that can affect to percolation threshold. Theoretically, the higher axial ratio structure, the less percolation threshold is predicted.

According to Xue [55], an effective conductivity of metal-polymer composite material can be calculated by using the Maxwell theory and the Effective medium theory. This calculation can consider influence of the filler aligning effect as well as the shape and size. For simplicity, we assume elastomeric matrix is compound of spherical particles and all the conductive fillers are the elliptical particles whose axial ratio is M $\left(M = \frac{a+t}{b+t}\right)$, where a, b, c(=b) are the radii. In this condition, the effective conductivity of the metal-polymer composite material can be expressed as

$$(1 - V_e) \cdot \sum_{k=x,y,z} \frac{\sigma_{eff,kk} - \sigma_{m,kk}}{\sigma_{eff,kk} + L_{mi,k} \cdot \left(\sigma_{m,kk} - \sigma_{eff,kk}\right)} + V_e \cdot \sum_{k=x,y,z} \frac{\sigma_{eff,kk} - \sigma_{c,kk}}{\sigma_{eff,kk} + L_{cj,k} \cdot \left(\sigma_{c,kk} - \sigma_{eff,kk}\right)} = 0 \quad (2.2)$$

where *Ve* are the total effective volume fraction of the metal particles; $L_{mi,k}$ and $L_{cj,k}$ are the depolarization factors of the *i*th matrix particle and the *j*th complex metal particle along k axis (*k* = *x*, *y*, *z*); σ_{eff}, σ_m, σ_c are the effective electric conductivity of the conductive composite material, electric conductivity of the matrix and the filler, respectively; L_m and L_c are the depolarization factors of the matrix and the filler, respectively.

In Equation (2.2), depolarization factors L_m and L_c can be varied with particle shapes. According to Giordano [19], the depolarization factors along each axes can be expressed below

$$L_x = \frac{a_x a_y a_z}{2} \int_0^{+\infty} \frac{ds}{(s+a_x^2)R(s)} \tag{2.3}$$

$$L_y = \frac{a_x a_y a_z}{2} \int_0^{+\infty} \frac{ds}{(s+a_y^2)R(s)} \tag{2.4}$$

$$L_z = \frac{a_x a_y a_z}{2} \int_0^{+\infty} \frac{ds}{(s+a_z^2)R(s)} \tag{2.5}$$

where a_x, a_y and a_z are the axes of the particles. When we assume elliptical particles, ($0 < a_x \leq a_y \leq a_z$, $0 <$ e $= \frac{a_x}{a_y} \leq 1$ and $0 <$ g $= \frac{a_y}{a_z} \leq 1$; e and g are eccentricities.) the depolarization factors can be expressed as below

$$L_x = \frac{1}{1-e^2} - \frac{e}{(1-e^2)\sqrt{1-e^2g^2}}E(v,q) \tag{2.6}$$

$$L_y = \frac{e(1-e^2g^2)}{(1-e^2)(1-g^2)\sqrt{1-e^2g^2}}E(v,q) - \frac{eg^2}{(1-g^2)\sqrt{1-e^2g^2}}F(v,q) - \frac{e^2}{1-e^2} \tag{2.7}$$

$$L_z = \frac{eg^2}{(1-g^2)\sqrt{1-e^2g^2}}[F(v,q) - E(v,q)] \tag{2.8}$$

Where $F(v,q)$ and $E(v,q)$ are the elliptical integrals.

When we consider once again, all the polymer matrix particles are sphere, and all the metal fillers are the same rotational elliptical particles whose axial ratio is *M* ($M = \frac{c+t}{a+t}$), where a, b(=a), c are the radius of each axes. In this condition, $L_{mi,k}$ and $L_{cj,k}$ are defined as,

$$L_{m,x} = L_{m,y} = L_{m,z} = 1/3 \tag{2.9}$$

$$L_{c,x} = L_{c,y} = \frac{1-L_{c,z}}{2} \tag{2.10}$$

$$L_{c,z} = \begin{cases} \frac{1}{1-M^2} + \frac{M}{\sqrt{(1-M^2)^3}} \cdot \ln\left(M + \sqrt{M^2-1}\right), & M > 1, \\ \frac{1}{1-M^2} + \frac{M}{\sqrt{(1-M^2)^3}} \cdot \cos^{-1} M, & M < 1, \end{cases} \tag{2.11}$$

We may verify that $2L_x + L_z = 1$ for any value of *M*. Equation (2.11) describes the behavior of a dispersion of aligned prolate ellipsoids [19]. Figure 2.2

shows depolarization factors of a prolate ellipsoid which is stretched along z-direction.

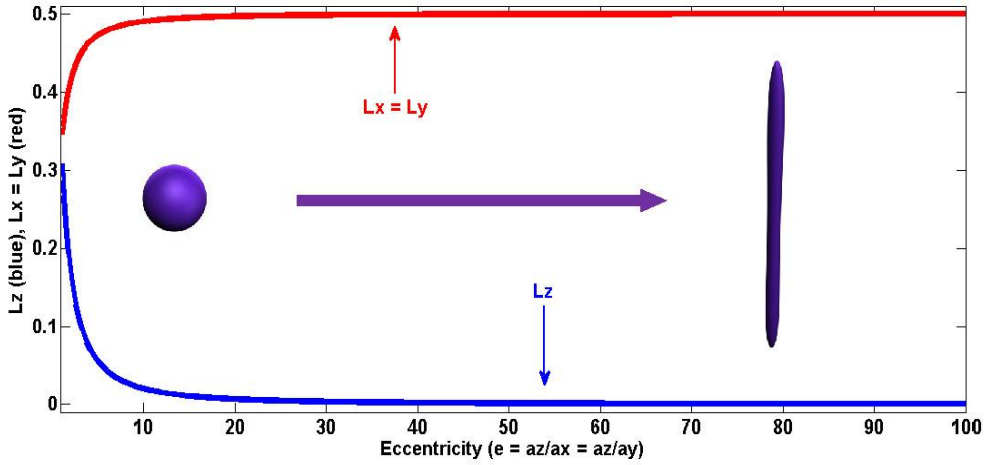

Figure 2.2 Variation of depolarization factors with eccentricity.

Finally, substituting Equations (2.9)-(2.11) into Equation (2.2), the effective electric conductivity of the metal-polymer composite is defined as,

$$9(1 - V_e) \cdot \frac{\sigma_{eff} - \sigma_m}{2\sigma_{eff} + \sigma_m} + V_e \cdot \left[\frac{\sigma_{eff} - \sigma_{c,z}}{\sigma_{eff} + L_{c,z} \cdot (\sigma_{c,x} - \sigma_{eff})} + 4 \cdot \frac{\sigma_{eff} - \sigma_{c,x}}{2\sigma_{eff} + (1 - L_{c,z}) \cdot (\sigma_{c,y} - \sigma_{eff})} \right] = 0 \qquad (2.12)$$

The electric conductivity of the metal–polymer composite is given by Equation (2.12). Figure 2.3 shows dependency of the percolation threshold with filler shape and orientation, based on Equation (2.12).

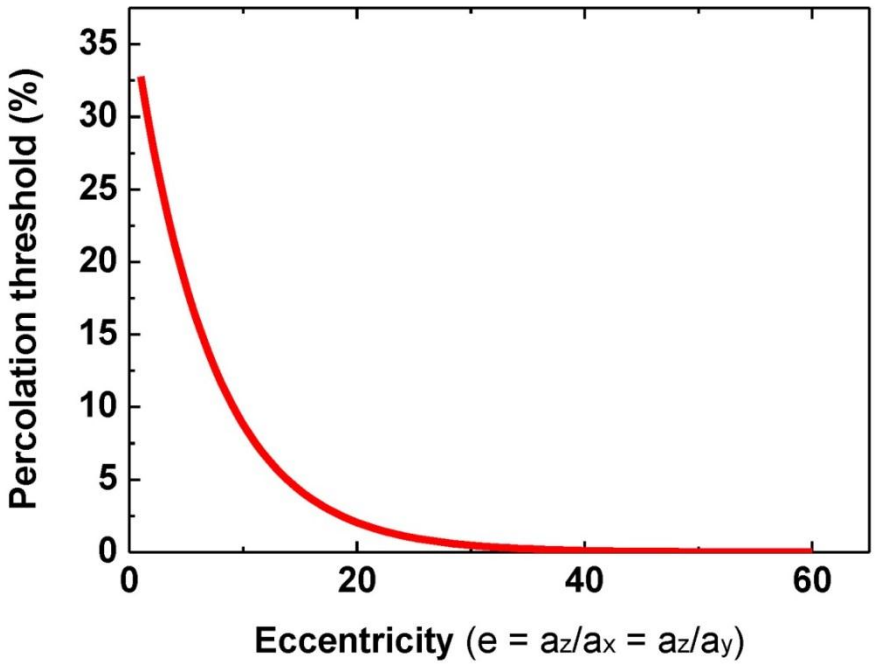

Figure 2.3 The dependency of the percolation threshold with filler shape and orientation.

2.3 Materials and Fabrication Method

Poly (dimethyloxane) (PDMS: Sylgard 184 from Dow Corning) was used as base material. And nickel powder(from Sigma Aldrich) was used as conductive filler which diameter is <150μm. PDMS base was mixed with hardener at 10:1 weight ratio. And then nickel powder was mixed into PDMS. Each PDMS/nickel composite material was mixed during at least 10minutes. After mixing, PDMS/nickel composite material was moved in vacuum chamber for degassing. Degassed PDMS/nickel composite material was poured onto flat aluminum mold. After the aluminum mold seal up, two neodymium permanent magnets were attached on top and bottom side of the aluminum mold. In this structure, magnetic field from the permanent magnets induced through the aluminum mold. While the magnetic field induced, nickel powder inside the PDMS mixture was aligned along the magnetic field direction. PDMS/nickel composite material was exposed to the magnetic field during 10 minutes. After finish exposing magnetic field, aluminum mold was moved on a hot plate and then cured. Curing condition is 10minutes at 150 °C. Figure 2.4 shows the all fabrication processes for the magnetically aligned nickel conductive composite materials.

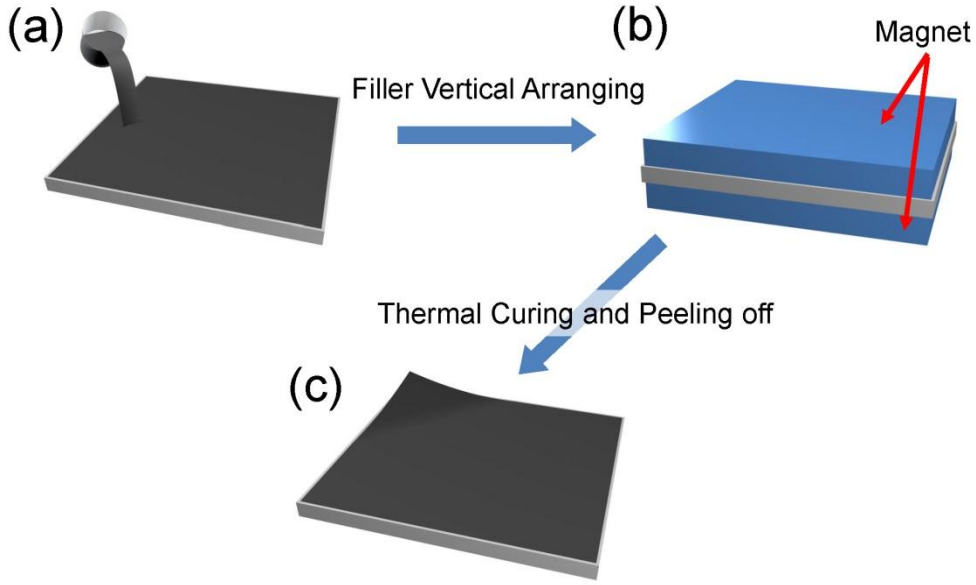

Figure 2.4 Processes for nickel conductive composite with magnetically filler aligning.

2.4 Results and Discussions

2.4.1 Optical Microscope Measurement

Figure 2.5 shows optical microscope images of nickel/PDMS mixture while the nickel inside the PDMS was aligned along with direction of external magnetic field. To make sure smooth moving of the nickel particles, nickel/PDMS was not cured. The uncured mixture was sealed between two sheets of slide glasses.

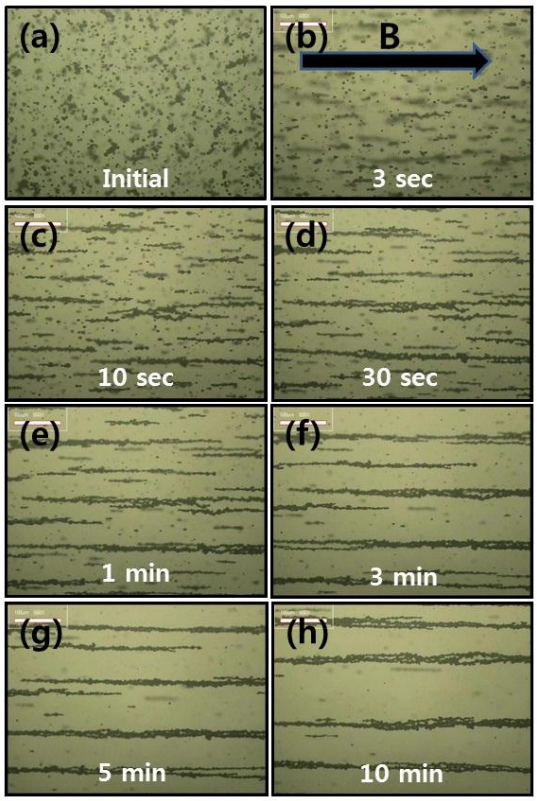

Figure 2.5 Optical microscope images of uncured nickel/PDMS mixture (Ni 5 wt.%) under external magnetic field during (a) 0 second, (b) 3 second, (c) 10 second, (d) 30 second, (e) 1 minute, (f) 3 minute, (g) 5 minute, and (h) 10 minute. Direction of the magnetic field is expressed in (b).

2.4.2 Electrical Characteristics

Figure 2.6 shows comparing of the percolation threshold variation with the magnetic field exposure time for 10 second, 1minute, 10 minute, and bare composite material. In case of the bare composite material, it showed nearly insulator characteristics until around 30 vol% of nickels, and then its percolation threshold was formed at slightly above 30 vol% of nickels. Further, resistivity was rapidly decreased until 40 vol% of nickels. Magnetically aligned conductive composite which was exposed to the magnetic field for 10 second showed a similar tendency

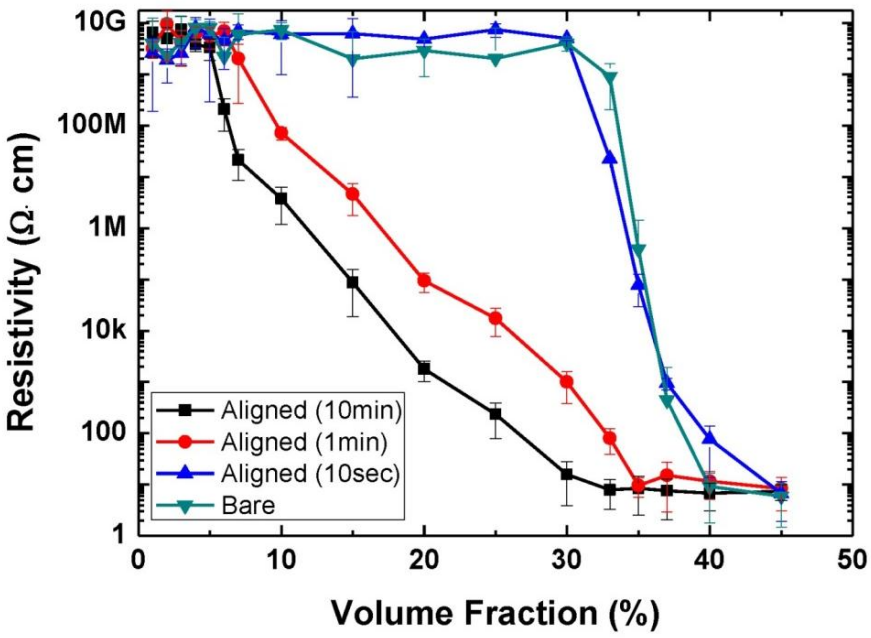

Figure 2.6 Variation of percolation threshold with magnetically aligning time.

with the bare conductive composite material. However, magnetically aligned conductive composite materials which were exposed to the magnetic field over 1 minute showed definitely different percolation thresholds and tendencies. These materials showed sharply reduced percolation threshold around 5 vol% of nickels and wide range of the smearing region.

To verify an effect of electrical characteristics improvement on sensor application, magnetically aligned conductive composite materials were prepared with various thicknesses of 250-μm, 500-μm, 750-μm, and 1-mm. All samples were made with the magnetic exposure in 10 minute. Figure 2.7 shows pressure sensing characteristics of the magnetically aligned nickel conductive composite materials. Resistance change was measured under continuously applied pressure changing condition with home-made pressure apply machine and Keithley 2400.

Due to the low young's modulus of PDMS, when pressure is applied on the conductive composites, the nickel conductive filler which in the composites comes into contact with one another in the composite more easily and a conducting path is formed, and vice versa. Because of this characteristic, when composite is pressed by external force, composite's bulk resistance decreases compared to the initial state. On the other hand, when the pressure is released, composite's bulk resistance increases compared to the initial state, because the conducting path is disconnected.

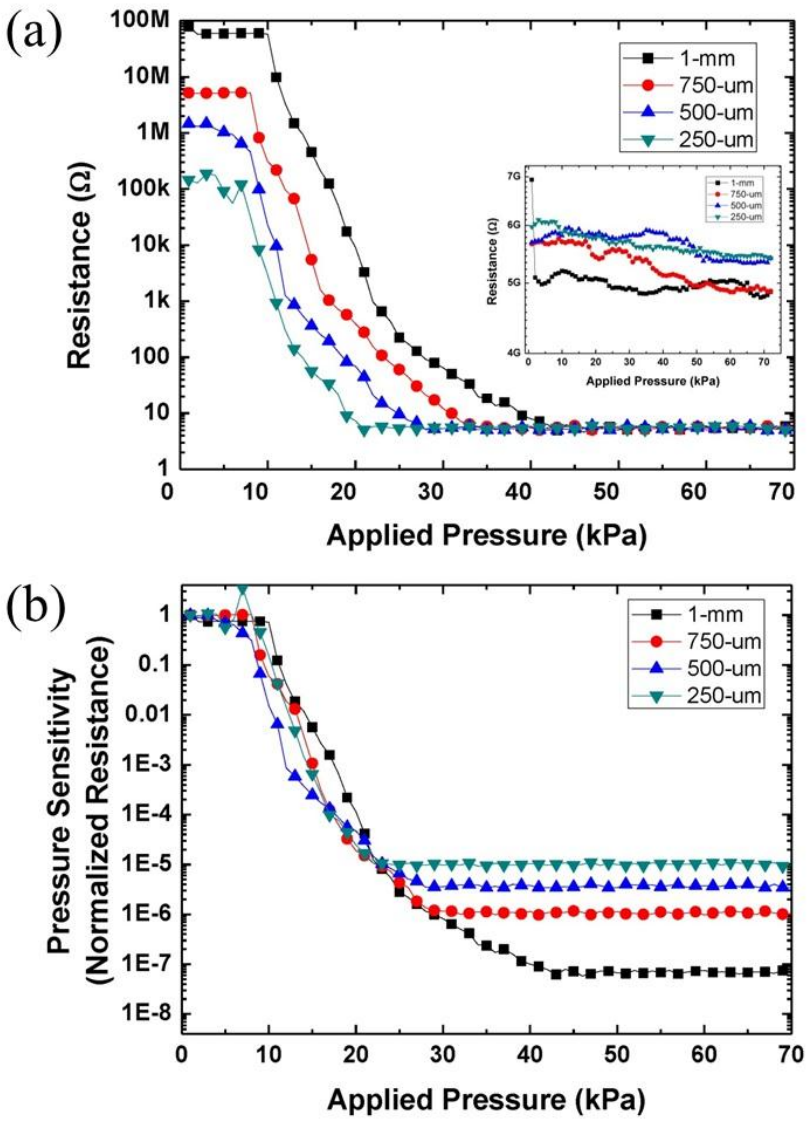

Figure 2.7 Pressure sensing characteristics of magnetically aligned nickel conductive composite materials. (a) Resistance changes in terms of applied pressure (Inset: non-aligned nickel conductive composite materials) and (b) sensitivities (normalized resistance), according to film thicknesses.

There was thickness dependency for applied pressure. Dynamic range became wider when the conductive composite film was thicker. Furthermore, minimum detectable pressure became slightly lower when the conductive composite film was thinner. 1-mm thick samples showed pressure sensitivity over seven orders with dynamic range from 10 kPa to 50 kPa. 250-μm thick sample showed pressure sensitivity over four orders with dynamic range from 7 kPa to 20 kPa. All sample showed monotonic resistance variations against the applied pressure.

Similar to pressure dependency, conductive composite material also has an electrical characteristic where resistance changes depending on external temperature. Volume of the PDMS is easily changed by ambient temperature change due to that the PDMS has a large coefficient of thermal expansion of about 310 μm/m-℃ or ppm. This property is also applied to the conductive composite material which based on the PDMS. When ambient temperature increases, volume of composite is increased and conductive path is disconnected. Then resistance is increased.

To measure the temperature characteristic of the magnetically conductive composite materials, we set the temperature changing environment by hotplate. We measured at 25℃ to 80℃, and each increment was 5℃. Figure 2.8 shows the response of the temperature sensor to the external temperature change. 250-μm thick sample showed temperature sensitivity around four orders.

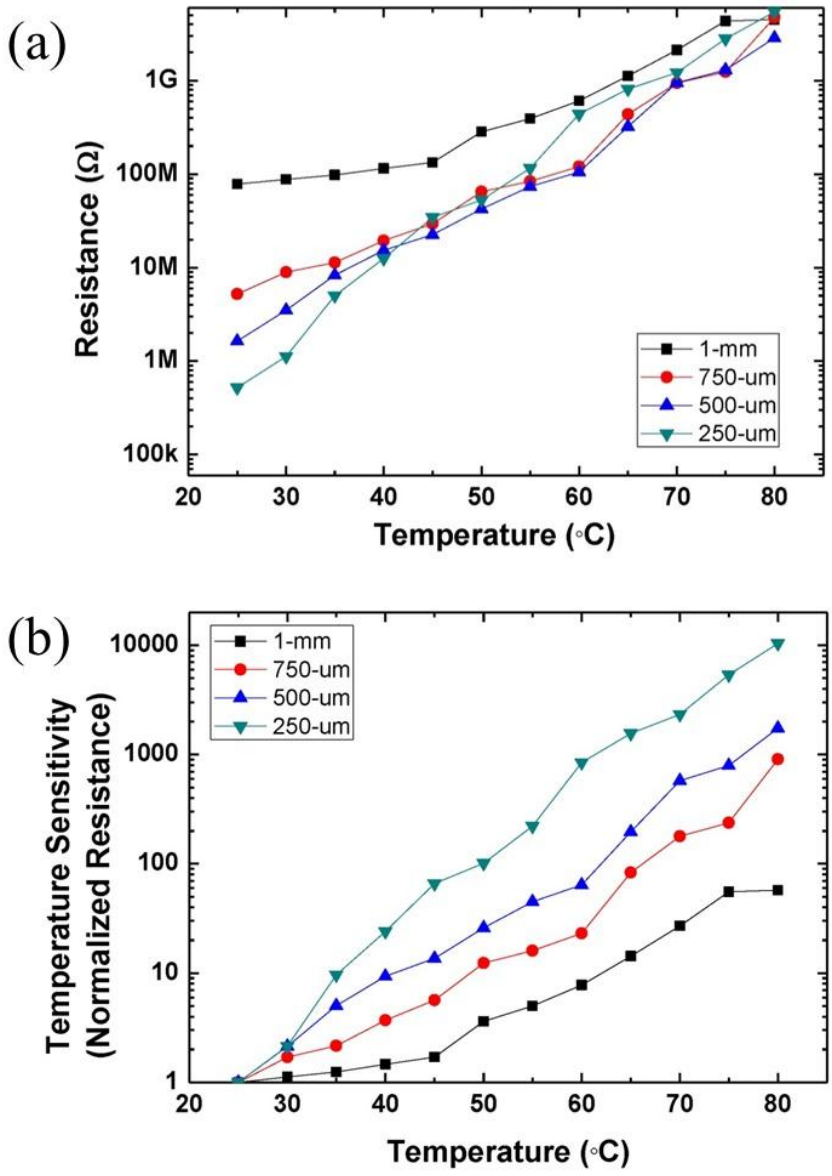

Figure 2.8 Temperature sensing characteristics of magnetically aligned nickel conductive composite materials. (a) Resistance changes in terms of external temperature and (b) sensitivities (normalized resistance), according to film thicknesses.

2.5 Conclusion

In this chapter, by using the magnetic aligning method, we successfully demonstrated high performance nickel based conductive composite materials. Filler aligning effect was theoretically analyzed by using percolation theory and effective medium theory. The magnetically aligned conductive composite material shows lower percolation threshold and higher pressure and temperature sensor characteristics than the bare conductive composite materials.

Reference

[1] W. Yi, Y. Wang, G. Wang, and X. Tao, “Investigation of carbon black/silicone elastomer/dimethylsilicone oil composites for flexible strain sensors,” Polymer Testing, vol. 31, no. 5, pp. 677–684, 2012.

[2] L. Wang, T. Ding, and P. Wang, “Thin Flexible Pressure Sensor Array Based on Carbon Black/Silicone Rubber Nanocomposite,” IEEE Sensors Journal, vol, 9, no. 9, pp. 1130–1135, 2009.

[3] X. Wang, and D. Chung, “Self-monitoring of fatigue damage and dynamic strain in carbon fiber polymer-matrix composite,” Composites Part B, vol. 29, no. 1, pp. 63–73, 1998.

[4] S. Wen, S. Wang, and D. Chung, “Piezoresistivity in continuous carbon fiber polymer-matrix and cement-matrix composites,” Journal of Materials Science, vol. 35, no. 14, pp. 3669–3675, 2000.

[5] T. Yasuoka, Y. Shimamura, and A. Todoroki, “Electrical Resistance Change under Strain of CNF/Flexible-Epoxy Composite. Advanced Composite Materials, vol. 19, no. 2, pp. 123–138, 2010.

[6] S. Y. Kwon, Y. K. Park, and M. S. Kim, “PIEZORESISTIVE PROPERTIES OF MULTI-WALLED CARBON NANOTUBE–POLY(DIMETHYLSILOXANE) COMPOSITES FOR LOW-PRESSURE-SENSING APPLICATIONS,” Nano,

vol. 07, no. 01, 1250005(5pages), 2012.

[7] J. J. Ku-Herrera, and F. Avilés, “Cyclic tension and compression piezoresistivity of carbon nanotube/vinyl ester composites in the elastic and plastic regimes,” Carbon, vol. 50, no. 7, pp. 2592–2598. 2012.

[8] S. Littlejohn, A. Nogaret, G. M. Prentice, and G. D. Pantos, “Pressure Sensing and Electronic Amplification with Functionalized Graphite-Silicone Composite,”Advanced Functional Materials, vol. 23, no. 43, pp. 5398-5402, 2013.

[9] D. T. Beruto, M. Capurro, and G. Marro, “Piezoresistance behavior of silicone–graphite composites in the proximity of the electric percolation threshold,” Sensors and Actuators A: Physical, vol. 117, no. 2, 301–308. 2005.

[10] R. Soltani, and A. A. Katbab, “The role of interfacial compatibilizer in controlling the electrical conductivity and piezoresistive behavior of the nanocomposites based on RTV silicone rubber/graphite nanosheets,” Sensors and Actuators A: Physical, vol. 163, no. 1, pp. 213–219. 2010.

[11] Y. Hou, D. Wang, X.-M. Zhang, H. Zhao, J.-W. Zha, and Z.-M. Dang, Z.-M., “Positive piezoresistive behavior of electrically conductive alkyl-functionalized graphene/polydimethylsilicone nanocomposites,” Journal of Materials Chemistry C, vol. 1, no. 3, pp. 515-521. 2012.

[12] Y. V. Syurik, M. G. Ghislandi, E. E. Tkalya, G. Paterson, D. McGrouther, O. A. Ageev, and J. Loos, “Graphene Network Organisation in Conductive Polymer Composites,” Macromolecular Chemistry and Physics, vol. 213, no. 12, pp. 1251–1258, 2012.

[13] Nurazreena, L. B. Hussain, H. Ismail, and M. Mariatti, “Metal Filled High Density Polyethylene Composites - Electrical and Tensile Properties,” Journal of Thermoplastic Composite Materials, vol. 19, no. 4, pp. 413–425, 2006.

[14] A. Maaroufi, K. Haboubi, El. A. Amarti, and F. Carmona, “Electrical resistivity of polymeric matrix loaded with nickel and cobalt powders,” Journal of Materials Science, vol. 39, no. 1, pp. 265–270, 2004.

[15] X. W. Zhang, Y. Pan, Q. Zheng, and X. S. Yi, “Piezoresistance of conductor filled insulator composites,” Polymer international, vol. 50, no. 2, pp. 229–236, 2001.

[16] H.-S. Chuang, and S. Wereley, “Design, fabrication and characterization of a conducting PDMS for microheaters and temperature sensors,” Journal of Micromechanics and Microengineering, vol. 19, no. 4, pp. 045010. 2009.

[17] Y. Kim, J. Zhu, B. Yeom, M. Di Prima, X. Su, J.-G. Kim, S. J. Yoo, C. Uher, and N. A. Kotov, “Stretchable nanoparticle conductors with self-organized conductive pathways,” Nature, vol. 500, pp. 59–63. 2013.

[18] S. Stassi, G. Canavese, V. Cauda, S. L. Marasso, and C. F. Pirri, “Evaluation of different conductive nanostructured particles as filler in smart piezoresistive composites,” Nanoscale research letters, vol.7, no.1, pp. 1–5, 2102.

[19] S. Giordano, “Effective medium theory for dispersions of dielectric ellipsoids,” Journal of Electrostatics, vol. 58, pp. 59-76, 2003.

[20] A. P. Soledad, G. Jorge, O. E. Perez, A. Butera, L. A. Gabriela,and N. R. Martín, “Magnetic and elastic properties of CoFe2O4- polydimethylsiloxane magnetically oriented elastomer nanocomposites,” Journal of applied physics, vol. 110, no. 4, pp. 043920. 2011.

[21] I. T. Kim, A. Tannenbaum, and R. Tannenbaum, “Anisotropic conductivity of magnetic carbon nanotubes embedded in epoxy matrices,” Carbon, vol, 49, no. 1, pp. 54–61, 2011.

[22] X. Wang, Z. Zhao, J. Qu, Z. Wang, and J. Qiu, “Fabrication and characterization of magnetic Fe3O4–CNT composites,” Journal of Physical and Chemistry of Solids, vol. 71, no. 4, pp. 673–676, 2010.

[23] O. K. Johnson, G. C. Kaschner, T. A. Mason, D. T. Fullwood, and G, Hansen, “Sensors and Actuators A: Physical. Sensors and Actuators A: Physical, vol. 166, no. 1, pp. 40–47, 2011.

[24] D. Bloor, A. Graham, E. J. Williams, P. J. Laughlin, and D. Lussey, “Metal–

polymer composite with nanostructured filler particles and amplified physical properties," Applied physics letters," vol. 88, no. 10, 102103. 2006.

[25] G. Canavese, M. Lombardi, S. Stassi, C. F. Pirri, "Comprehensive Characterization of Large Piezoresistive Variation of Ni-PDMS Composites," Applied Mechanics and Materials, vol.110, no. 116, pp. 1336–1344, 2011.

[26] R. Ma, S. Kwon, Q. Zheng, H.-Y. Kwon, J. I. Kim, H. R. Choi, and S. Baik, "Carbon-Nanotube/Silver Networks in Nitrile Butadiene Rubber for Highly Conductive Flexible Adhesives," Advanced Materials, vol. 24, no. 25, pp. 3344–3349, 2012.

[27] T. Oh, K.-Y. Chun, E, Lee, E., Y.-J.Kim, Y.aman Baik, S. "Functionalized nano-silver particles assembled on one-dimensional nanotube scaffolds for ultra-highly conductive silver/polymer composites," Journal of Materials Chemistry, vol. 20, no. 18, pp. 3579-3582, 2010.

[28] C.-C. Lin, W.-S. Lee, C.-C. Sun, and W.-H. Whu, "A varistor–polymer composite with nonlinear electrical-thermal switching properties," Ceramics International, vol. 34, no. 1, pp. 131–136, 2008.

[29] N. M., Sofian, & D. Rusu, "Mechanical and thermal properties of zinc powder filled high density polyethylene composites," Polymer Testing, vol. 20, no. 4, pp. 409–417, 2001

[30] Y.-Z Long, M.-M. Lu, C. M. Wan, J.-L. Duvail, Z. Liu, and Z. Fan, Z, “Recent advances in synthesis, physical properties and applications of conducting polymer nanotubes and nanofibers,” Progress in Polymer Science, vol. 36, no. 10, pp. 1415–1442, 2011.

[31] W. Gaynor, G. F. Burkhard, M. D. McGehee, and P. Peumans, “Smooth Nanowire/Polymer Composite Transparent Electrodes. Advanced Materials, vol. 23, no. 26, pp. 2905–2910, 2011.

[32] T. Nagai, N. Aoki, Y. Ochiai, and K. Hoshino, Electric Conductivity-Tunable Transparent Flexible Nanowire-Filled Polymer Composites: Orientation Control of Nanowires in a Magnetic Field. ACS Applied Materials & Interfaces, vol. 3, no. 7, pp. 2341–2348, 2011.

[33] J. C. Ramos, R. N. González, H. Macicior, T. Sikora, E. Ochoteco, and F. V. Verdú, “Tactile sensors based on conductive polymers,” Microsystem Technologies, vol. 16, no. 5, pp. 765–776, 2009.

[34] A. Vega, J. Sumfleth, H. Wittich, and K. Schulte, “Time and temperature dependent piezoresistance of carbon nanofiller/polymer composites under dynamic load,” Journal of Materials Science, vol. 47, no. 6, pp. 2648–2657, 2011.

[35] H.-S. Chuang, and S. Wereley, “Design, fabrication and characterization of a

conducting PDMS for microheaters and temperature sensors," Journal of Micromechanics and Microengineering, vol. 19, no. 4, 045010. 2009.

[36] S. V. Patel, M. W. Jenkins, R. C. Hughes, W. G. Yelton, and A. J. Ricco, "Differentiation of Chemical Components in a Binary Solvent Vapor Mixture Using Carbon/Polymer Composite-Based Chemiresistors," Analytical Chemistry, vol. 72, no. 7, pp. 1532–1542, 2000.

[37] J. Martin, R. Anderson, J. Odinek, D. Adolf, and J. Williamson, "Controlling percolation in field-structured particle composites: Observations of giant thermoresistance, piezoresistance, and chemiresistance," Physical Review B, vol. 67, no. 9, 094207. 2003.

[38] D. Stauffer, and A. Aharony "Introduction to percolation theory," London: Taylor and Francis; 1992, pp. 89-113.

[39] J. Li, and J.-K. Kim, "Percolation threshold of conducting polymer composites containing 3D randomly distributed graphite nanoplatelets," Composites Science and Technology, vol. 67, no. 10, pp. 2114–2120, 2007.

[40] Y. P. Mamunya, V. V. Davydenko, P. Pissis, E. V. Lebedev, Electrical and thermal conductivity of polymers filled with metal powders, European Polymer Journal, vol. 38, pp. 1887–1897, 2002.

[41] V.I. Roldughin, V.V. Vysotskii, "Percolation properties of metal-filled

polymer films, structure and mechanisms of conductivity," Progress in Organic Coatings, vol. 39, pp. 81–100, 2000.

[42] R. A. Antunes, M. C. L. de Oliveira, G. Ett, and V. Ett, "Carbon materials in composite bipolar plates for polymer electrolyte membrane fuel cells: A review of the main challenges to improve electrical performance," Journal of Power Sources, vol. 196, no. 6, pp. 2945–2961, 2011.

[43] M. Hussain, Y.-H. Choa, and K. Niihara, "Effects of nano ceramics on electrical resistivity of carbon filled rubber materials," Scripta materialia, vol. 44, no. 8, pp. 1203–1206, 2001.

[44] M. Hussain, Y.-H. Choa, and K. Niihara, "Conductive rubber materials for pressure sensors," Journal of materials science letters, vol. 20, no. 6, pp. 525–527, 2001.

[45] M. Hussain, Y.-H. Choa, and K. Niihara, "Fabrication process and electrical behavior of novel pressure-sensitive composites," Composites Part A, vol. 32, no. 12, pp. 1689–1696, 2001.

[46] G. Canavese, M. Lombardi, S. Stassi, and C. F. Pirri, "Comprehensive Characterization of Large Piezoresistive Variation of Ni-PDMS Composites," Applied Mechanics and Materials, vol. 110, no. 116, pp. 1336–1344, 2011.

[47] T. Kaully, A. Siegmann, and D. Shacham, "Mechanical behavior of highly

filled natural CaCO3 composites: Effect of particle size distribution and interface interactions," Polymer Composites, vol. 29, no. 4, pp. 396–408, 2008.

[48] Q, Lü, H. Cao, X. Song, H. Yan, Z. Gan, and S. Liu, "Improved electrical resistance-pressure strain sensitivity of carbon nanotube network/polydimethylsiloxane composite using filtration and transfer process," Chinese Science Bulletin, vol. 55, no. 3, pp. 326–330, 2010.

[49] B. G. Han, B. Z. Han, and X. Yu, :Experimental study on the contribution of the quantum tunneling effect to the improvement of the conductivity and piezoresistivity of a nickel powder-filled cement-based composite," Smart Materials and Structures, vol. 18, no. 6, 065007, 2009.

[50] S. Wang, P. Wang, and T. Ding, "Resistive viscoelasticity of silicone rubber/carbon black composite," Polymer Composites, vol. 32, no. 1, pp. 29–35, 2010.

[51] K.-Y. Chun, Y. Oh, J. Rho, J.-H. Ahn, Y.-J. Kim, H. R. Choi, and S. Baik, "Highly conductive, printable and stretchable composite films of carbon nanotubes and silver," Nature Nanotechnology, vo;. 5, no. 12, pp. 853–857, 2010.

[52] R. Ma, S. Kwon, Q. Zheng, H. Y. Kwon, J. I. Kim, H. R. Choi, and S. Baik, "Carbon-Nanotube/Silver Networks in Nitrile Butadiene Rubber for Highly

Conductive Flexible Adhesives," Advanced Materials, vol. 24, no. 25, pp. 3344–3349, 2012.

[53] T. Sekitani, Y. Noguchi, K. Hata, T. Fukushima, T. Aida, and T. Someya, "A Rubberlike Stretchable Active Matrix Using Elastic Conductors," Science, vol. 321, no. 5895, pp. 1468–1472, 2008.

[54] M. Park, J. Im, M. Shin, Y. Min, J. Park, H. Cho, S. Park, M.-B. Shim, S. Jeon, D.-Y. Chung, J. Bae, J. Park, U. Jeong, and K. Kim, "Highly stretchable electric circuits from a composite material of silver nanoparticles and elastomeric fibres," Nature Nanotechnology, vol. 7, no. 12, pp. 803–809, 2012.

[55] Q. Xue, "The influence of particle shape and size on electric conductivity of metal–polymer composites," European Polymer Journal, vol. 40, no. 2, pp. 323–327, 2004.

[56] B. Lundberg, and B. Sundqvist, "Resistivity of a composite conducting polymer as a function of temperature, pressure, and environment: Applications as a pressure and gas concentration transducer," Journal of Applied Physics, Vol. 60, pp. 1074-1079, 1986.

[57] J.-C. Huang, "Carbon Black Filled Conducting Polymers and Polymer Blends," Advanced Polymer Technique, vol. 21, pp. 299-313, 2002.

[58] P. J. Mather, and K. M. Thomas, "Carbon black/high density polyethylene

conducting composite materials," Journal of Material Science, vol. 32, pp. 401-407, 1997.

[59] H.-S. Chuang, and S. Wereley, "Design, fabrication and characterization of a conducting PDMS for microheaters and temperature sensors," Journal of Micromechanics and Microengineering, vol. 19, 045010, 2009.

[60] X. Niu, S. Peng, L. Liu. W. Wen, and P. Sheng, "Characterizing and Patterning of PDMS-Based Conducting Composites," Advanced Materials, vol. 19, pp. 2682-2686, 2007.

Chapter 3

Scalable and Stretchable Fully Integrated Pressure/Temperature Sensor Array with Magnetically Aligned and Patterned Nickel Conductive Composite Material

3.1 Introduction

Implementation of electronic artificial skin has been widely studied, from basic concept [1-3] to prototypes [4-6], for potential applications in robot engineering and prosthetic replacement. Artificial skin plays a key role of sensing external environment, such as pressure and temperature, and delivering transformed signals either to robot control or human nerve system. No matter what applications are, many researchers have tried to mimic human skin in terms of functionality and

sensitivity [12]. Although several types of sensing mechanisms based on resistive capacitive and optical devices have been used for sensing elements, unfortunately most of the research has been focused on pressure sensing devices.

In order to truly mimicking human skin, artificial skin at least needs to contain both pressure and temperature sensing elements in an array format. In fact, a couple of trials have been attempted to integrate sensing both elements onto single skin. Combination of commercial temperature sensing chips with printed pressure sensitive resistor or assembly of separately fabricated sensor arrays of each type [5] has been demonstrated. These hybrid type integration or assembly approach renders rather complicated processes and thus increases fabrication cost.

For sensing elements, conductive composite materials have been commonly used [7, 8, 14-18], whose resistance changes as geometrical dimension changes with applied pressure or temperature. In most cases, the conductive composite materials have been used only for single type of sensing element, either pressure or temperature [14, 17] sensor. It is challenging to differentiate two type of sensing part in one substrate with single conductive composite material and to independently read out each signal. Therefore, there have been no reported researches on using single conducting composite materials to a multi-sensing device.

In addition, the conductive composite materials were typically fabricated "on" either flexible or stretchable substrate only after readout active-matrix circuitry was

fabricated on the substrate [4, 5, 13, 19]. Therefore, there can be limitation in selection of materials and device structure, and process incompatibility that can makes mass manufacturing of the active-matrix sensor arrays difficult. However, when the sensor arrays are separately fabricated by embedding the sensing elements in the substrate, they can be easily incorporated into passive-matrix system or can be simply laminated on the separately fabricated active-matrix circuitry, as in case of the electronic paper front-plane technology.

In this chapter, we report a simple fabrication method of integrated pressure/temperature sensor arrays by embedding conductive nickel (Ni) particles in poly (dimethyloxane) (PDMS) medium. The pressure and temperature sensing parts are formed in one pixel but have different heights, which are implemented by introducing a corrugated structure to Ni/PDMS composite with a pre-patterned aluminum mold. Since Ni particles are ferromagnetic materials, we also patterned them by exposing Ni/PDMS to patterned magnetic fields produced with pre-patterned iron structure (we will call the structure "magnetic field modulator"), resulting in an embedded Ni dot array. Magnetic field exposure helped both lateral patterning and vertical particle alignment, which directly improved sensitivity and linearity of the sensor. Independent and stable read-out signals for pressure and temperature sensors are successfully obtained even under repeated measurements. Our technology has advantages of simple tuning for sensitivity and operation ranges

by changing particle concentration and device physical dimension, easy scaling-up to large area by seamlessly bonding small arrays or using large-area magnetic field modulator, and potential implementation of the sensor front-plane for active-matrix backplane read-out circuitry. Artificial skin passive-matrix system and active-matrix front-plane with about 10 ppi resolution with the integrated 16 by 16 pressure and 15 by 15 temperature sensor arrays have been finally demonstrated.

3.2 Materials and Fabrication Method

Poly (dimethyloxane) (PDMS: Sylgard 184 from Dow Corning) was used as base material. And nickel powder(from Sigma Aldrich) was used as conductive filler which diameter is <150μm. Figure 3.1 shows Fabrication processes of stretchable sensor array. PDMS base was mixed with hardener at 10:1 weight ratio. And then nickel powder was mixed into PDMS at 30wt.%. Each PDMS/nickel composite material was mixed during at least 10minutes. After mixing, PDMS/nickel composite material was moved in vacuum chamber for degassing. Degassed PDMS/nickel composite material was poured onto aluminum mold. After aluminum mold seal up, designed magnetic field modulator were attached on top and bottom side of aluminum mold. The magnetic field modulator has 481 tips (for 16 by 16 pressure sensor array and 15 by 15 temperature sensor array). Each tip has 1mm by 1mm area, and between the two closest tips distance is 1.77mm (=14dpi). And two neodymium permanent magnets were attached on outside of the each magnetic field modulator. In these all structure, magnetic field from permanent magnet was induced in each tips confront area through the aluminum mold. In this situation, nickel powder which was into the PDMS moved to the magnetic field induced area. Moving nickel powder by the patterned magnetic field means each sensor cell separate perfectly. Patterned magnetic field help cell separation as well as nickel powder align vertically in the PDMS elastomer. Vertically aligned sensor shows better electrical performance which like conductivity and uniformity than random

arranged sensor. PDMS/nickel composite material was exposed to the patterned magnetic field during 10 minutes. After finish exposing magnetic field, aluminum mold was moved on a hot plate and then cured. Curing condition is 10minutes at 150 °C. After curing, sensor sheet which has 481 sensor cells was completed. Each sensor cell size is 1mm by 1mm area. And pressure, temperature sensors thickness are 0.75mm and 0.25mm, respectively. Figure 3.2 shows Image of as-fabricated sensor array without electrodes. As a reference we fabricated same size sensor sheet but it was not exposure to magnetic field which means nickel powder was randomly arranged. To measure the sensor characteristics, we used printed silver electrode by inkjet printer (Dimatix 2800 series) on plastic substrate. To obtain good adhesion between printed silver electrode and sensor surface, we introduced large surface roughness on the sensor surface.[20] To introduce surface roughness on the sensor sheet, we use roughened aluminum mold which was made by wire-electro discharging machine (wire-EDM) method. The surface roughness was 1 to 1.5 μm in root-square-value and 4 to 6 μm in peak-to-valley value measured by atomic force microscopy (AFM) in non-contact mode**.** Resistance was measured by Keithley 2400. Pressure applied to the sensor cell by home-made machine with in-situ measurement of resistance change.

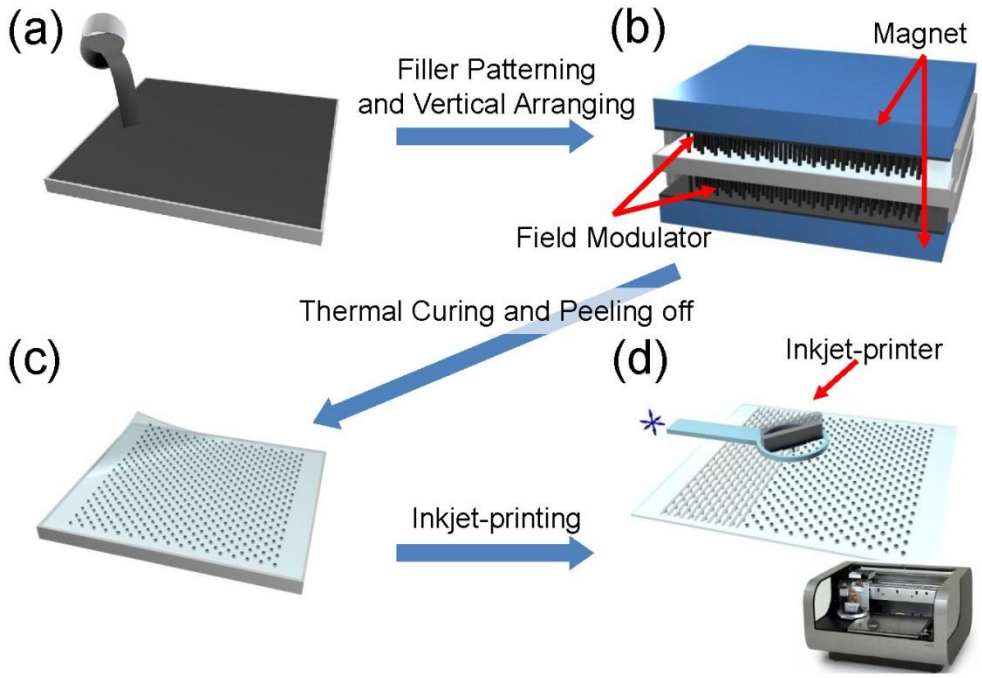

Figure 3.1 Fabrication processes of stretchable sensor array. (a) Nickel/PDMS mixture casting onto aluminum mold. (b) Nickel filler arranging and patterning by the magnetic field modulator. (c) Cured sensor array. (d) Inkjet-printing of silver electrodes onto sensor array.

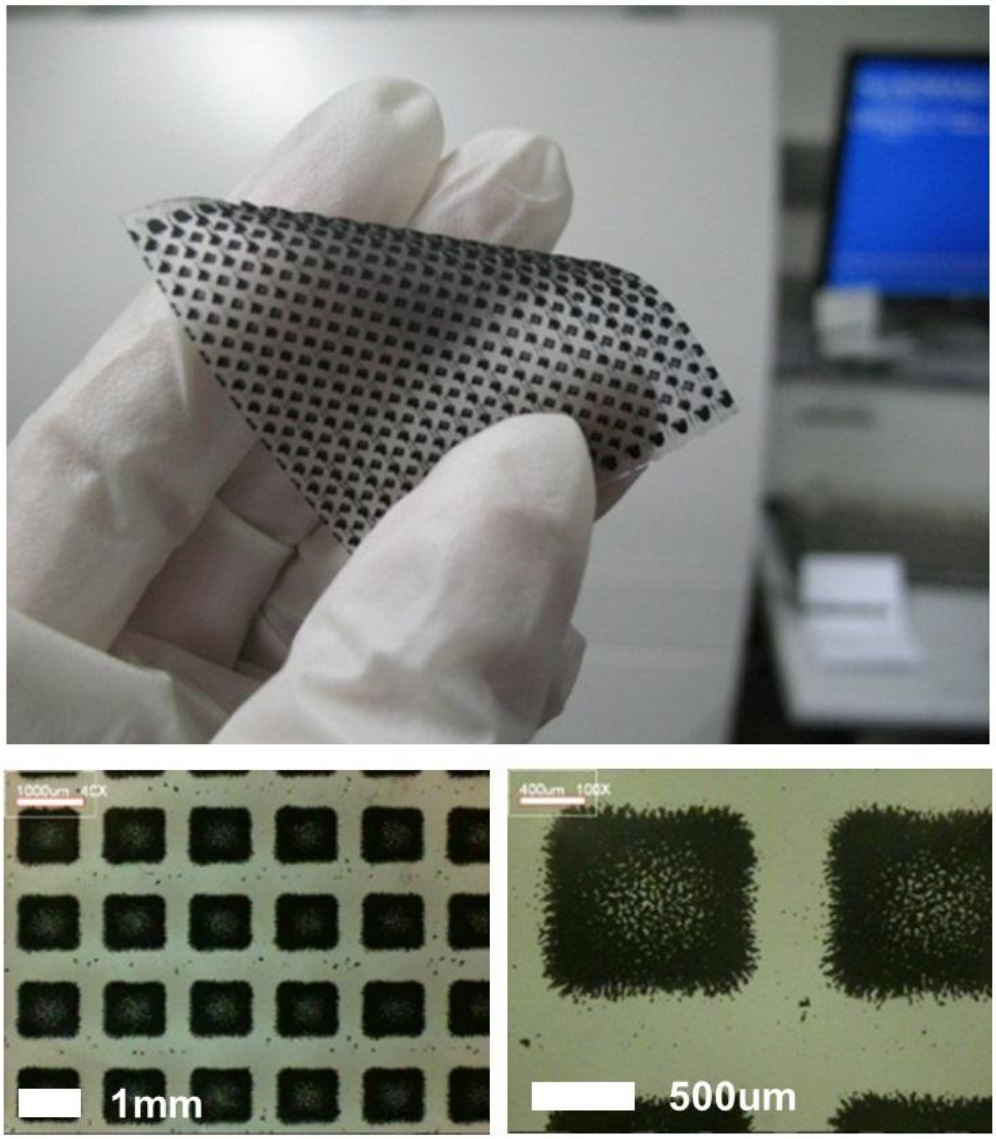

Figure 3.2 (Top) Image of as-fabricated sensor array without electrodes. (Bottom left) Optical microscope images of 40x magnifications and (Bottom right) 100x magnifications.

3.3 Finite Element Analysis for Patterning and Mechanical Characteristics

Feasible limit of the magnetically patterning method is a one of the important consideration. It is not easy to control shape of magnetic field precisely and minimum feature size or pitch of the patterned conductive composite is very important for various applications. Indeed, we are trying to develop better ways to improve the minimum feature size but for now, we are using field modulator to make patterns, whose shape and pattern will determine the final patterned conductive composite's shapes. Based on our electro-magnetic field simulation result that is based on the finite element analysis (FEA) (by the Maxwell 12 from ANSYS Ansoft), there are major parameters that determine minimum feature size of the patterned shapes on the assumption that all patterned shapes are square, such as line width (*W*) and spacing in between (*S*), (or pitch (*P*)), and thickness (*T*) of the patterned conductive composite. For the electro-magnetic field simulation, we prepared simplified model of the magnetic field modulator which is able to patterning of 13 square cells. Each pattern shape is 1000 μm by 1000 μm square and spacing is 770 μm, as shown in Figure 3.3.

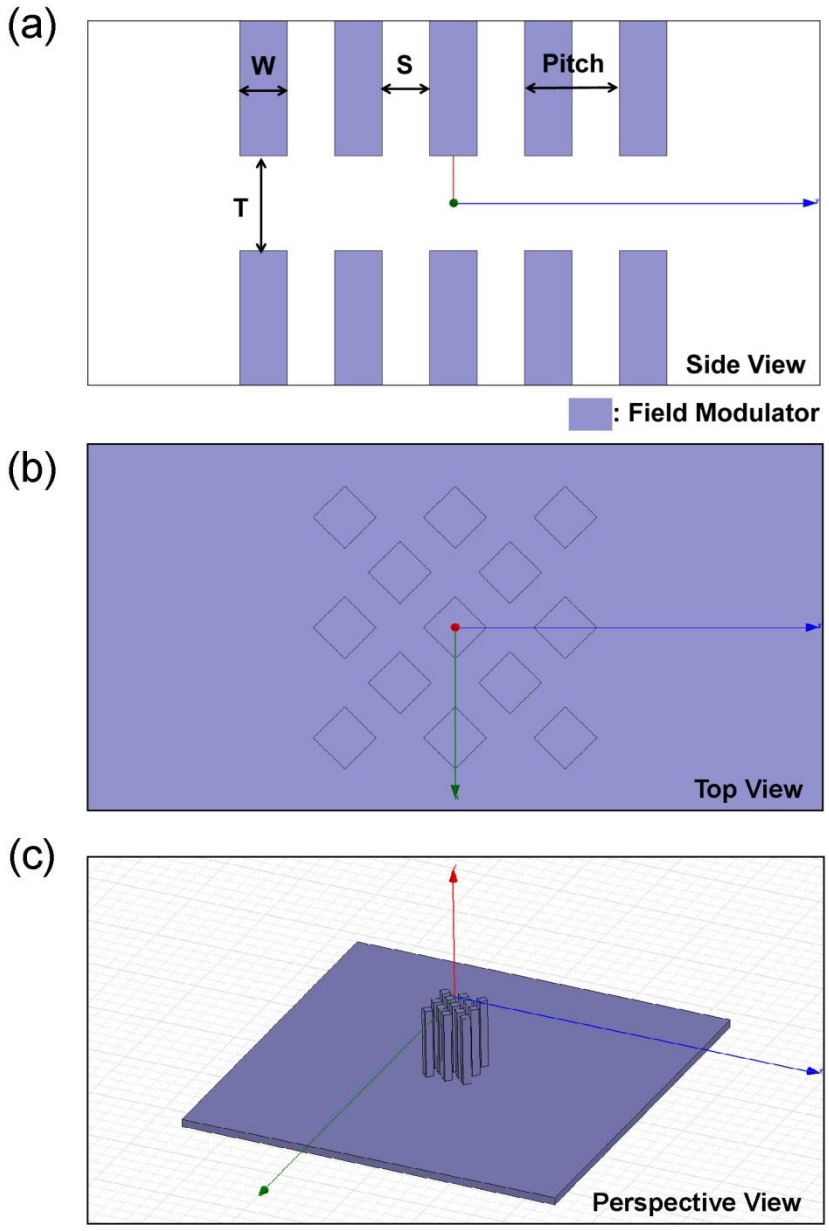

Figure 3.3 Simplified magnetic field modulator model for the electro-magnetic field simulation by using the MAXWELL 12, which is able to patterning of 13 square cells with 1000-μm width (*W*) and 770-μm spacing(*S*). (a) Side view of two face to face magnetic field modulators. (b) Top view. (c) Perspective view.

Based on our analysis, achievable minimum value of *W* and *S* (or *P*) is determined by the magnetic field distribution under the field modulation edges and closely related to *T*. When *T* is much larger than *W*, fillers are located at top and bottom area without being connected to each other. When *T* is much larger than *S*, lines can be connected to each other due to spreading of the magnetic field in the lateral direction. To verify the effect of the *T*, we accomplished the magnetic field simulation by using the simplified magnetic field modulator model with different values of *T* of 100um, 200um, 500um, 1000um, 2000um, and 5000um. Magnetic sources were two neodymium magnets with the coercivity of 890000 A/m. A shape of the each magnet was a box with area of 50 mm^2 square and thickness of 10 mm. Detail solution setup of the electro-magnetic simulation is a magneto-static with 20 numbers of passes and 0.1 percent error. Magnetic flux density [B] distributions of the electro-magnetic simulation are plotted in Figure 3.4. If the magnetic field exposure time is fully sufficient, the magnetic field gradient is more important than strength. When we compare the magnetic flux density distributions with different thicknesses, we can find a definite characteristic that the thickness of the patterned conductive composite increases, the shape of the pattern is a vaguer, as shown in Figure 3.4 (e) and (f). According to the electro-magnetic field simulation, we cannot definitely distinguish pattern by pattern above the thickness of 2000 um, when the condition of the pattern spacing is 770 um.

(a)

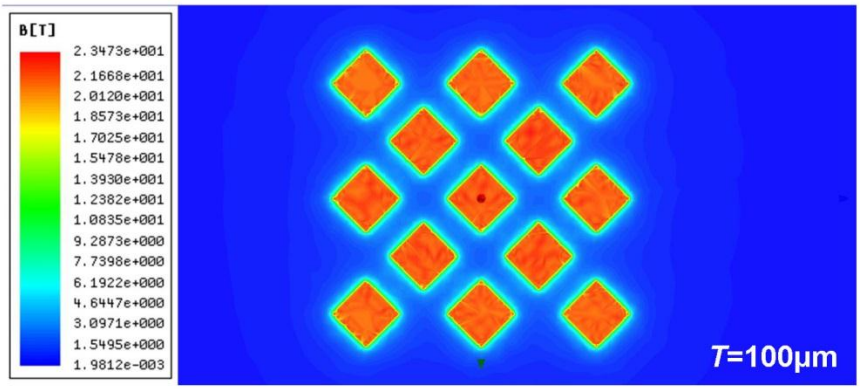
B[T]
2.3473e+001
2.1668e+001
2.0120e+001
1.8573e+001
1.7025e+001
1.5478e+001
1.3930e+001
1.2382e+001
1.0835e+001
9.2873e+000
7.7398e+000
6.1922e+000
4.6447e+000
3.0971e+000
1.5495e+000
1.9812e-003
T=100μm

(b)

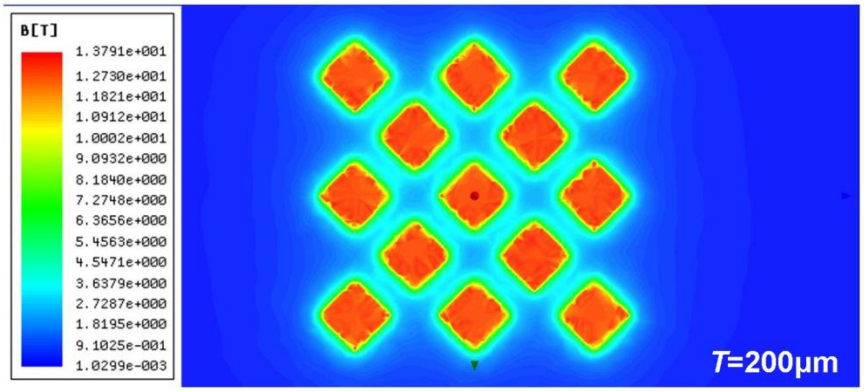
B[T]
1.3791e+001
1.2730e+001
1.1821e+001
1.0912e+001
1.0002e+001
9.0932e+000
8.1840e+000
7.2748e+000
6.3656e+000
5.4563e+000
4.5471e+000
3.6379e+000
2.7287e+000
1.8195e+000
9.1025e-001
1.0299e-003
T=200μm

(c)

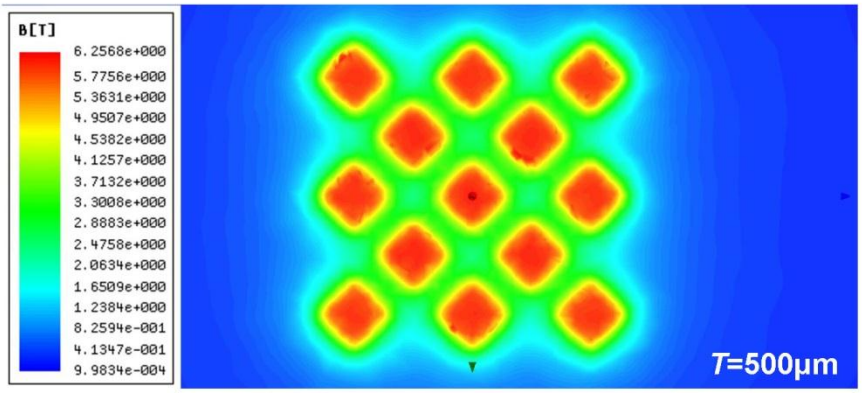
B[T]
6.2568e+000
5.7756e+000
5.3631e+000
4.9507e+000
4.5382e+000
4.1257e+000
3.7132e+000
3.3008e+000
2.8883e+000
2.4758e+000
2.0634e+000
1.6509e+000
1.2384e+000
8.2594e-001
4.1347e-001
9.9834e-004
T=500μm

(d)

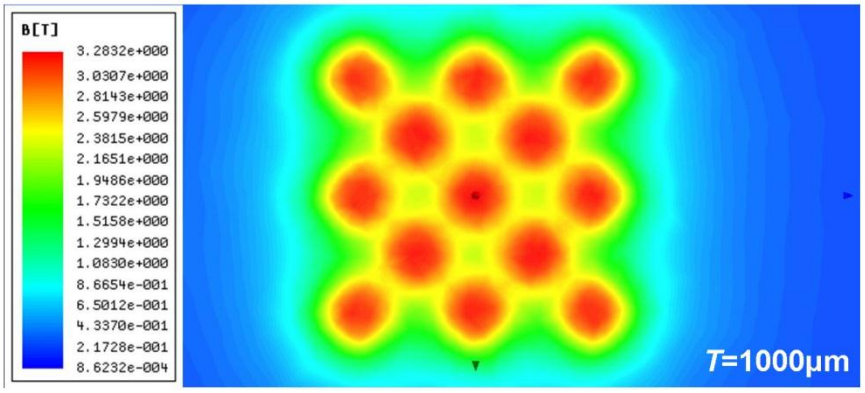
B[T]
3.2832e+000
3.0307e+000
2.8143e+000
2.5979e+000
2.3815e+000
2.1651e+000
1.9486e+000
1.7322e+000
1.5158e+000
1.2994e+000
1.0830e+000
8.6654e-001
6.5012e-001
4.3370e-001
2.1728e-001
8.6232e-004
T=1000μm

(e)

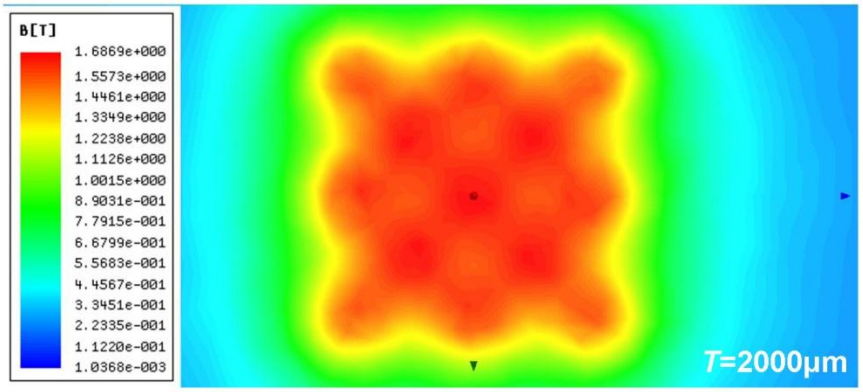

(f)

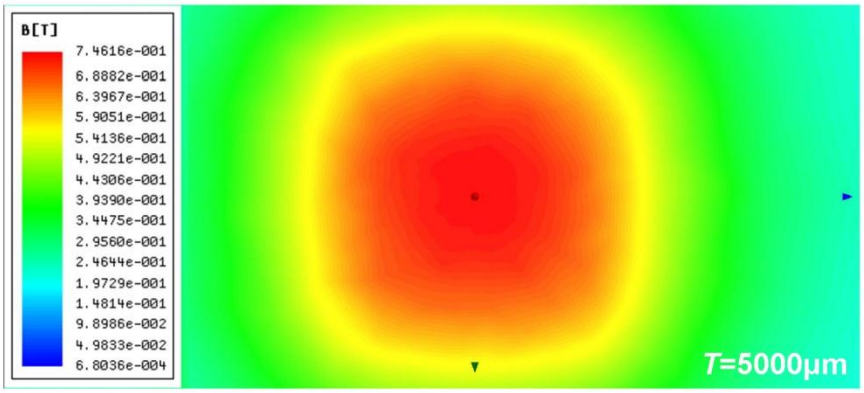

Figure 3.4 Magnetic flux density [B] distributions of the electro-magnetic simulation (by MAXWELL 12 from ANSYS Ansoft) with different values of *T* of (a) 100um, (b) 200um, (c) 500um, (d) 1000um, (e) 2000um, and (f) 5000um.

Therefore, theoretically, if we can reduce *T* as much as we can and we can focus the magnetic field (or we can produce the field modulator with edge dimension for *W* and *S*) to the similar scale of *T*, we can achieve smaller feature size (finer line patterns with fine spacing in between). However, since we think that particle size of the nickel may affect the maximum *T* needed for particle movement during the patterning process, the feasible minimum pattern size could be larger than the theoretical value. In addition, practically, it is hard to produce iron field modulator with very fine feature. In current work, *T* can be relatively easily controlled by the mold thickness. However, control of the *W* and *S* (or *P*) is much harder than *T* because they depend on geometry of the field modulator. The field modulator that was used in this work had been made by Electrical Discharge Machining (EDM) method. At present, as far as we know, EDM method has a limited resolution around 100 μm, in case of high aspect-ratio structure like our field modulator. If we can make a field modulator with finer pattern structure, we believe that we can further reduce the minimum feature size, considering the size (~5 μm) of the used nickel particles, from current 100 μm to around 50 μm.

When sensor cells are patterned in the PDMS matrix, there is another advantage in point of the stretchability of the sensor array beside cross talk and fabrication issues. Conductive composite materials show a resistivity variation by tensile strain as well as applied pressure. An elongation by an uniaxial tensile strain and a compression by an applied pressure with a transverse direction to the applied uniaxial tensile strain cause a similar effect to a resistivity variation along the applied pressure direction.

This phenomenon can be explained by the Poisson's ratio. The Poisson's ratio is the ratio of lateral contraction to longitudinal elongation. When a material is expanded (or compressed) in one direction, it usually tends to compress (or expand) in the other two directions perpendicular to the direction of expansion (or compression). We observed this phenomenon with two dimensional finite element analysis (2D-FEA) by using COMSOL MULTIPHYSICS from COMSOL Incorporation. To investigate the effect of magnetically patterning, we examined two different simplified models as compared with real fabricated one. First model is a sheet of a conductive composite material, that is composed of PDMS and 66.7 wt% of homogeneously mixed nickel, with 10-mm length, 10-mm width, and 250-um thickness. Second FEA model is also shown in Figure 3.5(a). Second model is a sheet of PDMS including magnetically patterned 13 conductive composite cells. Each cell's effective nickel weight fraction is 66.7 wt%. Whole sheet's dimension is

10-mm length, 10-mm width, and 250-um thickness and each conductive composite cell have 1-mm length, 1-mm width, 250-um thickness and cell's pitch is 1.77 mm. The FEA model for patterned conductive composite including cell arrangement is shown in Figure 3.5(b).

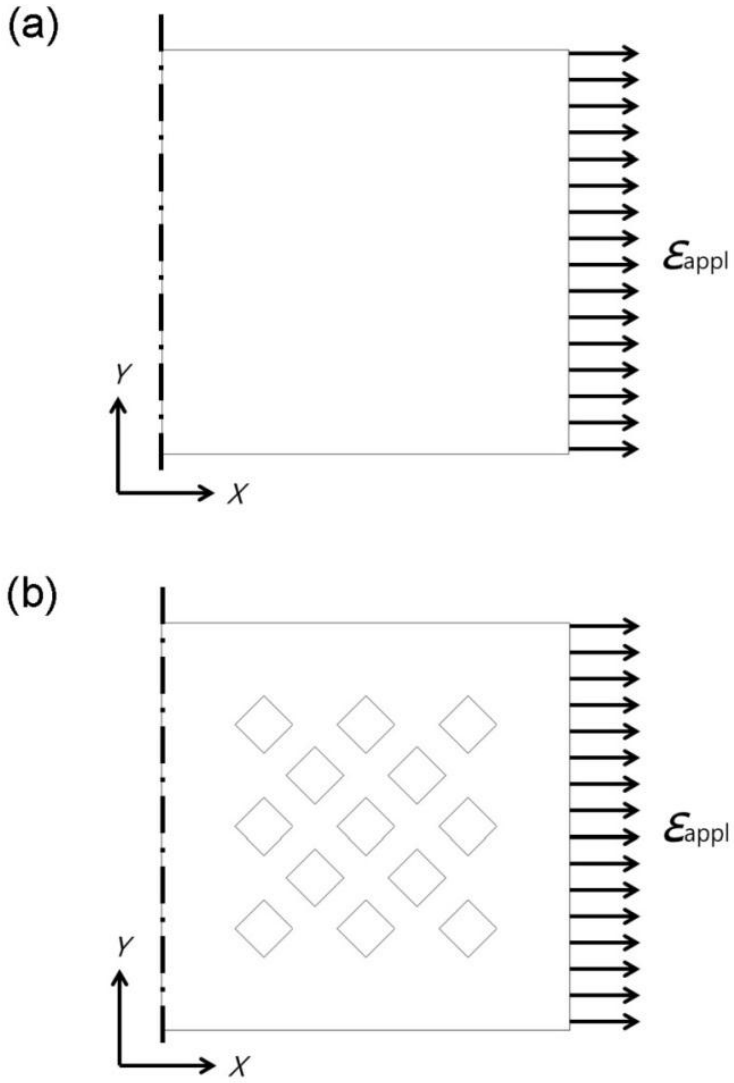

Figure 3.5 Finite element analysis (FEA) models for the tensile test. (a) Model for the sheet of bare conductive composite with 66.7 wt% of nickel fraction. Dimensions are 10-mm length, 10-mm width, and 250-um thickness. (b) Model for the sheet of patterned conductive composite. Effective nickel fraction of each patterned conductive composite is 66.7 wt%. Dimensions of the sheet are 10-mm length, 10-mm width, and 250-um thickness, and patterned conductive composite has 1-mm length, 1-mm width, and 250-um thickness.

To input physical parameters for FEA simulation, we measured physical properties of our materials such as the Young's modulus by tension test, as shown in Figure 3.6. The Young's modulus is measured with slightly differences as a measuring condition or details of the sample. Particularly, the Young's modulus of the PDMS is affected by various dependent factors such as a baking temperature and time, thickness of membrane, and ratio of the curing agent [21-23]. To measure the stress-strain curve, we prepared bare PDMS and magnetically aligned conductive composite materials with 10:1 ratio of PDMS base and curing agent, and for 30 minute baking time in convection oven at 130°C. And the sample thicknesses were fixed at 1 mm. Specimens were prepared by following the Korean Industrial Standards-KS M 6518 test standard for physical testing methods for vulcanized rubber [24]. Temperature and humidity of the testing environment were 23C and 30% RH, respectively. The tensile tester provided up to 200 N in tensile force and a 5 mm s^{-1} loading speed was chosen. The results of tension test of bare PDMS film and aligned conductive composite film with 1-mm thickness are shown in Figure 3.6. The tensile stress of the specimen was obtained by using the followed Equation (3.1),

$$\sigma_E = \frac{F}{A_0} \tag{3.1}$$

where F is the applied force, and A_0 is the original cross sectional area of the specimen. And the strain was obtained by using the followed Equation (3.2),

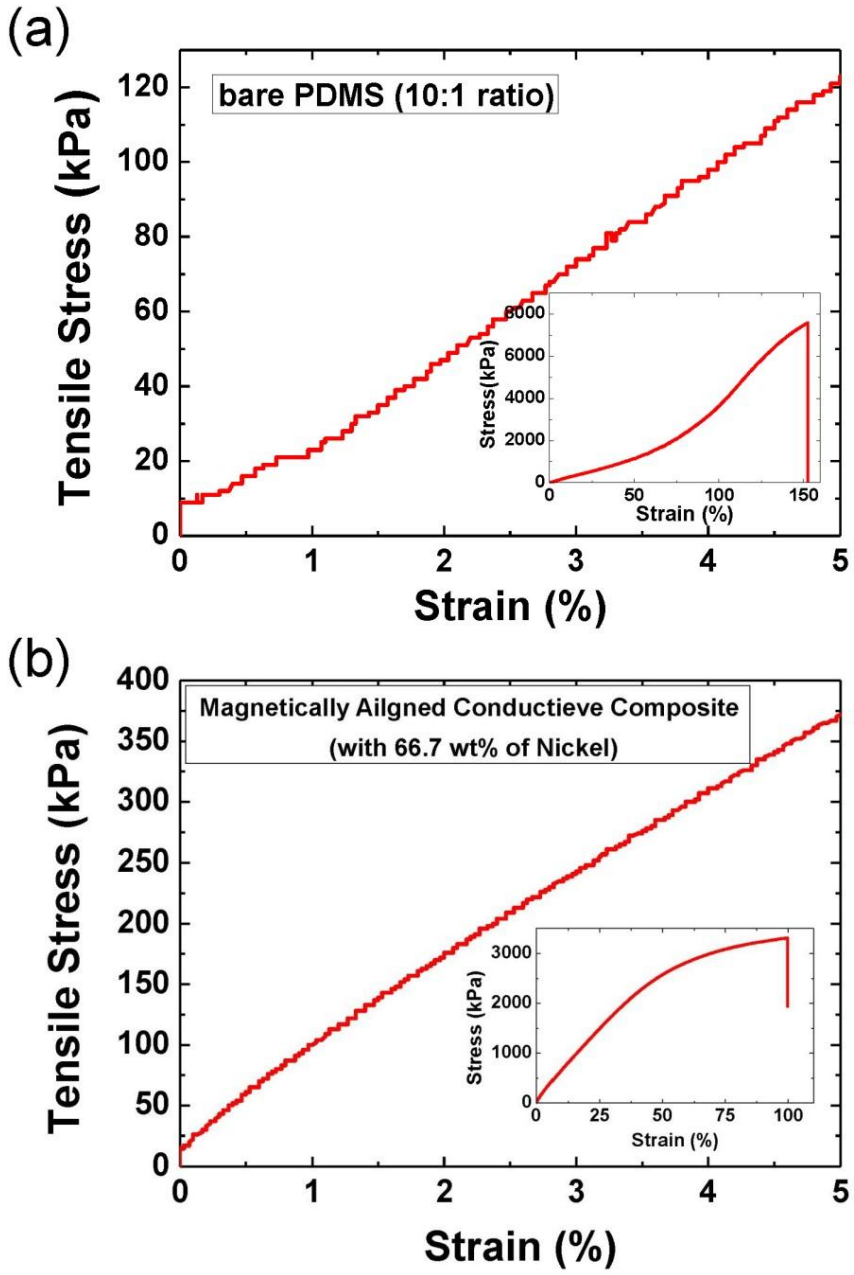

Figure 3.6 Tensile stress versus strain curves of (a) bare PDMS film of 10:1 ratio of base polymer and curing agent and (b) magnetically aligned conductive composite film with 66.7 wt% of nickel.

$$\varepsilon_E = \frac{\Delta L}{L_0} \tag{3.2}$$

Where ΔL is the elongation of the specimen and L_0 is the original length of the specimen. In addition, since PDMS and its composite materials are able to withstand large amount of tensile strain, we used true strain (ε*) and true stress (σ*) for the calculation of the Young's modulus, as followed equations.

$$\varepsilon^* = \ln(1 + \varepsilon_E) \tag{3.3}$$

$$\sigma^* = \sigma_E(1 + \varepsilon_E) \tag{3.4}$$

$$E = \frac{\sigma^*}{\varepsilon^*} \tag{3.5}$$

The Young's modulus was calculated from the slope within first linear region of the true stress/strain curves. In addition, density of conductive composite with 66.7 wt% of nickel was calculated by using well known densities of PDMS and nickel, 965 kg/m^3 and 8.908 g/cm^3, respectively.

The measurements indicate that the Young's modulus and Poisson's ratio for the bare PDMS, which is made with 10 : 1 weight ratio of a primary and curing agent, are 877 kPa and 0.499, respectively. And the Young's modulus and Poisson's ratio of a magnetically aligned conductive composite material with 66.7 wt% of

nickel were 9783 kPa and 0.64, respectively. In addition, the calculated density of conductive composite material is 6260 kg/m^3.

Surface strain distributions of a bare and patterned conductive composite sheet were computed, for the case of applied uniaxial tensile strain with different values of ε_{appl} = 10%, 30%, and 50%. Tensile strains were applied only one side of the boundary, however the opposite boundary was restricted as shown in Figure 3.5. In the case of the sheet of the bare conductive composite, similar level of the longitudinal strain (ε_{xx}) around 10% was occurred covering on whole surface when it is stretched by applied strain of 10%. And, around -6% of the transverse strain (ε_{yy}) was also occurred on whole surface. In the case of the sheet of the patterned conductive composite, however, a degree of occurred strain on areas of each sensor cell was extremely decreased. When 10% of uniaxial tensile strain was applied, the longitudinal strain and the transverse strain on the sensor cell are only around 0.7% and -0.5%, respectively. However, most of the bare PDMS matrix, that are located between patterned conductive composites, is received larger strains than the patterned conductive composite. The longitudinal strain and the transverse strain of the bare PDMS were around 15% and -8.5%, respectively. An effect of this strain minimization with isolation becomes more noticeable as larger strain is applied. In case of the applied strain of 30% and 50%, the sheet of bare conductive composite shows longitudinal strains of around 30% and 50%, while the patterned conductive

composite shows only around 2.3% and 3.8%, respectively.

Experimental results were consistent with simulation results. As shown in Figure 3.9(b), the magnetically patterned sensor array showed stable characteristics even at 30% tensile strain.

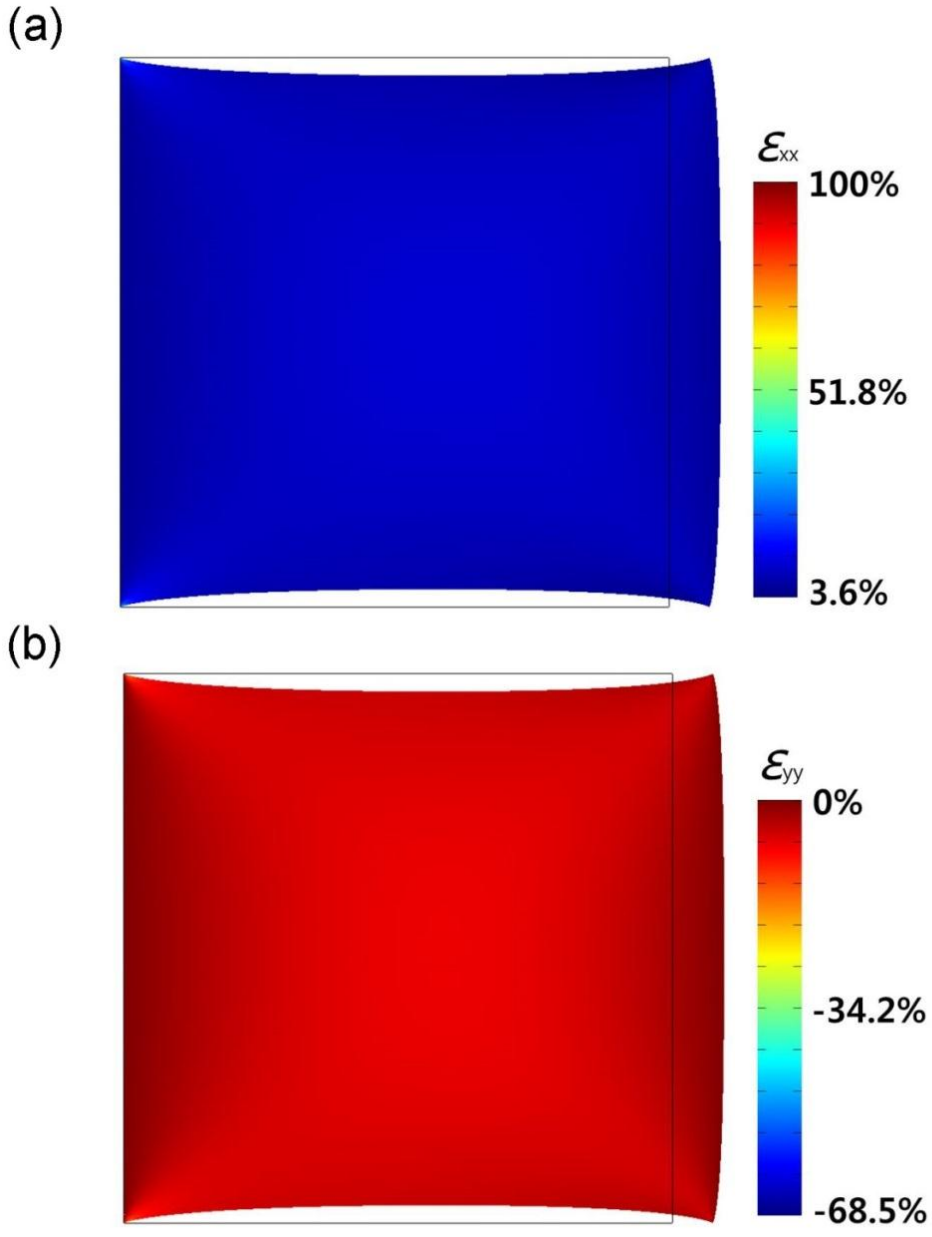
(a)
ε_{xx}
100%
51.8%
3.6%
(b)
ε_{yy}
0%
-34.2%
-68.5%

(c)

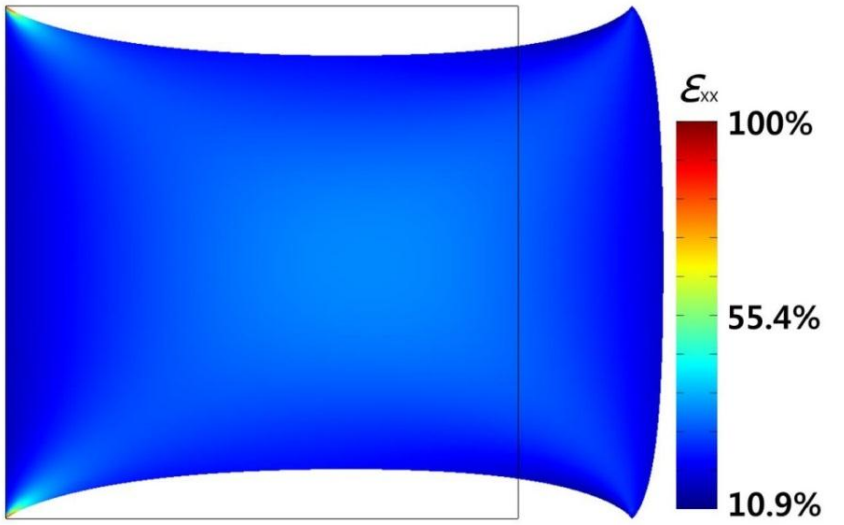

(d)

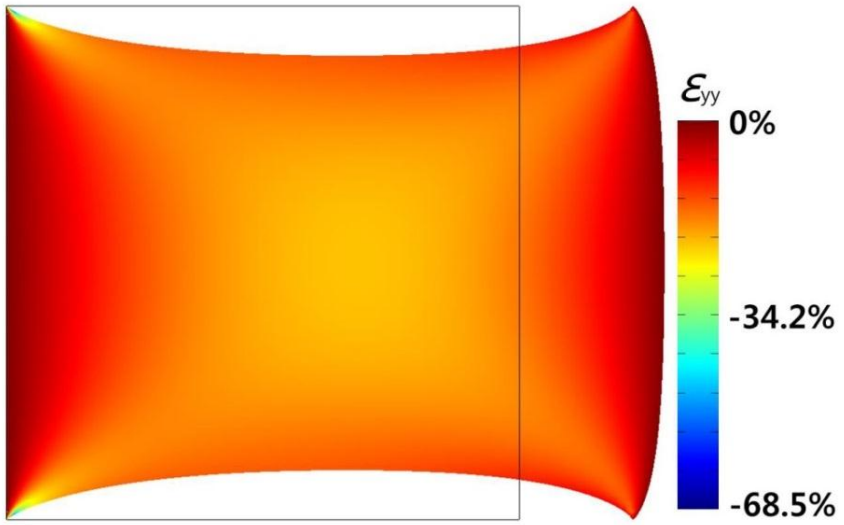

(e)

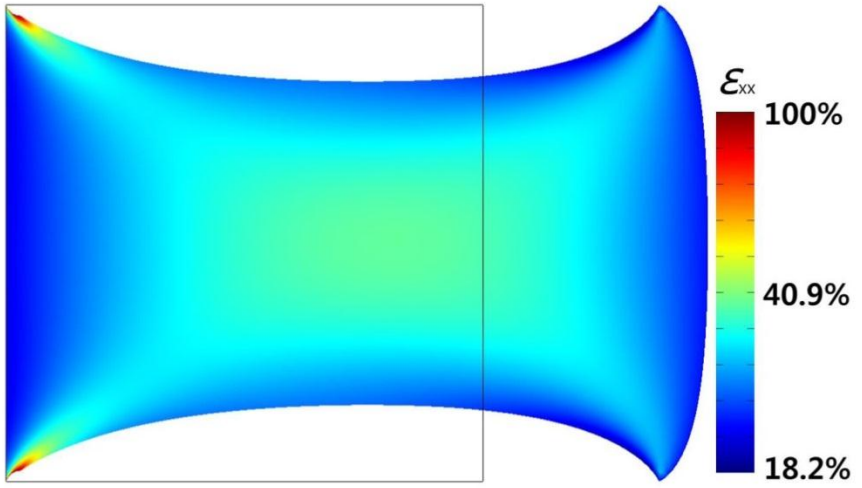

(f)

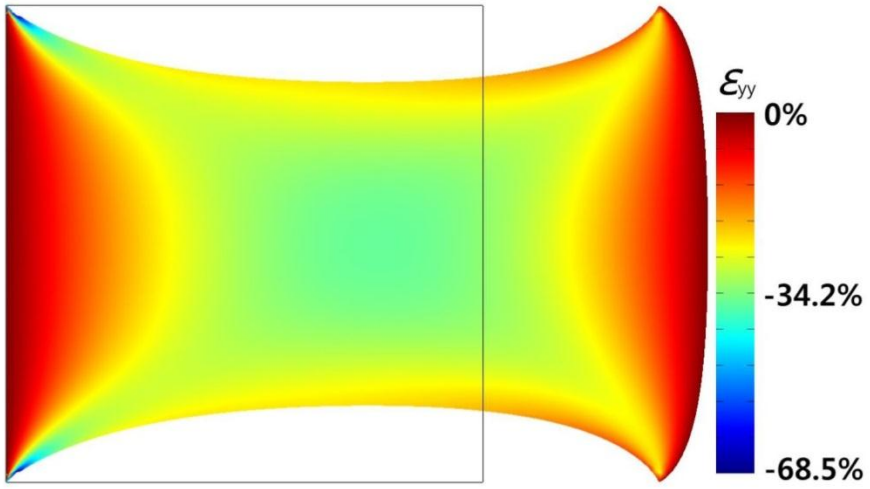

(g)

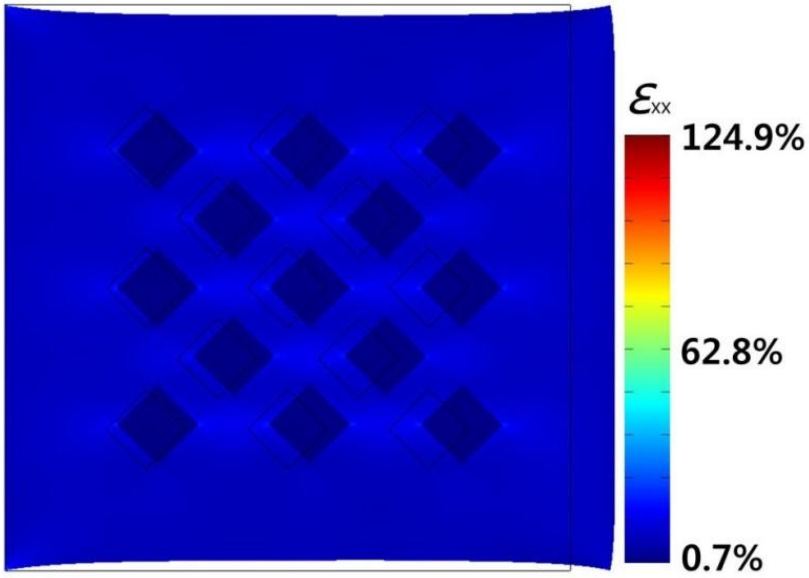

(h)

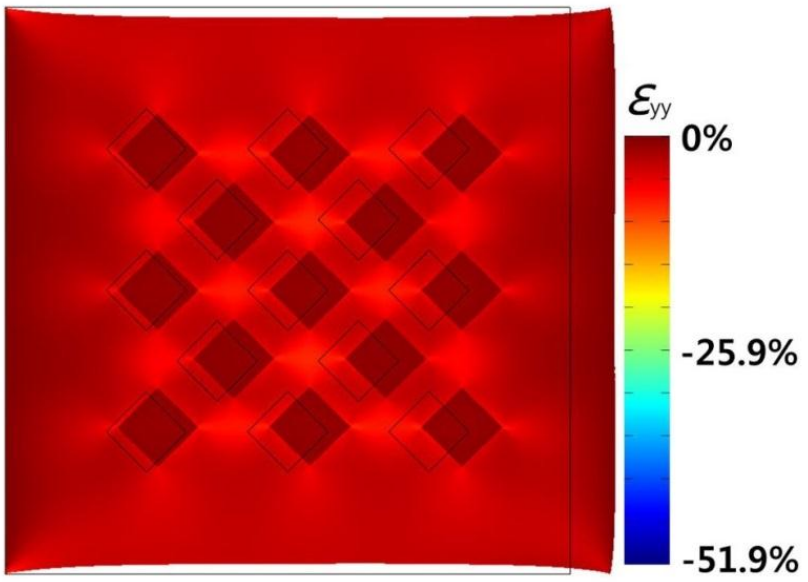

(i)

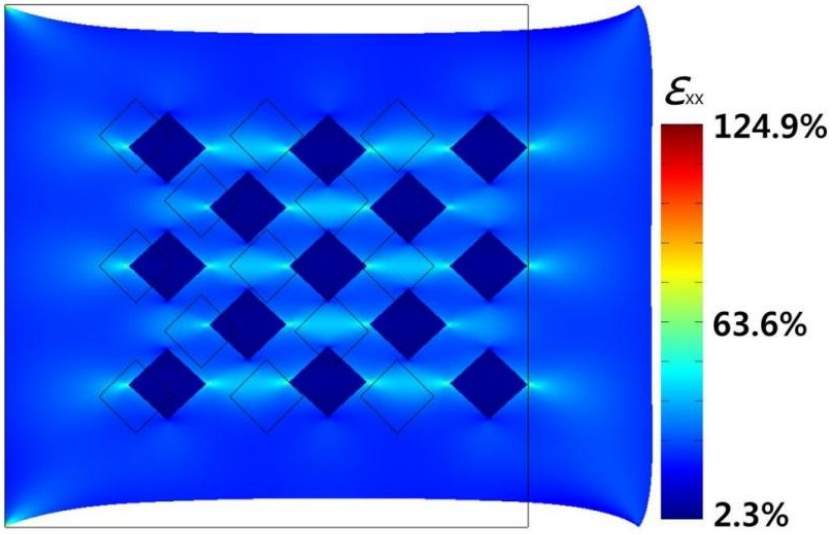

(j)

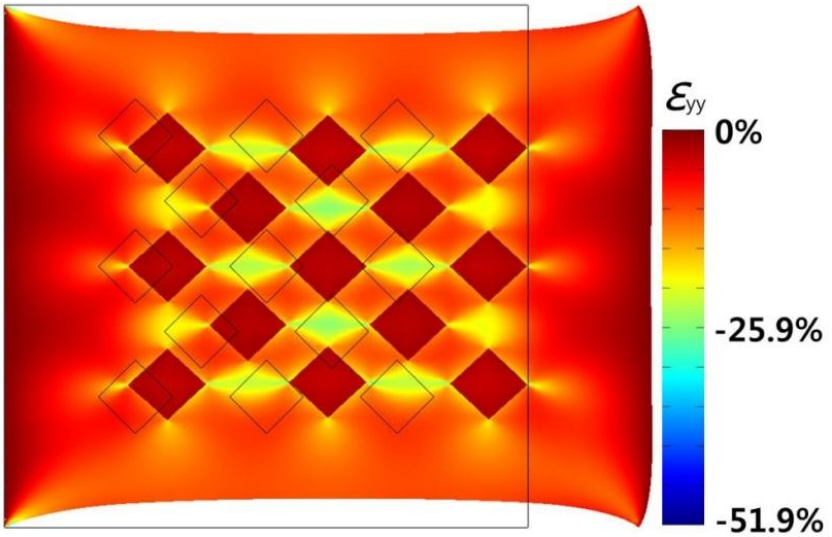

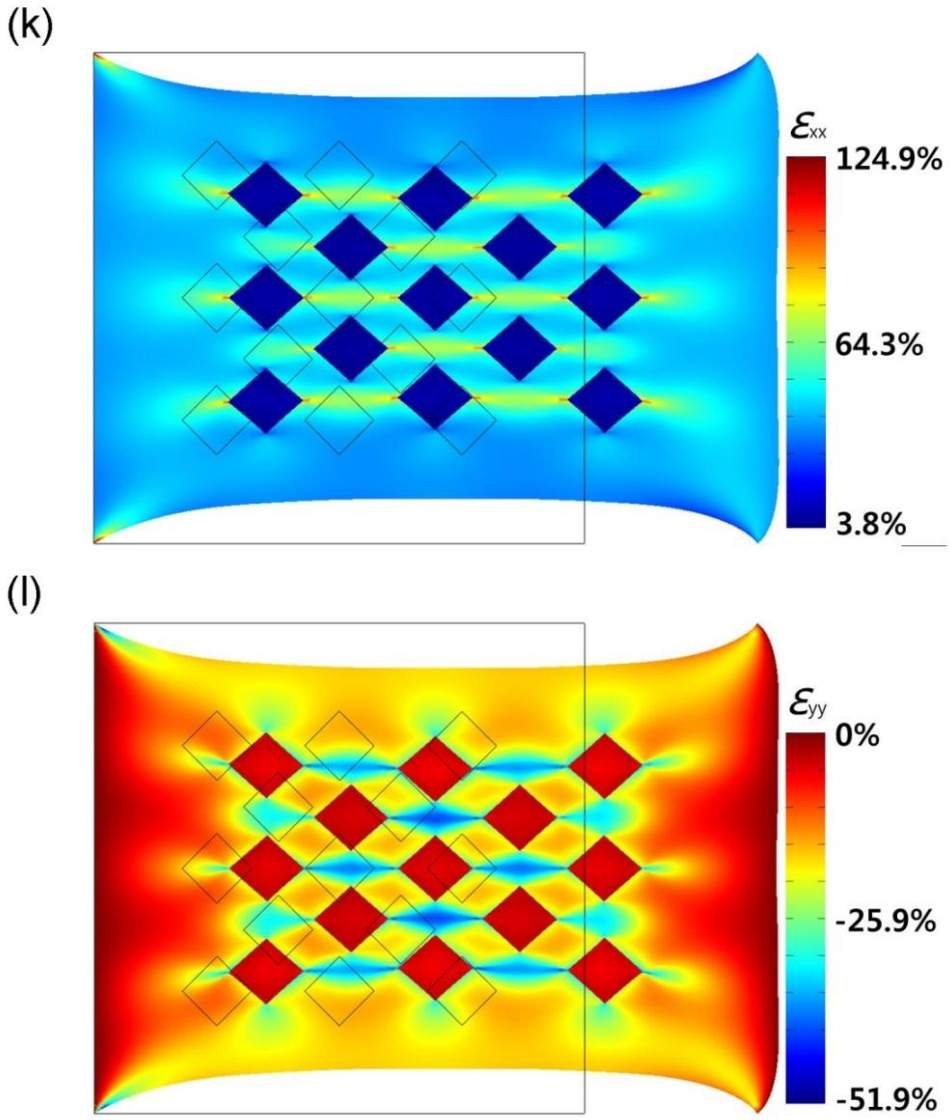

Figure 3.7 Surface strain distributions of the 2D-FEA simulation (by COMSOL MULTIPHYSICS from COMSOL Incorporation) for bare ((a)-(f)) and patterned conductive composite ((g)-(l)) with different values of applied strain of 10% ((a), (b), (g), (h)), 30% ((c), (d), (i), (j)), and 50% ((e), (f), (k), (l)).

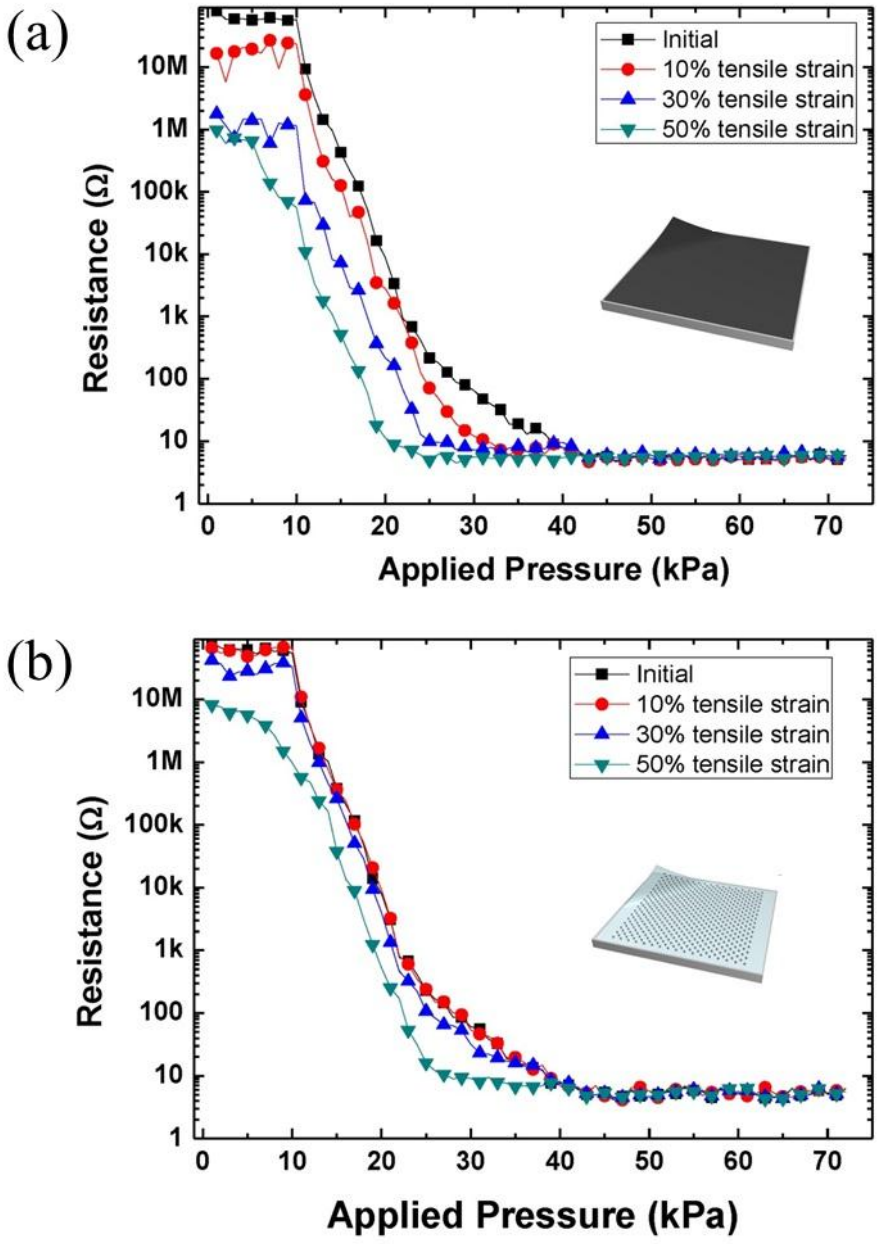

Figure 3.8 Pressure sensing characteristics shift according to 1D tensile strain of sheets of (a) non-patterned and (b) magnetically patterned nickel conductive composite materials.

3.4 Electrical Characteristics of Integrated Sensor Array

We accomplished array experiment with switching matrix system and Keithley 2400, in order to confirm operation of integrated pressure and temperature sensor array. We made three kinds of copper stamps shapes of alphabets S, N and U (**S**eoul **N**ational **U**niversity) respectively. Each alphabet stamp applies about 50 kPa to sensor array. We also set two different temperature conditions, which are room temperature and 70℃ respectively. Figure 3.10(a) shows room temperature condition experiment of 16 by 16 pressure sensor array. Time interval of measuring is 0.2 sec for 256 pressure sensor cells. In these re-constructed images, black area means low resistance area which was applied external pressure by copper stamp and white area means high resistance region which was not applied external pressure. As a result, we can recognize affected by copper stamps through applied pressure. Figure 3.10(b) shows 70℃ condition experiment of 15 by 15 temperature sensor array. The Stamp which was heated 70℃, on to the sensor array and measured. Like the preceding pressure sensor array result, we can recognize each character. To measure the pressure sensor characteristics in more actual situation, we applied several discrete forces by using pressure gauge manually. Figure 3.11(a) shows the result. Measured data is a slightly unstable because pressure was not applied by the mechanically. But the pattern of slightly resistance change is clearly recognizable. Figure 3.11(b) shows room temperature condition experiment of temperature sensor

while block applies pressure to entire sensor array. In the result, there is no significant resistance change. The reason is because temperature sensor which is part of our designed integrated sensor array is not affected by external applied pressure. Structurally, external force affects only pressure sensor if force resolution is bigger than 1.25mm. From these results, we confirm that applied pressure does not affect temperature sensor. This means that, temperature sensor can detects exact external temperature at any pressure applying condition. Accordingly, we can compensate detected pressure by post-data processing which is based on exact temperature result.

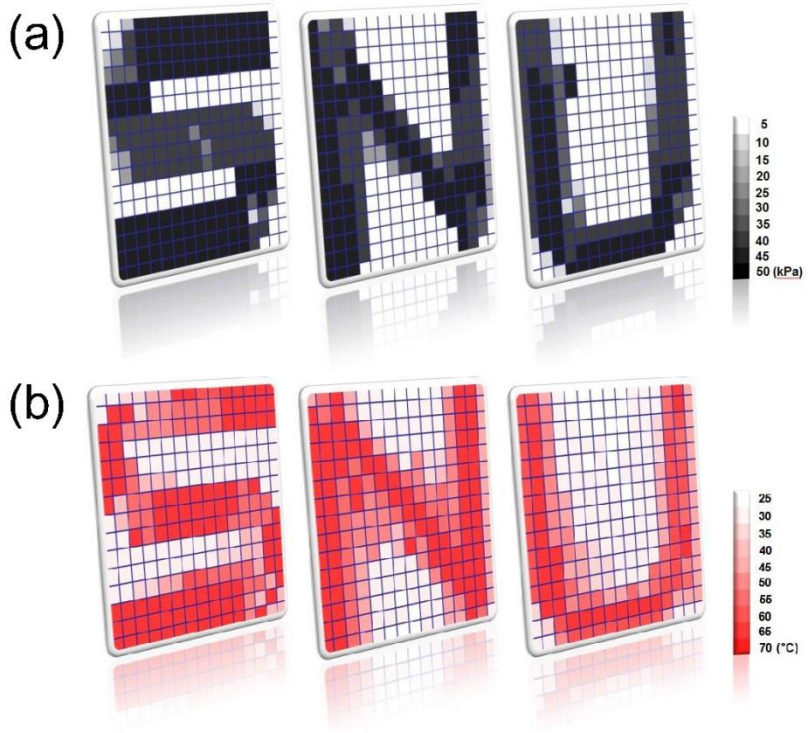

Figure 3.9 Two-dimensional mapping profiles obtained from experimental sensor cell responses. Characters ‘S’, ‘N’, and ‘U’, corresponding to the (a) applied pressure and (b) temperature

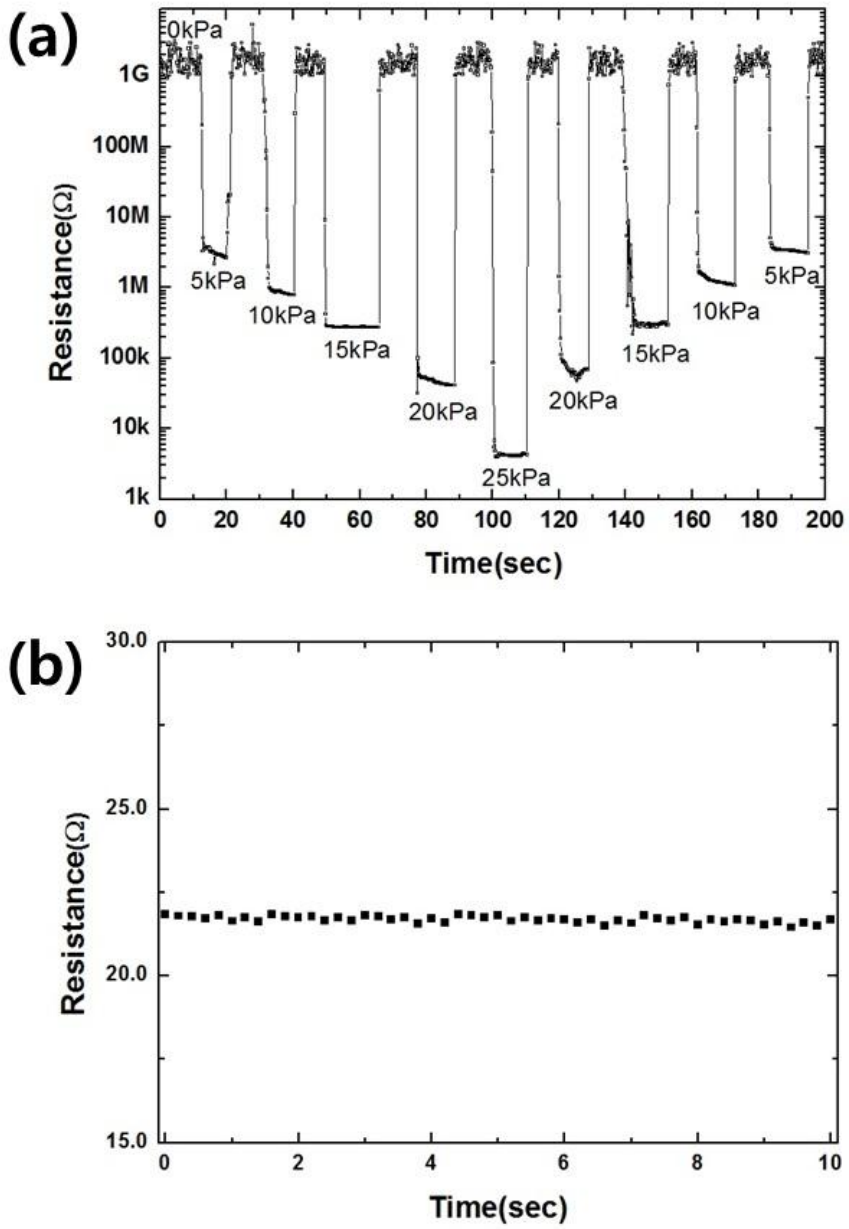

Figure 3.10 (a) Repeat operation characteristics of pressure sensor and (b) Stable operation characteristic of temperature sensor under external pressure applying.

3.5 Conclusion

In summary, we demonstrated stretchable pressure and temperature sensor integrated artificial skin by using conducting composite material and magnetically patterning method. Magnetically patterned sensor shows better sensing performance than bare sheet of conductive composite. Pressure and temperature sensitivities are 2mS/kPa and 0.713μS/°C, respectively. And two different sensors successfully integrated by import of uneven structure. Magnetically patterning method, which was introduced in this chapter, can be improved for high resolution and better sensing properties.

Reference

[1] V. J. Lumelsky, M. S. Shur, and S. Wagner, “Sensitive Skin," IEEE Sensors Journal. vol. 1, pp. 41-51, 2001.

[2] S. Wagner, S. P. Lacour, J. Jones, P. I. Hsu, J. C. Sturm, T. Li, and Z. Suo, “Electronic skin: architecture and components,” Physica E, vol. 25, pp. 326-334, 2004.

[3] R. Tajima, S. Kagami, M. Inaba, and H. Inoue, “Development of soft and distributed tactile sensors and the application to a humanoid robot,” Advanced Robotics, vol. 16, pp. 381-397, 2002.

[4] T. Someya, T. Sekitani, S. Iba, Y. Kato, H. Kawaguchi, T. Sakurai, “A large-area, flexible pressure sensor matrix with organic field-effect transistors for artificial skin applications,” Proceedings of the National Academy of Sciences, Vol. 101, pp. 9966-9970, 2004.

[5] T. Someya, Y. Kato, T. Sekitani, S. Iba, Y. Noguchi, Y., Murase, H. Kawaguchi, and T. Sakurai, “Conformable, flexible, large-area networks of pressure and thermal sensors with organic transistor active matrixes,” Proceedings of the National Academy of Sciences, vol. 102, pp. 12321-12325, 2005.

[6] J. Engel, J. Chen, and C. Liu, “Development of polyimide flexible tactile sensor skin,” Journal of Micromechanics and Microengineering, vol. 13, pp. 359-366,

2003.

[7] M. Hussain, Y.-H. Choa, and K. Niihara, “Conductive rubber materials for pressure sensors,” Journal of Material Science Letter, vol. 20, pp. 525-527, 2001.

[8] M. Shimojo, A. Namiki, M. Ishikawa, R. Makino, and K. Mabuchi, “A tactile sensor sheet using pressure conductive rubber with electrical-wires stitched method,” IEEE Sensors Journal, vol. 4, pp. 589-596, 2004.

[9] H.-K. Lee, S.-I. Chang, and E. A. Yoon, “Flexible polymer tactile sensor: fabrication and modular expandability for large area deployment,” Journal of Microelectromechanical System, vol. 15, pp. 1681-1686, 2006.

[10] H.-K. Kim, S. Lee, and K.-S. Yun, “Capacitive tactile sensor array for touch screen application,” Sensors and Actuators A: Physical, vol. 165, pp. 2-7, 2010.

[11] M. Rothmaier, M. P. Luong, and F. Clemens, “Textile pressure sensor made of flexible plastic optical fibers,” Sensors, vol. 8, pp. 4318-4329, 2008.

[12] S. C. B. Mannsfeld, B. C.-K. Tee, R. M. Stoltenberg, C. V. H.-H. Chen, S. Barman, B. V. O. Muir, A. N. Sokolov, C. Reese, ann Z. bao, “Highly sensitive flexible pressure sensors with microstructured rubber dielectric layers,” Nature Materials, vol. 9, pp. 859-864, 2010.

[13] K. Takei, T. Takahashi, J. C. Ho, H. Ko, A. G. Gillies, P. W. Leu, R. S. Fearing,

and A. Javei, “Nanowire active-matrix circuitry for low-voltage macroscale artificial skin,” Nature Materials, vol. 9, pp. 821-826, 2010.

[14] B. Lundberg, and B. Sundqvist, “Resistivity of a composete conducting po~ymer as a function of temperature, pressure, and environment: Appricatlons as a pressure and gas concentration transducer,” Journal of Applied Physics, vol. 60, pp. 1074-1079, 1986.

[15] J.-C. Huang, “Carbon Black Filled Conducting Polymers and Polymer Blends,” Advanced Polymer Technique, vol. 21, pp. 299-313, 2002.

[16] P. J. Mather, and K. M. Thomas, “Carbon black/high density polyethylene conducting composite materials,” Journal of Material Science, vol. 32, pp. 401-407 1997.

[17] H.-S. Chuang, and S. Wereley, “Design, fabrication and characterization of a conducting PDMS for microheaters and temperature sensors,” Journal of Micromechanics and Microengineering, vol. 19, 045010, 2009.

[18] X. Niu, S. Peng, L. Liu. W. Wen. and P. Sheng, “Characterizing and Patterning of PDMS-Based Conducting Composites,” Advanced Materials, vol. 19, pp. 2682-2686, 2007.

[19] Y.-J. Yang, M.-Y. Cheng, W.-Y. Chang, L.-C. Tsao, S.-A. Yang, W.-P. Shih, F.-Y. Chang, S.-H. Chang, and K.-C. Fana, “An integrated flexible temperature and

tactile sensing array using PI-copper films," Sensors and Actuators A: Physical, vol. 143, pp. 43-153, 2008.

[20] J. Jeong, S. Kim, J. Cho, D. Kim, and Y. Hong, "Stretchable low thick silver electrode on PDMS compliant elastomeric substrate," Japanese Journal of Applied Physics, vol. 49, 05EB09, 2010.

[21] D. Fuard, T. Tzvetkova-Chevolleau, S. Decossas, P. Tracqui, and P. Schiavone, "Optimization of poly-di-methyl-siloxane (PDMS) substrates for studying cellular adhesion and motility," Microelectronic Engineering, vol. 85, pp. 1289–1293, 2008.

[22] M. Liu, J. Sun, Y. Sun, C. Bock, and Q. Chen, "Thickness-dependent mechanical properties of polydimethylsiloxane membranes," Journal of Micromechanics and Microengineering, vol. 19, 035028, 2009.

[23] E. Gutierrez, A. Groisman, "Measurements of Elastic Moduli of Silicone Gel Substrates with a Microfluidic Device," PLoS ONE, vol. 6, e25534, 2011.

[24] The Korean Industrial Standards KS M 6518 test standard for physical testing methods for vulcanized rubber from: http://www.standard.go.kr/code02/user/0B/03/SerKs_View.asp?ks_no=KSM6518.

Chapter 4

Negatively Strain-Dependent Electrical Resistance of Magnetically Arranged Nickel Composite : Its Application to Highly Stretchable Electrode and Stretchable Lighting Devices

4.1 Introduction

In recent years, there has been an increasing interest in stretchable electronics. It has great potential in future electronics such as flexible display, wearable electronics and biomedical applications [1, 2]. With recent progress in stretchable electronics, electronic devices on the stretchable substrates can be protected from mechanical deformation by allowing the stretchable electrodes to undergo most of

the mechanical stress [3]-[6]. Previous stretchable electrodes were mainly realized by either vacuum deposition or inkjet-printing of metal thin film on elastomeric substrates [7]-[12]. These stretchable electrodes show very good electrical performance at relatively low tensile strain conditions typically lower than 30% elongation.

In order to realize stretchable electrode that can well sustain electrical performance at higher tensile strain conditions (over 30% elongations), conductive composite materials have also been widely used. Generally, conductive composite materials which are composed of elastomeric matrix and conductive fillers such as metal powder [13, 14], carbon black [15, 16], and graphite [17] show relatively high initial resistance to be used as interconnection between electronic devices. Recently carbon nanotube (CNT)-based conductive composite materials have been reported to stretchable electrode applications.[1, 18, 19] With special treatment, these materials show superior electrical property at over 30% tensile strain. In view of practical use, however, they require complex fabrication process to attain high initial conductivity and show significant decrease in conductivity with increasing tensile strain. Furthermore, patterning of the embedded conductive materials is also challenging for previously reported methods. Table 4-1 shows summary of recent representative conductive composites and their electrical characteristics with mechanical stretching, including our results. This comparative chart shows a typical tendency of most

conductive composites. It is hard to maintain initial conductivity under the tensile strain even if they have remarkable initial conductivity and can mechanically sustain at high tensile strain.

It is noted that most conductive materials show positively strain-dependent resistance change, i.e. resistance increases with the applied tensile strain, while our material shows opposite behavior. This unique property can be used as a device supplying power at high tensile strain conditions because the electrodes show low resistance when elongated. In addition, when combined with the inorganic metal films with very low initial resistance, high-performance stretchable electrodes with low resistance at both low and high tensile strain conditions can be implemented. Furthermore, our materials are ferromagnetic and thus can be patterned by a patterned magnetic field in a simple manner. Therefore, depending on the configuration of our composite-only and metal film electrodes, we can fabricate a new conceptual device, such as a stretchable lighting or display device with constant image resolution even under tensile strain conditions.

In this study, we report a novel property of negatively strain-dependent electrical resistance change of a composite where nickel powder conductive filler is embedded in an elastomeric medium. When the conductive fillers in the composite were arranged in a direction perpendicular to the strain plane under the magnetic field, the composite showed negative strain-dependency. When we used the

patterned magnetic field with the pre-patterned ferromagnetic iron structure, patterned and embedded composite electrodes were also simultaneously formed. Details of this process will be later described. In order to fabricate a highly stretchable electrode with a very low initial resistance (a few ohms for 10 mm long electrode), we combined the inkjet-printed silver thin film on the magnetically patterned and arranged conductive composite materials. Silver thin film provides very low initial resistance and maintains the value at low tensile strain range. As the tensile strain increases, the conductive composite with the negative strain-dependency takes over and maintains its resistance low at high tensile strain range. In addition, we also implemented a resolution-sustainable, stretchable lighting device, by appropriately configuring both composite-only and silver-covered composite electrodes as interconnecting lines for surface-mount light-emitting diodes (LEDs). In this conceptual device, hidden LED pixels are located between on-pixels and connected to the composite-only electrodes so that they supply power to and turn on the hidden pixels, maintaining the resolution of the lighting device, when the distance between on-pixels increases under the tensile strain.

Table 4.1 Mechanical and electrical properties of various conductive composite materials.

Ref.	Materials			Mechanical and Electrical Properties			Patterning Demonstration
	Conductive filler	Elastomeric and insulating matrix	Composition ratio	Failure strain [%]	Electrical Properties		
					Conductivity at applied strain (S/cm)		
					Initial	At high strain	
[17]	EG[a]	PDMS	PDMS with 15wt% of EG	30	~0.1	~0.1 at 30% strain	N/A
[20]	Carbon black	Silicon rubber	Silicon rubber with 15 wt% of carbon black	50	0.16	0.12 at 50% strain	N/A
[21]	Carbon fiber	Epoxy	Epoxy with 65 vol% of carbon fiber	N/A	N/A	7% increase in resistance at 1.6% strain	N/A
[22]	MWNT	SEBS[c]	SEBS with 15 wt% of MWNT	611	5.16	~10-4 at 300% strain	N/A
[19]	nAg-MWNT[d], Ionic liquid, Silver flake	PVDF[e]	(nAg-MWNTs, 100 mg; ionic liquid, 200mg; PVDF, 8.2 g) with 8.60 wt% silver flake, Post treated by hot-roll	140	5,710	20 at 140% strain	N/A
[23]	MWNT forest	Polyurethane	N/A	>1400	0.1-0.2	>4 times increase in resistance at 300% strain	N/A
[24]	MWNT, Ionic liquid, Silver nanoparticle	SIS[f]	1:2.6:45.4:51 (MWNTs:ionic liquid:SIS:Ag nanoparticle)	288	~3,700	~50 at 100% strain	Screen printing w/ contact mask
[25]	MWNT, Graphene	PDMS	PDMS with 1.3 wt% of grapheme/MWNT aerogel	N/A	2.8	~30% decreases in conductivity at 30% strain	N/A
[26]	SWNT	PDMS	SWNT densities in composite were ~10 mg/mL	250	108	~16% increases in resistance at 100% strain	N/A
[27]	SWNT, Ionic liquid	Silicone rubber	Silicone rubber with 4 wt% SWNT and 1:3 ratio of ionic liquid(relative to SWNTs weight), Post treated by nitric acid vapor	200	~63	~20 at 200% strain	Spray coating w/ contact mask
[18]	SG-SWNT[g], Ionic liquid	PVDF	SG-SWNTs, 50 mg; ionic liquid, 50 mg; PVDF, 100 mg; 4-methyl-2-pentanone, 8 ml	134	57	6 at 134% strain	N/A
[1]	SG-SWNT, Ionic liquid	PVDF	SG-SWNTs, 30 mg; ionic liquid, 60 mg; 4-methyl-2-pentanone, 100 ml; PVDF, 1500 mg)	118	9.7	9.7 at 118% strain	Screen printing w/ shadow mask
[28]	Silver platelet	PDMS	PDMS with 86 wt% of silver platelet	N/A	~170	~300 at 80% strain	Soft lithography
[14]	Copper powder	PMMA	PMMA with 40 vol% of copper	N/A	~1.25	N/A	N/A
[13]	Nickel micro-particle	Silicone rubber	Silicone rubber with 24 vol% of nickel particle	N/A	~0.1	N/A	N/A
[29]	Silver powder	PDMS	PDMS with 21 vol% of silver and benzophenone	57	~100	N/A	Photo lithography
[30]	Silver coated fly ash cenosphere	Silicone rubber	N/A	N/A	N/A	58 times increase in resistance at 64% strain	N/A
[31]	PEDOT[h]	Polyurethane	Polyurethane with 50 wt% of PEDOT	N/A	120	~35 at 200% starin	N/A
[32]	Bacterial cellulose	PDMS	N/A	118	0.20-0.41	50% increase in resistance at 118% strain	N/A
This work	Nickel	PDMS	PDMS with 18.3 vol% of nickel (*:combined with inkjet-printed silver)	>200 (*>200)	0.34 (*45.73)	115 at 100% strain (*116 at 100% strain)	Magnetic field & inkjet-printing

[a] Exfoliated Graphite
[b] Cyclic test was performed by PDMS with 5 wt.% EG sample
[c] Poly[styrene-*b*-(ethylene-*co*-butylene)-*b*styrene]
[d] Silver nanoparticle decorated MWNT
[e] Polyvinylidenefluoride
[f] Polystyrene–polyisoprene–polystyrene
[g] Super growth SWNT (>1 mm in length)
[h] Poly(3,4-ethylenedioxythiophene):*p*-tosylat

4.2 Experimental

To implement the stretchable electrodes, we used poly(dimethylsiloxane) (PDMS; Sylgard 184 from Dow Corning) for elastomeric medium and nickel powder (203904; average particle size ~5 μm, 99.99% from Sigma Aldrich) for conductive fillers. Filler volume ratio can be varied to optimize the performance of the conductive composite.

Figure 4.1 shows fabrication flow of the composite-only and silver-covered composite electrodes. Various volume ratio of nickel powder (average particle size ~5 μm, 99.99% from Sigma Aldrich) was mixed with 10 : 1 weight ratio mixture of poly(dimethylsiloxane) (PDMS; Sylgard 184 from Dow Corning) base and curing agent with a hand blender for 10 minute and then was put in a desiccator for 1 hour to degas air in it. The degassed PDMS/nickel mixture was cast onto a flat aluminum mold (see Figure 4.1 (a)) and then the mold was placed between two pre-made iron structures (we will call the structure "magnetic field modulator") and two neodymium permanent magnets (4,000 G) as shown in Figure 4.1 (b). During this process, magnetic field from magnets is focused at closest confronting area of the two magnetic field modulators. The nickel powder inside the mixture moves laterally under the focused area, making electrode patterns similar to the shape of the magnetic field modulator. At the same time, the nickel powder was vertically

arranged due to the magnetic field, direction of which is perpendicular to the composite plane. It is noted that, we can produce various shapes such as wavy lines or circles in addition to the straight lines if we use magnetic field modulators with corresponding patterns. However, our method has limitation in producing very fine features because feature sizes are directly related to the minimum feature size of the shape of the magnetic field modulator and the thickness of the nickel-embedded PDMS. Since our field modulator is made by an electrical discharge machining (EDM) method and has high aspect ratio structure, its pattern pitch (or line width and spacing) is limited to around 100 μm due to the intrinsic EDM limitation. The important point is that the designed pattern pitch and PDMS thickness should be similar in order to obtain desirable pattern quality. The time required for patterning/arrangement process depends on volume ratio of the nickel powder, mixture viscosity, and magnetic field strength at the confronting surface. Finally, the patterned and arranged mixture was thermally cured in a convection oven at 130 ℃ for 30 min. The fully cured arranged conductive composite electrodes (we call this "exposed composite-only electrodes") have 10-mm length, 1-mm width and 1-mm thickness as shown in Figure 4.1 (c). On top of the fully cured exposed composite-only electrodes, silver thin films were inkjet-printed (see Figure 4.1 (d), we call this "exposed silver-covered composite electrodes") by using the printing conditions, details of which have been reported in our previous papers [11, 12]. On top of the

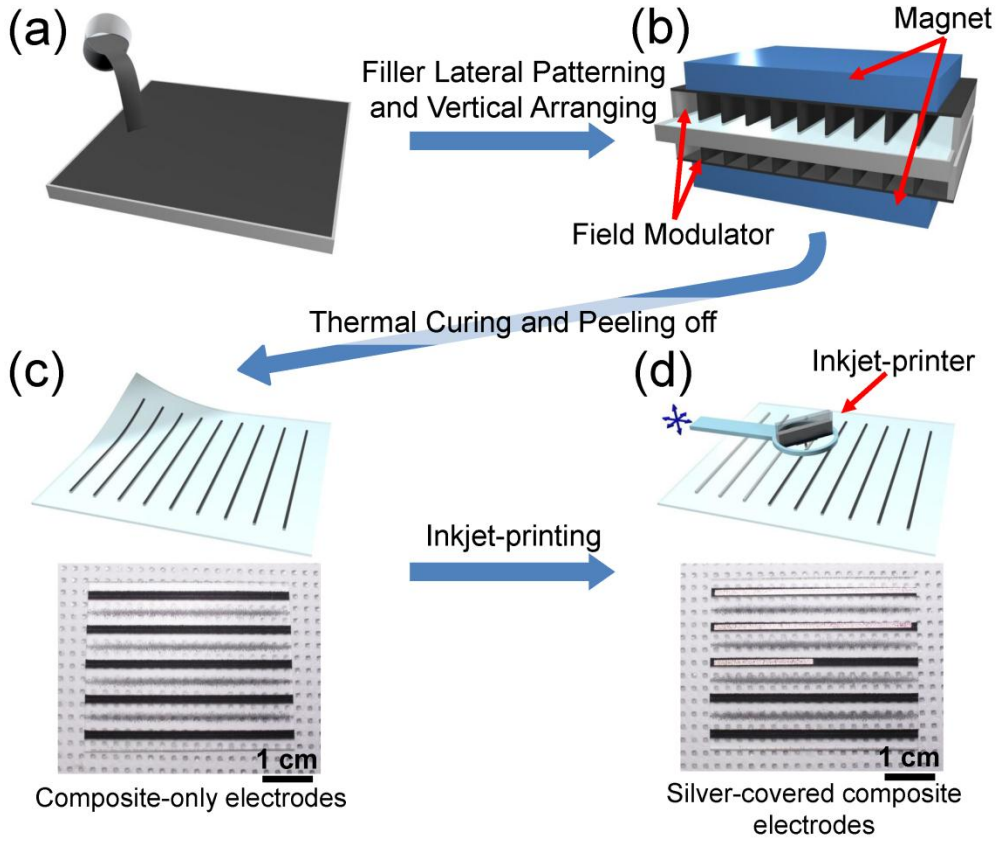

Figure 4.1 Fabrication process of stretchable electrodes. (a) Nickel/PDMS mixture casting onto aluminum mold. (b) Nickel filler arranging and patterning by the magnetic field modulator. (c) Cured exposed composite-only electrodes. (d) Inkjet-printing of silver electrodes onto exposed composite-only electrodes.

fully cured exposed composite-only electrodes, silver thin films were inkjet-printed. Nanoparticle type silver ink (DGP-40 from ANP Corp.) was inkjet-printed by using a piezo electric inkjet-printer (DMP-2831 from Dimatix Corp.) after the composite surface was treated with UV ozone cleaner (AH1700 from AHTECH LTS) for 10 minutes to increase the surface energy to be more hydrophilic. Power of the UV light was 28 $mWcm^{-2}$. Inkjet-printing parameters such as the cartridge temperature, stage temperature, ink drop speed and drop spacing were 30 ℃, 60 ℃, 6 ms^{-1} and 25 μm, respectively. The inkjet-printed silver electrode was sintered on a hot plate at 100 ℃ for 1h. For comparison, we also fabricated two additional types of electrodes: nickel conductive composite electrodes without exposure to magnetic field (we call this "unexposed composite-only electrode") and inkjet-printed silver electrodes on the PDMS substrate.

It is noted that, we can produce various shapes such as wavy lines or circles in addition to the straight lines if we use magnetic field modulators with corresponding patterns, as shown in Figure 4.2. However, our method has limitation in producing very fine features because feature sizes are directly related to the minimum feature size of the shape of the magnetic field modulator and the thickness of the nickel-embedded PDMS. Since our field modulator is made by an electrical discharge machining (EDM) method and has high aspect ratio structure, its pattern pitch (or line width and spacing) is limited to around 100 μm due to the intrinsic EDM

limitation. The important thing is that the designed pattern pitch and PDMS thickness should be similar in order to obtain desirable pattern quality.

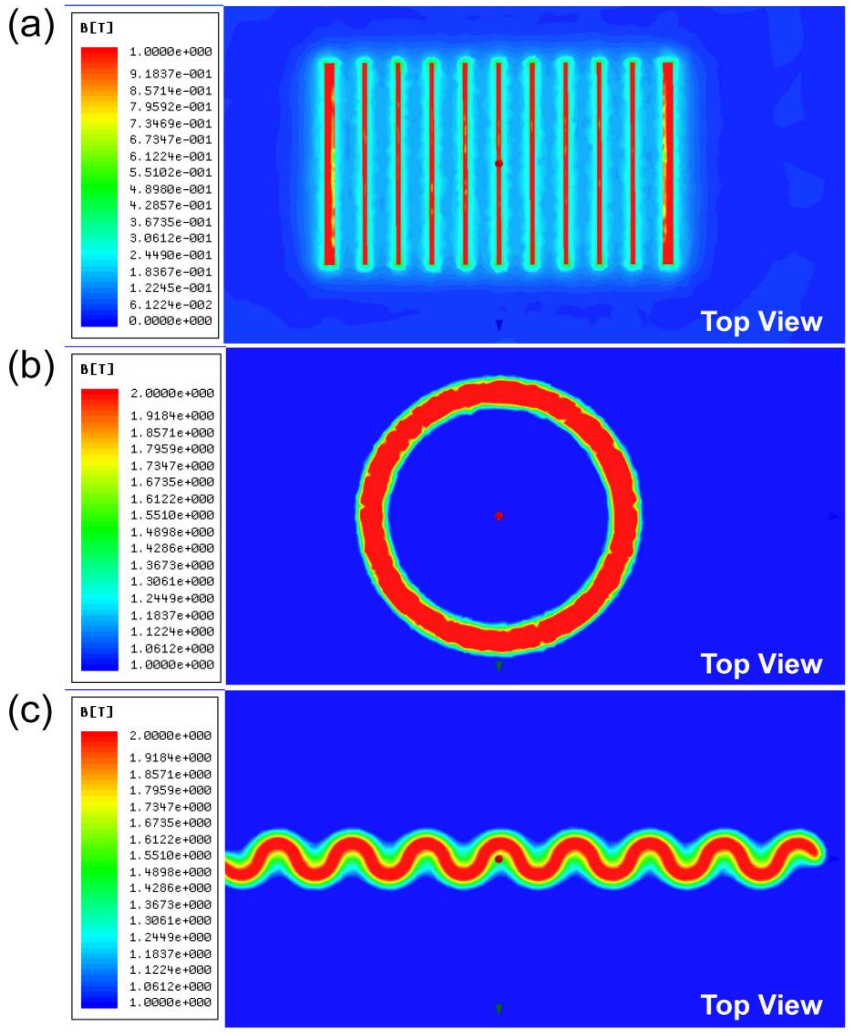

Figure 4.2 Magnetic field simulation results with various shapes. (a) Parallel straight lines (1-mm line width, 1-mm thickness and 6.3-mm spacing) (b) Circle (1-mm line width, 1-mm thickness) (c) Wavy line (100-μm line width, 100-μm thickness)

4.3 Results and Analysis

4.3.1 Electrical Characteristics with Tension Test

Figure 4.3 shows resistance change of the unexposed and exposed composite-only electrodes with the tensile strain for different filler concentrations of 5.3 to 18.3 vol% (lines with symbol). Tensile strain was applied using a home-made stretching equipment that can be programmed to control stretching amount and speed. Electrical property was measured using digital sourcemeter (Keithley 2420) that is controlled by a computer. All samples have 10-mm length, 1-mm width, and 1-mm thickness. The tensile strain was applied at 16.7 μm/s, and electrical resistance was measured every 0.2 sec.

It is noted that volume fraction was calculated from the measured weight of PDMS and nickel powder and literature values of their density (1.03 and 8.908 g/cm3 for PDMS and nickel, respectively) and indicates the volume fraction at the homogeneous mixture state. For exposed composite, resistance at the same tensile stress decreases with the filler concentration because the more nickel powder exists per volume, the more conduction paths are formed in the composite electrodes. The same behavior was also observed for the unexposed ones, which is not shown here. Resistance of the exposed composite-only electrodes rapidly decreases with the tensile strain at low strain region, and then is saturated at around 40% strain. Electrical conductivity that was calculated from resistance and volume of the

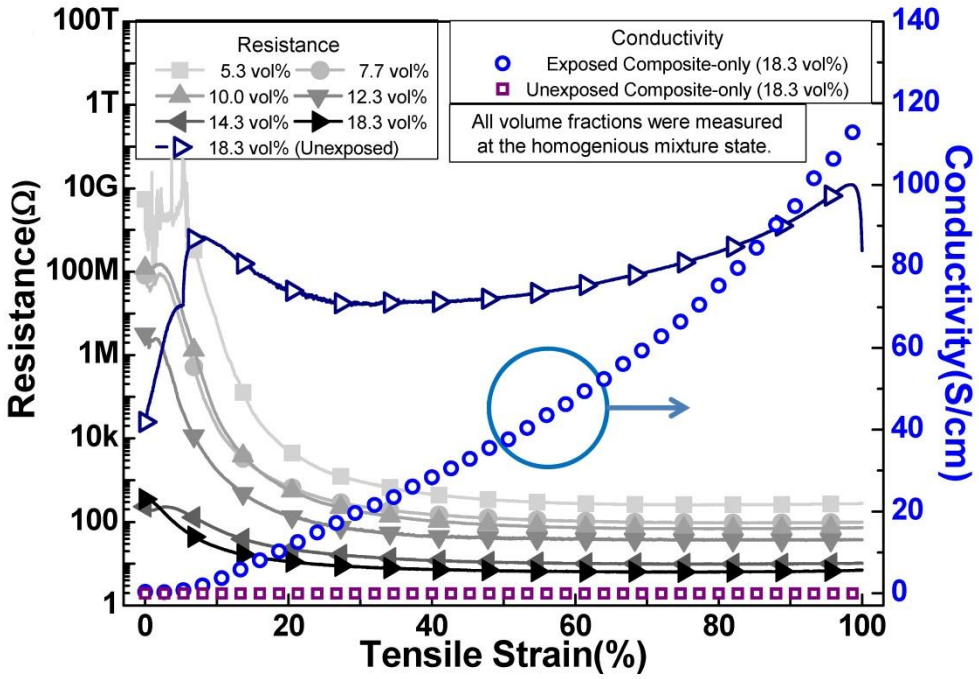

Figure 4.3 Resistance and conductivity change in terms of tensile strain for exposed and unexposed composite-only electrodes. (All volume fractions were measured at the homogeneous mixture state.)

composite was about 115 S/cm at 100% tensile strain. However, for unexposed composite, opposite properties, i.e. increase of resistance with the tensile stress, have been observed. In addition, its initial resistance was also very large in comparison with the exposed composite.

4.3.2 Analysis with Three-dimensional Percolation Theory

As mentioned before, it should be noted that the conductive composite materials that have been previously reported generally showed properties of increasing resistance with the tensile strain like our unexposed composite [13-19]. This general property seems to be caused by decrease of the conductive filler volume fraction in the composite with the tensile strain and can be explained by a three-dimensional percolation theory [19]. The electrical conductivity of the conductive composite is given by the power law relationship as shown in Equation (4.1).

$$\sigma = \sigma_0(V_f - V_c)^s \tag{4.1}$$

where σ is the electrical conductivity of composite, σ_o is the electrical conductivity of the filler, V_f is the filler volume fraction, V_c is the percolation threshold and s is the fitting exponent. In this equation, only V_f depends upon tensile strain, but other parameters were presumed to be constant.

The V_f is obtained by following equations, when tensile strain ε was applied to the composite along length direction [S5],

$$L_2 = L_1 \cdot (1 + \varepsilon) \tag{4.2}$$

$$T_2 = T_1 \cdot (1 - \nu_t \varepsilon) \tag{4.3}$$

$$W_2 = W_1 \cdot (1 - \upsilon_w \varepsilon) \tag{4.4}$$

$$V_2 = L_2 \cdot T_2 \cdot W_2 = L_1 T_1 W_1 (\upsilon_t \upsilon_w \varepsilon^3 + (\upsilon_t \upsilon_w - \upsilon_t - \upsilon_w)\varepsilon^2 - (\upsilon_t + \upsilon_w - 1)\varepsilon + 1) \tag{4.5}$$

$$V_f = \frac{V_{filler}}{V_2} \quad (4.6)$$

where L_1, T_1, W_1 and L_2, T_2, W_2 are the length, thickness, width of the composite before and after strain applying, respectively. V_2 is the volume of the composite after elongation. υ_t and υ_w are Poisson's ratios in the thickness and width direction of that were experimentally determined .

Typically, Poisson's ratio of most conductive composites is low value around 0.2~0.3. The volume of the conductive composite increases with the tensile strain for the composites with low Poisson's ratio, according to the Equation 4.5. This result leads to the material's electrical conductivity decreasing with the tensile stress. (Equation 4.1 and 4.6) However, our exposed composite has high Poisson's ratio (18.3 vol%; υ_t=0.26, υ_w=0.66) compared to the unexposed composite with same filler volume fraction (υ_t=0.24, υ_w=0.22), where, υ_t and υ_w are Poisson's ratio in the directions of thickness and width, respectively. For such a large Poisson's ratio, the volume of the composite decreases with the tensile strain (Equation 4.5). Volume variation of our nickel filler embedded medium in each case was calculated according to the tensile strain as shown in Figure 4.4. The exposed composite shows volume decrease tendency with the tensile strain, whereas unexposed composite does not. This volume decrease results in increase of the nickel filler volume

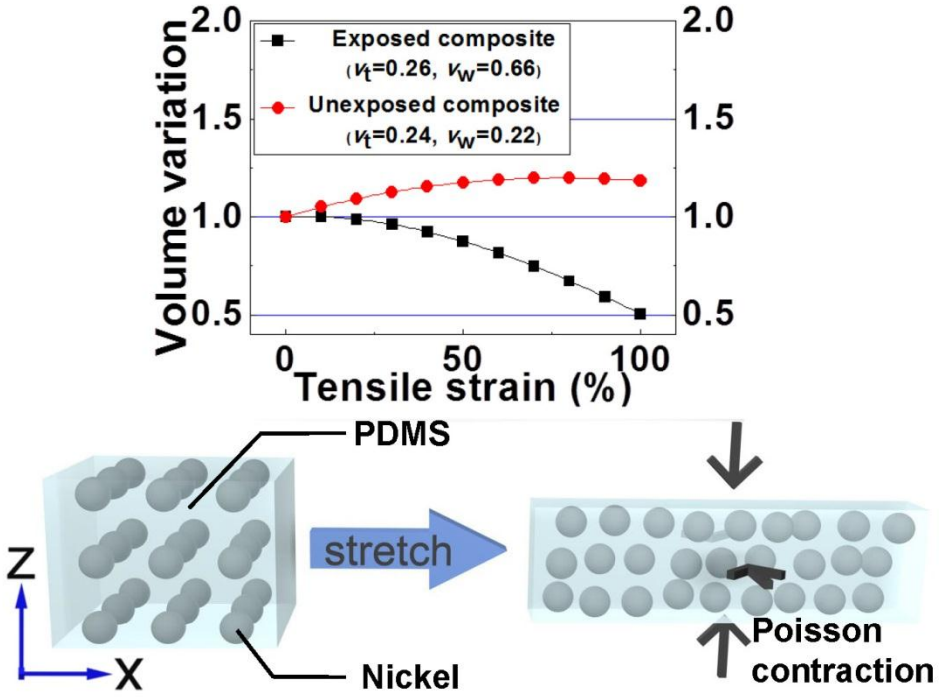

Figure 4.4 Graph: Volume variation calculation with tensile strain of exposed and unexposed composites. Schematic illustration: Volume decrease and nickel filler volume fraction increase with the tensile strain in exposed composite. Considered as composite with 18.3 vol% of nickel filler (vt=0.26, vw=0.66), and longitudinally 100% stretched. (stretching direction: x, magnetic field (or flux) direction: z)

fraction. The exposed composite-only electrodes showed conductive path increasing, which is verified from the cross-sectional scanning electron microscope (SEM) image with the tensile strain. Figure 4.5 (b) shows that electrical conduction paths are more formed between nickel powders as the tensile strain increases. This unique property of the exposed composite-only electrode plays the key role in reduction of the electrical resistance with the tensile strain.

SEM specimen preparation for a stretched electrode is shown in Figure 4.6. First, exposed composite-only electrode was cut in half (Figure 4.6 (a), (b), and (c)), along the center line in its stretching direction. Then, specimen was stretched and fixed at a specific tensile strain by using the manually implemented stretching machine (Figure 4.6 (d)). The stretched specimen which is fixed on the manual stretching machine was carefully and firmly adhered to SEM specimen holder by using conductive carbon tape under the specimen and kapton tape on the side area of the specimen (Figure 4.6 (e)) in order to maintain the stretched state after removing the stretching machine. As shown in the Figure 4.6 (f), the tapes can hold the stretched specimen without the stretching machine. SEM images were taken by field emission SEM. (Model S-4800 from Hitachi)

(a)

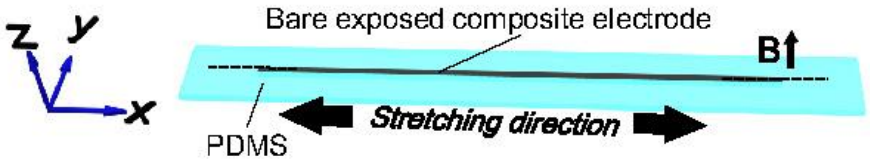
z
y
x
Bare exposed composite electrode
B
Stretching direction
PDMS

(b)

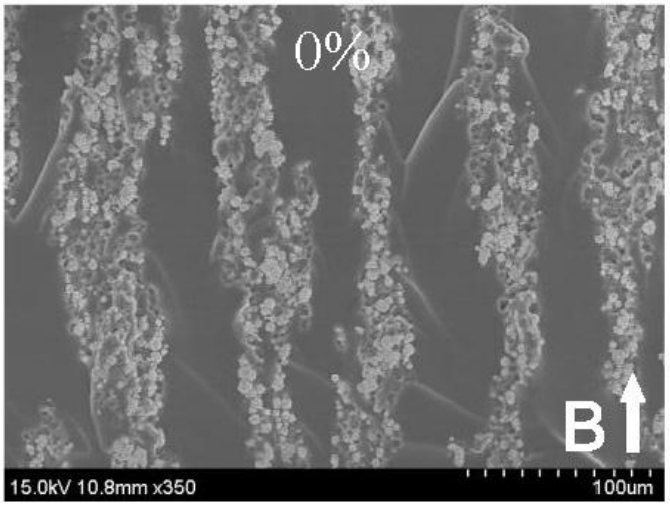
0%
B
15.0kV 10.8mm x350
100um

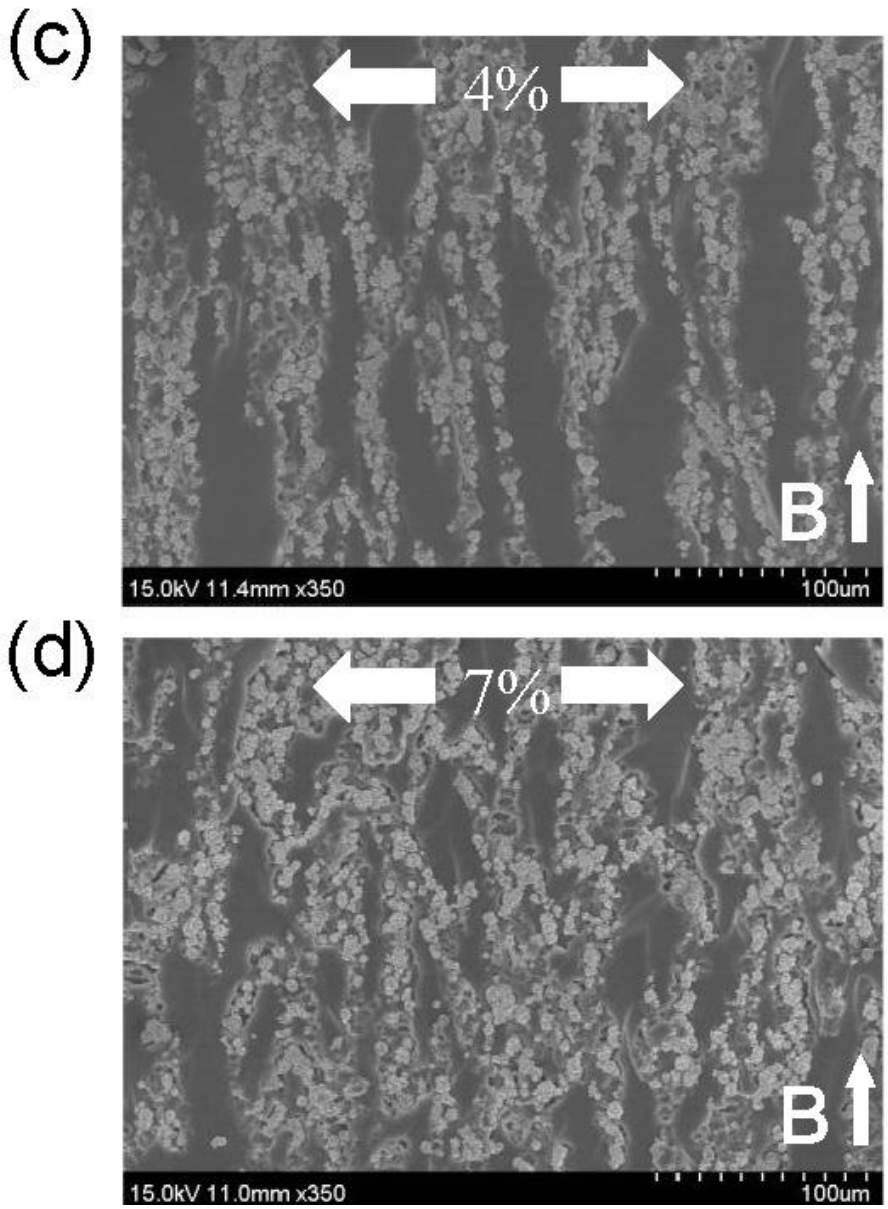

Figure 4.5 (a) Schematic illustration of the exposed composite-only electrode and its cross sectional SEM images under various tensile strain of (b) 0%, (c) 4%, and (d) 7%. (Magnetic field direction: z, stretching direction: x, SEM image: xz-plane through dashed line)

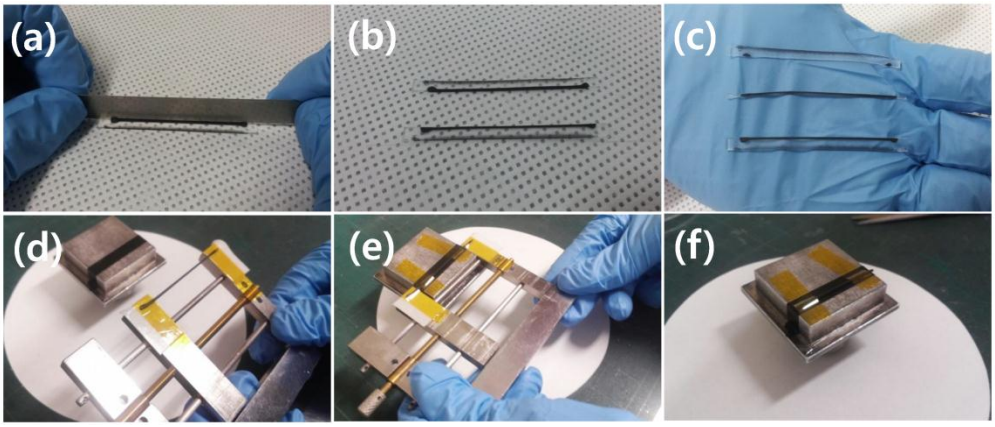

Figure 4.6 (a, b, c) First, exposed composite-only electrode was cut in half, along the center line in its stretching direction. (d) Then, specimen was stretched and fixed at a specific tensile strain by using the manually implemented stretching machine. (e) The stretched specimen which is fixed on the manual stretching machine was carefully and firmly adhered to SEM specimen holder by using conductive carbon tape under the specimen and kapton tape on the side area of the specimen in order to maintain the stretched state after removing the stretching machine. (f) The tapes can hold the stretched specimen without the stretching machine.

4.3.3 Highly Stretchable Electrode with Ink-jet Printed Silver

However, the exposed composite-only electrode still has high initial resistance, which limits its applications to practical devices and interconnections. To solve this issue, we fabricated additional inkjet-printed silver thin films on top of the exposed composite-only electrodes. Typical silver or gold electrodes keep their low resistance at low tensile strain, but lose their initial properties at higher strain. [7-12] Therefore, it is expected that two opposite behaviors of the exposed composite-only and silver electrodes would compensate for each other, resulting in an extremely highly stretchable electrode property. Figure 4.7 shows properties of the inkjet-printed silver electrode on PDMS substrate, the exposed composite-only electrode, (14.3 vol%) and the exposed silver-covered composite electrode. (14.3 vol%) The initial resistance of the inkjet-printed silver, exposed composite-only and silver-covered composite electrodes were 3.2, 237.4 and 2.2 Ω, respectively. The inkjet-printed silver electrode showed a good electrical performance at low tensile strain condition (under 20%). However, its electrical resistance rapidly increased with the tensile strain and it loses electrical conduction at above 38% tensile strain. This increase in resistance originates from the appearance of metal cracks under the tensile strain.[7-12] The exposed composite-only electrode showed poor electrical performance at low tensile strain condition but its electrical resistance decreased with the tensile strain. The resistance reached 20 Ω at 21% tensile strain and it

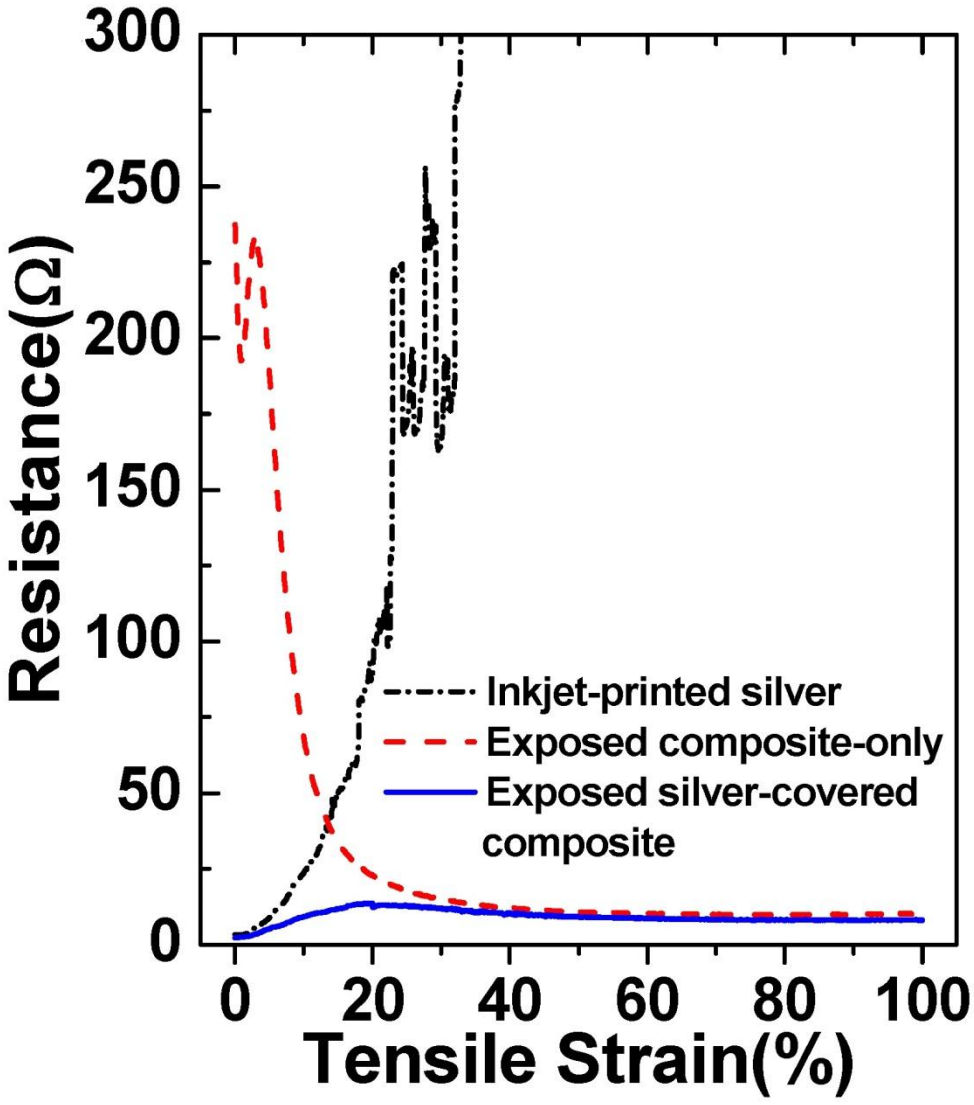

Figure 4.7 Resistance changes in terms of tensile strain for inkjet-printed silver, exposed composite-only and exposed silver-covered composite.

remained under 20 Ω up to 100 % tensile strain. When combined together, the exposed silver-covered composite electrodes showed low resistance at both low and high strain conditions. It showed resistance lower than 20 Ω within range of the experimented tensile strain conditions. Its resistance increased gradually but slightly up to 20% strain, mainly due to crack formation of the inkjet-printed silver thin films. As the tensile strain further increased, the resistance of the exposed silver-covered composite electrodes decreased and became saturated.

For visual demonstration, we connected commercial blue light emitting diodes (LEDs) with the stretchable electrodes and monitored the light emission under various tensile strain conditions. Their light-emission images at 0, 15, 30, 50 and 100% tensile strain conditions are included in Figure 4.8. The operating results are consistent with the measured electrical resistance variation with the tensile strain for three types of electrodes. It is noted that the electrical resistance of the composite-based electrode can be varied if there is any resistive heating. Since temperature dependency of the resistance of the composite-based electrode is common observation, [33, 34] if we want to use our electrodes for high power applications, heating effect should be considered accordingly.

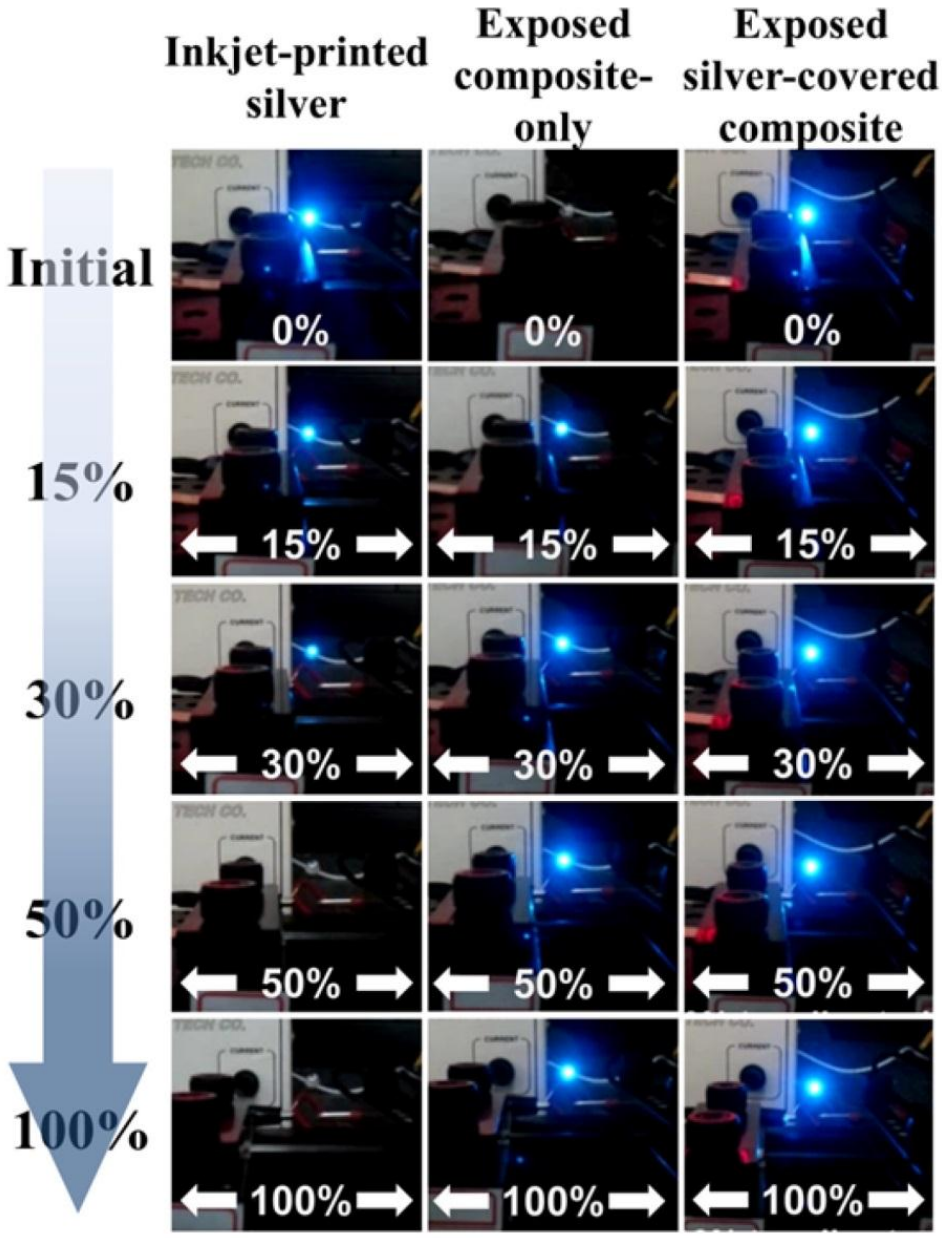

Figure 4.8 Luminance change of LED which was connected inkjet-printed silver, exposed composite-only and exposed silver-covered composite respectively, with tensile strain.

4.4 Resolution Sustainable Stretchable Lighting Device

Another promising application of this negative strain-dependency of the exposed composite-only electrodes is implementation of the stretchable display or lighting device with constant image resolution under the tensile strain conditions. It should be noted that most of the previous reports demonstrated stretchable lighting device but with decreasing image resolution with the tensile strain [1, 35]. However, in our approach, we can configure hidden pixels between light-emitting pixels so that the hidden pixels are turned on to maintain the original image resolution when the tensile strain is applied. When the exposed composite-only and exposed silver-covered composite electrodes are appropriately configured, we can produce a resolution-sustainable stretchable lighting device, where number of lighting pixels per unit area can be maintained same under the tensile strain. Figure 4.10 (a) shows a demonstration of one-dimensional stretchable lighting device with five surface mount LEDs. Three parallel exposed composite-only electrodes embedded in single PDMS matrix were fabricated using the same method as mentioned above. Then, silver thin films were inkjet-printed onto two outer exposed composite-only electrodes. Anode and cathode of the five surface mount LEDs were attached between the exposed silver-covered composite and composite-only electrodes. Those of the first, third, and fifth LEDs were connected to two exposed silver-covered composite electrodes via inkjet-printed silver. Polyimide films were located

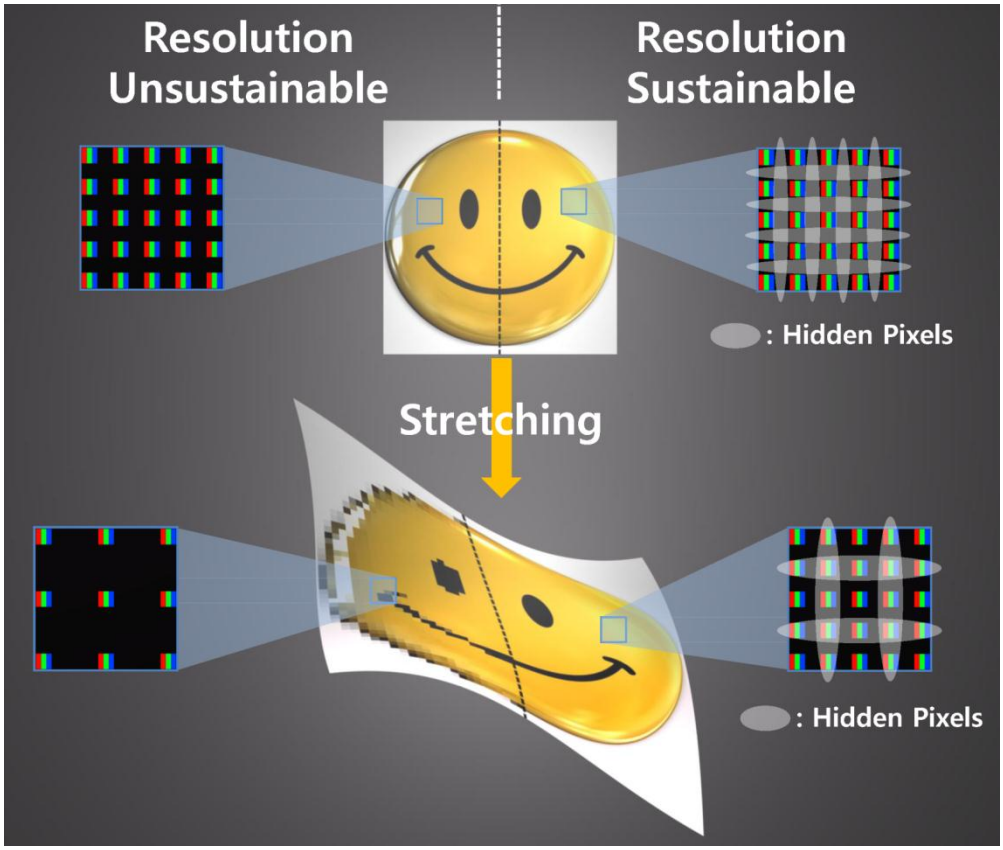

Figure 4.9 Conceptual image of a resolution sustainable stretchable display.

on the exposed composite-only electrode in order to prevent unwanted electrical connections. The anode and cathode of the second and fourth LEDs were connected to composite-only electrodes and exposed silver-covered composite, respectively, via inkjet-printed silver.

Three constantly on (1, 3, 5) and two hidden (2, 4) LEDs are connected to exposed silver-covered composite and exposed composite-only electrodes, respectively, so that the hidden LEDs are turned on when tensile strain is applied. As the tensile strain increases, the distance between constantly on pixels increases, resulting in reduction of the image resolution. However, at certain tensile strain, the hidden pixels start to be turned on and they will maintain the initial image resolution of the lighting device. Figure 4.10 (b) shows images taken at various strain conditions up to 20%. The hidden (2, 4) LEDs become turned on with the tensile strain and showed their full brightness at around 15% tensile strain, maintaining it up to 20%. It is noted that resistance of the exposed composite-only electrode becomes similar to that of the exposed silver-covered electrode around 20% tensile strain as shown in Figure 4.7. Therefore, we observed similar brightness from the LEDs connected to each electrode. When we optimize the concentration of fillers and improve connection between LEDs themselves with the electrodes, we can control turn-on strain for the hidden LEDs and apply higher tensile strain to our devices.

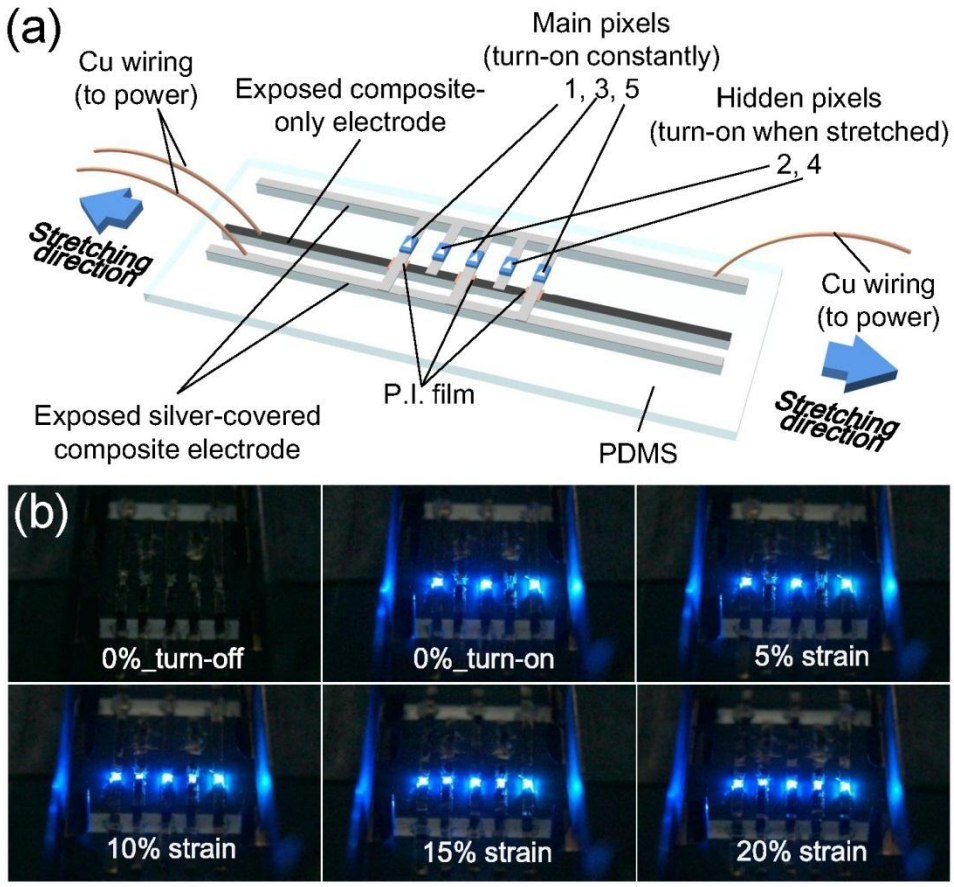

Figure 4.10 (a) Schematic illustration of resolution-sustainable stretchable lighting device with tensile strain. (b) Luminance change of resolution-sustainable stretchable lighting device with tensile strain.

4.5 Conclusion

In conclusion, we have developed a highly stretchable electrode and demonstrated a resolution sustaining lighting device by fully utilizing unique property of the negative strain-dependency in electrical resistance of the magnetically patterned and arranged nickel composite. Resistance of the exposed silver-covered composite electrode was maintained below 20 Ω even up to 100% tensile strain. Although cyclic behavior of pure nickel composite needs more improvement, nickel-based composite materials have excellent advantages over other materials in terms of simple patterning and in-situ embedding in the matrix. In addition, when nickel-containing composite, such as nickel-combined CNT [36] or nickel-attached polymer [37], is used, it is expected that more stable, highly-stretchable, patterned interconnecting electrodes can be implemented. Finally, from the conceptual demonstration of the resolution-sustainable lighting device, we believe that our novel technology would be one of the key enabling technology in implementing future stretchable electronic display devices.

Reference

[1] T. Sekitani, H. Nakajima, H. Maeda, T. Fukushima, T. Aida, K. Hata, and T. Someya, "Stretchable active-matrix organic light-emitting diode display using printable elastic conductors," *Nat. Mater.*, vol. 8, pp. 494-499, May 2009.

[2] T. Someya, Y. Kato, T. Sekitani, S. Iba, Y. Noguchi, Y. Murase, H. Kawaguchi, T Sakurai, "Conformable, flexible, large-area networks of pressure and thermal sensors with organic transistor active matrixes," *Proc. Natl. Acad. Sci*., vol. 102, no. 35, pp. 12321-12325, July 2005.

[3] D.-Y. Khang, H. Jiang, Y. Huang, and J. A. Rogers, "A Stretchable Form of Single-Crystal Silicon for High-Performance Electronics on Rubber Substrates," *Science*, vol. 311, no. 5768, pp. 208-212, January 2006.

[4] D.-H. Kim, J.-H. Ahn, W. M. Choi, H.-S. Kim, T.-H. Kim, J. Song, Y. Y. Huang, Z. Liu, C. Lu, and J. A. Rogers, "Stretchable and Foldable Silicon Integrated Circuits," *Science*, vol. 320, no. 5875, pp. 507-511, April 2008.

[5] M. Kubo, X. Li, C. Kim, M. Hashimoto, B. J. Wiley, D. Ham, and G. M. Whiteside, "Stretchable Microfluidic Radiofrequency Antennas," *Adv. Mater.*, vol. 22, no. 25, pp. 2749-2752, July 2010.

[6] I. M. Graz, D. P. J. Cotton, A. Robinson, and S. P. Lacour, "Silicone substrate with in situ strain relief for stretchable thin-film transistors," *Appl. Phy. Lett.*, vol. 98, no. 12, 124101 (3pp), March 2011.

[7] S. P. Lacour, J. Jones, Z. Suo, and S. Wagner, “Design and performance of thin metal film interconnects for skin-like electronic circuits,” *IEEE Electron Device Lett.*, vol. 25, no. 4, pp. 179-181. April 2004.

[8] S. P. Lacour, S. Wagner, Z. Huang, and Z. Suo, “Stretchable gold conductors on elastomeric substrates,” *Appl. Phys. Lett.*, vol. 82, no. 15, pp/ 2404-2406, April 2003.

[9] J. Jeong, S. Kim, J. Cho, and Y. Hong, “Stable Stretchable Silver Electrode Directly Deposited on Wavy Elastomeric Substrate,” *IEEE Electron Device Lett.*, vol. 30, no. 12, pp. 1284-1286, December 2009.

[10] J. Jeong, S. Kim, J. Cho, D. Kim, and Y. Hong, “Stretchable Low Resistance Thick Silver Electrode on Poly(dimethylsiloxane) Compliant Elastomeric Substrate,” *Jpn. J. Appl. Phys.*, vol. 49, 05EB09 (4pp), May 2010.

[11] S. Chung, J. Lee, H. Song, S. Kim, J. Jeong, and Y. Hong, “Inkjet-printed stretchable silver electrode on wave structured elastomeric substrate,” *Appl. Phys. Lett.*, vol. 98, no. 15, 153110 (3pp), April 2011.

[12] J. Lee, S. Chung, H. Song, S. Kim, and Y. Hong, “Lateral-crack-free, buckled, inkjet-printed silver electrodes on highly pre-stretched elastomeric substrates,” *J. Phys. D: Appl. Phys*., vol. 46, no. 10, 105305 (5pp), February 2013.

[13] G. Ausanio, A. C. Barone, C. Campana, V. Iannotti, C. Luponio, G. P. Pepe, and L. Lanotte, “Giant resistivity change induced by strain in a composite of

conducting particles in an elastomer matrix," *Sens. Actuators A*, vol. 127, no. 1, February 2006.

[14] R. Mukhopadhyay, S. K. De, and S. Basu, "Effect of metal concentration on the electrical conductivity and some mechanical properties of poly(methyl methacrylate)–copper composites," *J. Appl. Polym. Sci*., vol. 20, no. 9, pp. 2575-2580, September 1976.

[15] NC Das, TK Chaki, and D. Khastgir, "Effect of axial stretching on electrical resistivity of short carbon fibre and carbon black filled conductive rubber composites," *Polym. Int.*, vol. 51, no. 2, pp. 156-163, February 2002.

[16] M. Knite, V. Teteris, A. Kiploka, and I. Klemenoks, "Reversible Tenso-Resistance and Piezo-Resistance Effects in Conductive Polymer-Carbon Nanocomposites," *Adv. Eng. Mater.*, vol. 6, no. 9, pp. 742-746, September 2004.

[17] M. Kujawski, J. D. Pearse, and E. Smela, "Elastomers filled with exfoliated graphite as compliant electrodes," *Carbon*, vol. 48, no. 9, pp. 2409-2417, August 2010.

[18] T. Sekitani, Y. Noguchi, K. Hata, T. Fukushima, T. Aida, and T. Someya, "A Rubberlike Stretchable Active Matrix Using Elastic Conductors," *Science*, vol. 321, no. 5895, pp. 1468-1472, September 2008..

[19] K.-Y. Chun, Y. Oh, J. Rho, J.-H. Ahn, Y.-J. Kim, H. R. Choi, and S. Baik, "Highly conductive, printable and stretchable composite films of carbon nanotubes and silver," *Nat. Nanotechnol.*, vol. 5, pp. 853-857, November 2010.

[20] J. Kost, M. Narkis, and A. Foux, "Effects of axial stretching on the resistivity of carbon black filled silicone rubber," *Polym. Eng. Sci*., vol. 23, no. 10, pp. 567-571, July 1983.

[21] E. Sevkat, J. Li, B. Liaw, and F. Delale, "A statistical model of electrical resistance of carbon fiber reinforced composites under tensile loading," *Compos. Sci. Technol*., vol. 68, no. 10-11, pp. 2214-2219, August 2008.

[22] Y. Li, and H. Shimizu, "Toward a Stretchable, Elastic, and Electrically Conductive Nanocomposite: Morphology and Properties of Poly[styrene-b-(ethylene-co-butylene)-b-styrene]/Multiwalled Carbon Nanotube Composites Fabricated by High-Shear Processing," *Macromolecules*, vol. 42, no. 7, pp. 2587-2593, March 2009.

[23] M. K. Shin, J. Oh, M. Lima, M. E. Kozlov, S. J. Kim, and R. H. Baughman, "Elastomeric Conductive Composites Based on Carbon Nanotube Forests," *Adv. Mater*., vol. 22, pp. 2663-2667, May 2010.

[24] K.-Y. Chun, S. H. Kim, M. K. Shin, Y. T. Kim, G. M. Spinks, A. E. Aliev, R. H. Baughman, and S. J. Kim, "Free-standing nanocomposites with high

conductivity and extensibility," *Nanotechnology,* vol. 24, no. 16, 165401 (9pp), March 2013.

[25] M. Chen, T. Tao, L. Zhang, W. Gao, and C. Li, "Highly conductive and stretchable polymer composites based on graphene/MWCNT network," *Chem. Commun*., vol. 49, pp. 1612-1614, January 2013.

[26] K. H. Kim, M. Vural, and M. F. Islam, "Single-Walled Carbon Nanotube Aerogel-Based Elastic Conductors," *Adv. Mater*., vol. 23, no. 25, pp. 2865-2869, July 2011.

[27] T. A. Kim, H. S. Kim, S. S. Lee, and M. Park, "Single-walled carbon nanotube/silicone rubber composites for compliant electrodes," *Carbon*, vol. 50, no. 2, pp. 444-449, February 2012.

[28] X. Niu, S. Peng, L. Liu, W. Wen, and P. Sheng, "Characterizing and Patterning of PDMS-Based Conducting Composites," *Adv. Mater*., vol. 19, no. 18, pp. 2682-2686, September 2007.

[29] H. Cong, and T. Pan, "Photopatternable Conductive PDMS Materials for Microfabrication," *Adv. Func. Mat*., vol. 18, no. 13, pp. 1912-1921, July 2008.

[30] S.-F. Hu, C. Zhang, M. Zhao, W. Chen, and S.-X. Peng, "Effect of tensile strain on the electrical resistivity of silver-coated fly ash cenospheres/silicone-rubber composites," *Polym. Bull*. vol. 66, no. 7, pp. 955-963, April 2011.

[31] T. S. Hansen, K. West, K. West, O. Hassager, and N. B. Larsen, “Highly Stretchable and Conductive Polymer Material Made from Poly(3,4-ethylenedioxythiophene) and Polyurethane Elastomers,” *Adv. Funct. Mater*., vol. 17, no. 16, pp. 3069-3073, November 2007.

[32] H.-W. Liang, Q.-F. Guan, Z.-Zhu, L.-T. Song, H.-B. Yao, X. Lei, and S.-H. Yu, “Highly conductive and stretchable conductors fabricated from bacterial cellulose,” *NPG Asia Mater*., vol.4, e19 (6pp), June 2012.

[33] L. Lamaignere, F. Carmona and D. Sornette, “Static and dynamic electrical breakdown in conducting filled-polymers,” *Physica A*, vol. 241, no, 1-2, pp. 328-333, July 1997.

[34] A. Vega, J. Sumfleth, H. Wittich and K. Schulte, “Time and temperature dependent piezoresistance of carbon nanofiller/polymer composites under dynamic load,” *J. Mat. Sci*., vol. 47, no. 6, pp. 2648-2657, March 2012.

[35] R.-H. Kim, M.-H. Bae, D.-G. Kim, H. Cheng, B. H. Kim, D.-H. Kim, M. Li, J. Wu, F. Du, H.-S. Kim, D. Estrada, S. W. Hong, Y. Huang, E. Pop, and J. A. Rogers, “Stretchable, Transparent Graphene Interconnects for Arrays of Microscale Inorganic Light Emitting Diodes on Rubber Substrates,” *Nano Lett*., vol. 11, no. 9, pp. 3881-3886, July 2011.

[36] C. Bittencourt A. Felten, J. Ghijsen, J. J. Pireaux, W. Drube, R. Erni, and G. V. Tendeloo, “Decorating carbon nanotubes with nickel nanoparticles,” *Chem. Phys. Lett*., vol. 436, no. 4-6, pp. 368-372, March 2007.

[37] B. C-K. Tee, C. Wang, R. Allen, and Z. Bao, “An electrically and mechanically self-healing composite with pressure- and flexion-sensitive properties for electronic skin applications,” *Nat. Nanotechnol*., vol. 7, pp. 825-832, November 2012.

Chapter 5

Conclusion

In this these, we report the fully integrated pressure/temperature sensor array based on nickel conductive composite. By enhancing and optimizing the conductive composite materials for stretchable sensor, magnetic field alignment method is used.

By using the magnetic aligning method, we successfully demonstrated high performance nickel based conductive composite materials. It shows low percolation threshold with good pressure and temperature sensor characteristics. We fully analyzed filler alignment effect by using percolation theory and effective medium theory.

By using the magnetic patterning method, we report a simple fabrication method of integrated pressure/temperature sensor arrays by embedding conductive nickel (Ni) particles in poly (dimethyloxane) (PDMS) medium. The pressure and

temperature sensing parts are formed in one pixel but have different heights, which are implemented by introducing a corrugated structure to Ni/PDMS composite with a pre-patterned aluminum mold. Since Ni particles are ferromagnetic materials, we also patterned them by exposing Ni/PDMS to patterned magnetic fields produced with pre-patterned iron structure, resulting in an embedded nickel dot array. Magnetic field exposure helped both lateral patterning and vertical particle alignment, which directly improved sensitivity and linearity of the sensor. Independent and stable read-out signals for pressure and temperature sensors are successfully obtained even under repeated measurements. Our technology has advantages of simple tuning for sensitivity and operation ranges by changing particle concentration and device physical dimension, easy scaling-up to large area by seamlessly bonding small arrays or using large-area iron structure, and potential implementation of the sensor front-plane for active-matrix backplane read-out circuitry. Artificial skin passive-matrix system and active-matrix front-plane with about 10 ppi resolution with the integrated 16 x 16 pressure and 15 x 15 temperature sensor arrays have been finally demonstrated.

We also reported a highly stretchable electrode and demonstrated a resolution sustaining lighting device by fully utilizing unique property of the negative strain-dependency in electrical resistance of the magnetically patterned and arranged nickel composite. Resistance of the silver-covered composite electrode was maintained

below 20 Ω even up to 100% tensile strain. Although cyclic behavior of pure nickel composite needs more improvement, nickel-based composite materials have excellent advantages over other materials in terms of simple patterning and in-situ embedding in the matrix. In addition, when nickel-containing composite, such as nickel-combined CNT or nickel-attached polymer is used, it is expected that more stable, highly-stretchable, patterned interconnecting electrodes can be implemented. Finally, from the conceptual demonstration of the resolution-sustainable lighting device, we believe that our novel technology would be one of the key enabling technology in implementing future stretchable electronic display devices.

Publication and Conference Presentation

International Journal

6. S. Kim, J. Byun, S. Choi, D. Kim, T. Kim, S. Chung, and Y. Hong*, "Negatively Strain-Dependent Electrical Resistance of Magnetically Arranged Nickel Composite: Its Application to Highly Stretchable Electrode and Stretchable Lighting Devices," *Advanced Materials*, Accepted, 2013.

5. J. Lee, S. Chung, H. Song, **S. Kim**, and Y. Hong*, "Lateral-crack-free, buckled, inkjet-printed silver electrodes on highly pre-stretched elastomeric substrates," *Journal of Physics D: Applied Physics*, Vol. 46, 105305 (5pp), 2013.

4. S. Chung, J. Lee, H. Song, **S. Kim**, J. Jeong, and Y. Hong*, "Inkjet-Printed Stretchable Silver Electrode on Wave Structured Elastomeric Substrate," *Applied Physics Letters*, vol. 98, no. 15, 153110 (3pp), 2011.

3. J. Jeong, **S. Kim**, J. Cho, D. Kim, and Y. Hong*, "Stretchable Low Resistance Thick Silver Electrode on PDMS Compliant Elastomeric Substrate," *Japanese Journal of Applied Physics*, Vol. 49, 02EB09 (4pp), 2009

2. J. Jeong, **S. Kim**, J. Cho, and Y. Hong*, "Stable Stretchable Silver Electrode Directly Deposited on Wavy Elastomeric Substrate," *IEEE Electron Device Letters*, Vol. 30, no. 12, pp. 1284-1286, 2009

1. K.-J. Cho, J.-S. Koh, **S. Kim**, W.-S. Chu, Y. Hong, and S.-H. Ahn*, "Review of

Manufacturing Processes for Soft Biomimetic Robots," *International Journal of Precision Engineering and Manufacturing*, Vol. 10, No. 3, pp. 171-181, 2009.

International Conference Presentation

13. J. Byun, **S. Kim**, S. Chung, and Y. Hong*, "High-Performance Stretchable Silver Electrode with Scalable Inkjet-Patterned Photo-curable Strain Modulators," *2013 Materials Research Society Fall Meeting,* Boston, USA, Nov. 2013.

12. T. Kim, Y. Joo, **S. Kim**, J. Byun, and Y. Hong*, "A Highly Sensitive and Repeatable Strain Sensor Based on Inkjet-printed Single Walled Carbon Nanotube," *2013 Materials Research Society Fall Meeting,* San Francisco, USA, Apr. 2013.

11. S. Kim, J. Byun, S. Choi and Y. Hong*, "Flexible High-resolution Pressure Sensor Array Using Simply Patternable Conductive Composite Material for Electronic Skin Application," *2013 Materials Research Society Fall Meeting,* San Francisco, USA, Apr. 2013.

10. J. Byun, **S. Kim**, S. Chung, H. Im and Y. Hong*, "Controlled Wrinkling via Artificially Modulated Surface Stress using Inkjet-Printed Transparent Rigid Island Structures," *2012 Materials Research Society Fall Meeting,* Boston, USA, Nov. 2012.

9. Farah A.-N., **S. Kim**, Y. Park, J. Byun, H. Song and Y. Hong*, "Temperature sensor devices based on carbon nanotubes ink," *The 12th International Meeting on Information Display (IMID 2012),* Daegu, Korea, Aug. 2012.

8. S. Kim, J. Byun, S. Chung, D. Kim and Y. Hong*, "Extremely Stretchable Electrode based on Combination of Inkjet-Printed Silver and Conductive Composite

for Stretchable Lighting Applications," *Tech Connect World Conference & Expo 2012*, Santa Clara, USA, Jun. 2012.

7. S. Kim, J. Byun, and Y. Hong*, "Conductive Composite Materials for Extremely Stretchable Electrode Application," *2011 Materials Research Society Fall Meeting*, Boston, USA, Nov. 2011.

6. S. Chung, J. Lee, H. Song, **S. Kim**, J. Jeong, and Y. Hong*, "Inkjet-Printed Silver Electrode for Stretchable Electronics Application," *2011 Materials Research Society Fall Meeting*, Boston, USA, Nov. 2011.

5. Y. Hong*, S. Chung, J. Lee, H. Song, **S. Kim**, and J. Jeong, "Inkjet-Printed Thin Films and Their Applications in Flexible and Stretchable Electronics" 2011 *International Conference on Materials for Advanced Technologies*, Suntec, Singapore, Jun. 2011.

4. S. Kim, M. Kwon, J. Cho, D. Kim, J. Jeong, and Y. Hong*, "Pressure Sensor Array Fabrication Using Novel Magnetically Patternable Conducting Powders," *2010 Materials Research Society Spring Meeting*, San Francisco, USA, Apr. 2010.

3. M. Kwon, J. Jeong, **S. Kim**, D. Kim, and Y. Hong*, "All Solution Processed Integrated Temperature / Pressure Sensor Array," *2010 Materials Research Society Spring Meeting*, San Francisco, USA, Apr. 2010.

2. J. Jeong, J. Cho, **S. Kim**, and Y. Hong*, "Silver Electrodes on Elastomeric Substrates for Stretchable Electronics Applications," *2010 Materials Research*

Society Spring Meeting, San Francisco, USA, Apr. 2010.

1. Y. Hong*, J. Jeong, J. Kim, **S. Kim**, M. Kwon, and S. Chung, “Technical Issues and Applications of Printed Thin-Film Devices,” *2008 Asia-Pacific Workshop on Fundamentals and Applications of Advanced Semiconductor Devices*, Sapporo, Japan, Jul. 2008.

Proceeding Publication

1. **S. Kim**, J. Byun, S. Chung, D. Kim and Y. Hong*, "Extremely Stretchable Electrode based on Combination of Inkjet-Printed Silver and Conductive Composite for Stretchable Lighting Applications," *Tech Connect World Conference & Expo 2012*, Santa Clara, USA, Jun. 2012.

국문 초록

전자 인공 피부의 구현은, 시험적인 기초적 개념부터 로봇 엔지니어링과 인공 보철을 위한 응용까지, 폭넓은 범위에서 연구되고 있다. 인공 피부는 압력이나 온도와 같은 외부의 환경을 감지하고, 로봇 제어 시스템이나 인간의 신경계에 변환된 신호를 전달하는 과정에서 중요한 역할을 담당한다.

실제 인간의 피부가 가지는 특성을 제대로 모사하기 위해서는, 인공 피부는 어레이 형태를 지녀야 함과 동시에 최소한 압력과 온도의 두 가지 환경 변화를 감지해야 한다. 지금까지 단일 인공 피부 내부에 압력과 온도 두 가지 센서 요소를 집적하기 위한 몇몇 시도가 있어왔다. 상용화된 온도 센서 칩과 압력 감지 가능한 복합재료의 집적이나, 각기 따로 제작된 센서 어레이들의 조합과 같은 방법들이 구현돼 왔다. 이와 같은 이종 요소들간의 집적이나 조합의 방법들은 복잡한 제작 공정과 공정 비용의 증가를 불러 일으켰다.

센서 요소에 있어서는, 인가 압력이나 온도에 대해 구조적 변화와 동시에 전기 저항이 변화하는 전도성 복합 재료가 일반적으로 널리 사용되고 있다. 많은 경우에 있어서, 전도성 복합 재료는 압력 혹은 온도 센서로서 오직 한 가지 종류의 환경 감지만 가능하도록 사용되고 있다. 동일한 전도성 복합 재료를 사용해 확연히 구분되는 두 가지 종류의 센서 요소를 같은 기판위에 형성하고, 서로간의 간섭 없이 측정 신호를 읽어온다는 것은 매우 어려운 일이다. 이와

같은 이유로, 단일 전도성 복합 재료를 이용해 다감각 감지가 가능한 장치를 개발한 연구는 발표된바 없다.

또, 일반적으로 전도성 복합 재료는 신호 처리를 위한 능동형 매트릭스 회로가 제작된 유연성 기판 위에 제작되었다. 그러므로, 재료나 소자의 구조 선택에 많은 제한점이 존재할 수 있고, 능동 구동 가능한 센서 에러이의 대량 생산을 어렵게 만드는 공정 방법의 부적합성 등이 존재할 수 있다. 그러나, 기판내부에 각각의 센서 요소들이 내장되는 방식을 통해 독립적으로 센서 어레이가 제작된다면, 그 자체로서 수동형 매트릭스 시스템으로 응용이 가능할 뿐만 아니라, 이에 더하여, 마치 전자 종이에서의 front-plane 기술과 같이, 개별적으로 제작된 능동형 매트릭스 회로 위에 매우 쉬운 적층이 가능할 것이다.

이 논문에서는, poly (dimethyloxane) (PDMS) 매트릭스 내부에 전도성 니켈 입자들이 내장되는 방식을 통한, 매우 간단한 압력/온도 집적화된 센서 어레이의 제작 방법을 보고한다. 압력 센서와 온도 센서들은 동일한 면적을 가지는 하나의 픽셀로서 형성되지만, 요철 구조를 가지는 알루미늄 몰드를 이용해 제작되는 니켈-PDMS 전도성 복합재료 기판의 도입을 통해 서로 다른 높이를 가진다. 니켈 입자는 강자성 물질이기 때문에, 니켈-PDMS 전도성 복합재료에 특정한 구조로 설계된 철 구조물을 거치며 형성되는 패터닝된 외부 자기장을 노출시킴으로써 니켈을 패터닝해 PDMS 내부에 니켈 점들을 어레이 모양으로 제작할 수 있다. 자기장의 노출은 평면 차원으로의 패터닝 뿐 아니라, 수직 방향으로의 니켈

정렬에도 영향을 주고, 이는 민감도나 선형도와 같은 센서의 특성 향상에 직접적인 효과를 불러온다. 이렇게 제작된 센서 어레이는, 반복적인 측정 조건 아래에서도, 각각의 압력과 온도 센서 요소간에 서로 독립적이고 안정적인 결과를 얻을 수 있었다. 이 기술은, 전도성 필러의 함량이나 물리적 크기의 조절을 통해 민감도나 동적 범위와 같은 센서 특성의 쉬운 조절이 가능케하고, 대면적 제작이 용이하다. 또한, 능동 매트릭스 회로와의 쉬운 접합이 가능할 것으로 기대된다. 최종적으로 이 연구에서, 10 ppi 의 해상도를 가지며 16 by 16 의 압력 센서 어레이와 15 by 15 의 온도 센서 어레이가 집적된 수동형 인공 피부를 구현했다.

추가적으로, 자기장을 통한 니켈의 패터닝과 정렬 기술을 이용하여, 고신축성 신축 전극 및 이를 활용한 해상도 유지 가능한 신축성 발광 소자 시스템을 구현했다. 이렇게 제작된 신축정 전극은 인가 인장에 대해 역방향으로 전기 저항이 감소하는 매우 특이한 특성을 보였다. 비록, 반복적인 동작 특성은 추후 개선이 필요하지만, 쉬운 패터닝과 기판 내장 기술의 측면에서는 아주 좋은 장점을 가지고 있다. 본 논문에서 제안하는 기술은 미래의 신축성 전자 소자 기술에서 중요한 역할을 담당할 것으로 기대한다.

주요어: 전자 인공 피부, 전도성 복합 재료, 자기장 패터닝/정렬, 신축성 전극, 신축성 전자 소자

학번 : 2008-20840